

This is to certify that the

thesis entitled

VORTEX RING/MOVING WALL INTERACTIONS

presented by

STEVEN YUEHSAN LIANG

has been accepted towards fulfillment of the requirements for

MASTER OF SCIENCE degree in MECHANICAL ENGINEERING

Major professor

Date 23 Feb 84

0-7639

MSU is an Affirmative Action/Equal Opportunity Institution



RETURNING MATERIALS:

Place in book drop to remove this checkout from your record. FINES will be charged if book is returned after the date stamped below.

104

VORTEX RING/MOVING WALL INTERACTIONS

Ву

Steven Yuehsan Liang

A THESIS

Submitted to
Michigan State University
in partial fulfillment of the requirements
for the degree of

MASTER OF SCIENCE

Department of mechanical Engineering

1984

To My Parents

ABSTRACT

VORTEX RING/MOVING WALL INTERACTIONS

By

Steven Yuehsan Liang

An experimental investigation has been performed to study the evolutions that the interactions between a vortex ring and a moving wall can have. The evolutions range from interactions in which a ring redistributes wall layer vorticity but emerges from the interaction essentially unchanged, to interactions in which the ring goes completely unstable and strong mixing effects take place. The sensitivity of the evolution to ring/wall velocity ratio, ring core diameter/wall layer thickness, and the angle of interaction is presented via stability maps. The photochromic tracer technique was used to obtain velocity profiles and boundary layer thicknesses on the moving wall. Results are compared with the turbulence production mechanism near walls.

ACKNOWLEDGEMENTS

I would like to acknowledge the Air Force Office of Scientific Research for their financial support throughout this investigation. I wish to express my appreciation to Dr. Robert E. Falco, my major professor, for his guidance and assistance throughout this research program. I would also like to thank the other members of my master committee, Dr. John F. Foss and Dr. Richard W. Bartholomew, for their time and advise. In addition, I wish to acknowledge Mr. Jim Adair for processing some of the visualization data obtained in this study. Thanks are also due Mrs. Janet Martin, Mr. Nasser Rashidnia, and Mr. C. C. Chu for their discussion, assistance, and friendship.

TABLE OF CONTENTS

			Page
LIST 0	F FI	GURES	νi
LIST 0	F TAE	BLES	ix
LIST 0	F SYN	MBOLS	x
CHAPTE	:R		
1	INTRO	DDUCTION	1
2	DESC	RIPTION OF EXPERIMENTS	6
	2.1	Experimental Apparatus	6 7 10 13
	2.2	Visualization Technique	13
	2.3	Photochromic Tracer Technique	16 16 18 18
	2.4	Data Reduction	20
		2.4.1 Acquisition of Data for Vortex Ring/Moving Wall Interactions	20
		2.4.2 Acquisition of Data for Boundary Layer Thickness	23
3	RESUL	TS	26
	3.1	Features of Different Evolutions	26 27 30
	3.2	Stability Maps	35 35

		The Boundary Layer on the WallStability Maps	
4	DISCUSSION		49
5	CONCLUSIONS		58
REFE	RENCES		6 0
FIGU	RES		62
TARL	-5		108

· LIST OF FIGURES

Figure	2	Page
2.1	Vortex Ring Generating System	63
2.2	Dimensions of Ring Generator	64
2.3	Ring Core Diameter for Various Solenoid Valve Opening Times and Head Heights of Dye Reservoir	65
2.4	Ring Core Diameter for Various Ring Speeds and Traveling Distances	66
2.5	Ring Speed for Various Solenoid Valve Opening Times and Head Heights of Dye Reservoir	67
2.6	The Onset of the Azimuthal Instability of a Traveling Vortex Ring	68
2.7	Traveling Distance for the Onset of the Azimuthal Instability of Vortex Rings of Various Reynolds Number	69
2.8	Moving Belt System	70
2.9	Test Section for Vortex Ring/Moving Wall Interactions	71
2.10	Block Diagram of the Timer	72
2.11	Laser Illumination System	73
2.12	Arrangement for Split-Field Photography	74
2.13	Background Lighting and Filter Arrangement	75
2.14	Arrangement for Photochromic Tracer Technique	76
2.15	Divergence of Laser Beam after a F-500 mm Convex Lens	77
2.16	Arrangement to Maintain the Same Ring Traveling Distance for Different Generator Angles	78

2.17	Calibration Ruler	79
2.18	An Unstable Interaction at 15 Degrees	80
2.19	A Stable Interaction at 15 Degrees	81
2.20	An Unstable Interaction at 9 Degrees	82
2.21	A Stable Interaction at 9 Degrees	83
2.22	An Unstable Interaction at 3 Degrees	84
2.23	A Stable Interaction at 3 Degrees	85
2.24	Photochromic Time Lines (1)	86
2.25	Photochromic Time Lines (2)	87
2.26	Velocity Profile in the Boundary Layer on the Moving Wall	88
2.27	Boundary Layer Thickness at $U_W=1.35\ cm/sec$	89
2.28	Boundary Layer Thickness at U_W =2.68 cm/sec	90
2.29	Boundary Layer Thickness at U_W =5.01 cm/sec	91
2.30	Boundary Layer Thickness at U_W =6.57 cm/sec	92
2.31	Boundary Layer Thickness at U_W =9.84 cm/sec	93
2.32	Boundary Layer Thickness at U_W =11.42 cm/sec	94
2.33	Boundary Layer Thickness at U_w =13.30 cm/sec	95
2.34	Boundary Layer Thickness at U_W =19.20 cm/sec	96
3.1	An Unstable Interaction at 15 Degrees	97
3.2	A Stable Interaction at 15 Degrees	98
3.3	Measurement Error Introduced by the Thickness of Trace and the Wall Surface	99
3.4	Interaction Stability under Various Conditions (15 degrees, U _r =5.50 cm/sec)	100

3.5	Interaction Stability under Various Conditions (15 Degrees, U _r =6.42 cm/sec)	101
3.6	Interaction Stability under Various Conditions (9 Degrees)	102
3.7	Interaction Stability under Various Conditions (3 Degrees)	103
3.8	Stability Map for Interaction Angle of 15 Degrees	104
3.9	Stability Map for Interaction Angle of 9 Degrees	105
3.10	Stability Map for Interaction Angle of 3 Degrees	106
3 11	Overall Stability Man	107

LIST OF TABLES

Table		
1	A Typical Set of Wall Speed Calibration Date	109
2	Initial Conditions for Figure 2.18 through 2.23	110
3	Boundary Layer Thicknesses for Various Time Durations and Wall Speeds	111

LIST OF SYMBOLS

Dr	Ring core diameter
F	Focal Length
Re_{D}	Reynolds number based on ring core diameter
t	Time
Т	Duration of wall movement
U	Velocity
Ur	Velocity of vortex ring
U _W	Velocity of wall
X	Streamwise direction
У	Height above the wall
Υ	Direction normal to the wall
Z	Transverse direction
8	Boundary layer thickness
δ99	The distance, y, of which velocity is 1% less than the
	wall velocity
ν	Kinematic viscosity

CHAPTER 1

INTRODUCTION

A series of experimental investigations have been performed to study the viscosity initiated instability of a vortex ring as it comes into contact with a moving wall. Details of the interactions were studied to gain insight into the physics associated with the various types of evolutions that occur between a vortex ring and a moving wall. Furthermore, the sensitivity of the interaction to the governing parameters was investigated. Falco (1977) has shown that the turbulence production mechanism near a wall is closely related to the formation and evolution of a localized flow module which is created in the wall region of a turbulent boundary layer as the result of the interactions of vortex-ring-like eddies with the viscous The study of vortex ring/moving wall interacsublayer. tions thus provides information to further understand the mechanism governing turbulence production near walls, which is of great importance in the transfer of momentum, heat, and energy from surfaces moving in fluids.

The fundamental features of the dynamics and kinematics of vortex rings have been described in detail by Lamb (1945), Sommerfeld (1950), Batchelor (1967), and many others. Experimental investigations have been conducted on

the behavior of vortex rings over the decades. Maxworthy (1971) used dye and hydrogen-bubble techniques to observe the evolutions of vortex rings and proposed a simplified theoretical model to explain the characteristics seen. Furthermore, flow visualization and laser-doppler measurements were used by Maxworthy (1977) to study their behavior at high Reynold number (about 10°). Flow measurement using the variation of transportation times of sound signals was performed by Borner et al (1982) to study the evolution of vortex rings with homogeneous vorticity distributions.

A number of researchers have studied vortex rings when they interacts with other objects. Linden (1972) shot vortex rings across density interfaces and studied their interactions to model the turbulent entrainment pro-Yamada et al (1980) studied the flow field produced cess. by a normally impinging vortex ring in the vicinity of a flat wall. Two smoke wires were used: one was stretched across the ring generator to visualize the vortex ring, and the other was stretched above the wall to observe the flow field near the wall. As the ring approached the plane wall, he observed that a boundary layer was formed on the wall by the flow induced by the vortex ring. the flow separated from the wall and grew into a secondary vortex ring. Meanwhile, the main ring ceased to approach the wall and moved away.

A series of studies were made by Falco (1977-1982) on evolutions of a vortex ring as it comes into contact with a flat solid surface. He used droplets of ink solution introduced into a water tank, and slugs of dye injection manifold to produce vortex released from an rings in water. The rings then interacted with a smooth surface plate inclined an angle to the ring path. He also used acoustic pulses to create smoke rings in a wind tunnel and investigated their interactions with the wall. In all of these experiments, it was observed that fluid was lifted up from the wall region and then moved around the part of the ring which first come into contact with the This lifted fluid then caused "loops" to be ejected wall. out from the back side of the ring. The ring layed down on the wall followed by a breaking up of its structure. Also studied were the effects on the interactions by polyox additive which turned out to delay the onset of the evolutions (Falco and Wiggert, 1980). Falco (1981) also investigated the interactions between a vortex ring and a moving wall, in which case close comparisons could be made with the turbulence production mechanism near walls since these experiments have taken into account the high shear region near a wall. In these experiments it was observed under certain conditions the ring could be made to interact with the wall and leave the interaction intact.

The objective of the present study is to quantify the

parameters involved in the stable/unstable interaction process. New results from this experimental investigation on vortex ring/moving wall interactions are focused on more detailed and quantitative descriptions concerning various types of evolutions, and quantitative analysis of the main factors governing the stability of the interac-All interaction experiments were performed in a water tank. A gravity driven soleniod-timer system erated vortex rings which were made to approached the wall with various shallow angles. The wall had the capability of being started implusively and moved in the direction of the ring. The scales and the traveling velocities of the vortex ring, and the speeds of the belt were highly reproducible and were calibrated before each experiment. Laser sheet/flood light were used to illuminate different fluorescent dyes for the ring and for the belt. Color separation techniques and back lighting photography were applied to acquire split-field picture data with high contrast and resolution. Different types of evolutions for the interaction between vortex ring/moving wall were stu-The critical parameters dominating the stability of the evolutions were found to be the ratio of the ring velocity to the wall velocity, the ratio of boundary layer thickness to the ring core diameter, and the angle of interaction. Using two of these variables as coordinates, data were plotted on the stability maps which showed the

sensitivities of the stability to these parameters. The photochromic tracer technique, which involved the use of an ultra violet excimer laser and an organic solvent, was applied to measure the boundary layer thicknesses and velocity distributions in the wall region and to compare these with several analytical solutions. These data concerning the behavior of the boundary layer then can be use to describe the conditions on the wall which the vortex ring enters into, and the sensitivity can be properly non-dimensionalized and shown in the stability maps.

CHAPTER 2

DESCRIPTION OF EXPERIMENTS

The experimental investigations performed during this research work were made in the Turbulence Structure Laboratory of the Department of Mechanical Engineering. The first step was to qualitatively study and categorize different types of vortex ring/moving wall interaction using visualization techniques. The second step was to find the important parameters which governed the stability of the interactions, and to quantitatively map out the relationship between the stability and these parameters. The third step was to measure the boundary layer thickness on the moving wall, which is one of the dominating parameby means of photochromic tracer technique. Results of the third step were then input to the second step in mapping out the dependence of interaction stabilities upon the boundary layer thicknesses. Experimental devices and data acquisition processes are discussed in this chapter.

2.1 Experimental Apparatus

Experiments were performed in two tanks of the same size: 40.5 cm by 32.4 cm by 243.8 cm. One was filled with water and the other with kerosene. The experimental

aparatus in the water tank included a vortex-ring generating device, a moving belt, a triggering timer, and visualization settings. The kerosene tank had in it a moving belt, a motor-timer device, and the facilities for the photochromic tracer technique.

2.1.1 Ring Generating System

Vortex rings were generated by the system shown in figure 2.1. The constant head reservoir (6) was filled with a mixture of 10 ppm fluorescent Sodium Salt Sigma No.F-6377 green dye and water solution. As the solenoid valve (2) opened, a slug of dyed fluid was released from the generator (1) by head pressure of the dye reservoir and rolled up into a vortex-ring.

The ring generator (1) had the dimensions shown in figure 2.2. It was made of lucite and the portion of the supply line (4) that was submerged in the water was made of aluminum (refer to figure 2.1). The high thermal conductivity of aluminum equalized the temperatures of the water in the tank and that of dyed water in the supply line of the ring generator so that the buoyancy effects were not introduced. A loop of clear plastic tubing was mounted between the solenoid valve and the aluminum pipe. There were two reasons for doing this: the first was that when the solenoid valve suddenly opened, a non-axial

vibration was created by the mechanical motion and this vibration was absorbed by the plastic loop without being transmitted to the ring generator which would perturb the vortex ring. The second reason was to allow us to see air bubbles. Air bubbles in the piping system would compress during the solenoid cycle, and we found that the rings created with air bubbles present were not as stable as those created with no air in the system. Putting a section of clear tubing in the highest position enabled us to visualize if the tube was free of air bubbles. If it was not, bubbles could be released from the valve (5).

The diameter of the ring generated depended upon both the opening duration time of the solenoid valve and height of the dye reservoir for a fixed orifice. Figure 2.3 shows the variations of ring diameter with valve opening time and head height of dye reservoir. The ring diameter defined as the diameter of the dyed ring core as seen was in the laser sheet (see figure 2.4). Measurements were taken 10 cm downstream of the ring generator, which corresponds to 4.5 ring diameters. T. Maxworthy (1972) observed that as the vortex ring proceeded downstream, fluid from ambient would be entrained into the back of the ring and the ring would become larger in size and slower in speed. In this study, the variation in ring diameters during the first several diameters of traveling distance was less than the error in our measurements. Figure 2.4

gives the ring diameters in different downstream positions and shows that it was almost a constant up to at least a traveling distance of ten ring generator diameters for each specified ring speed. Vortex-ring/wall interactions were always made to occur before 17.2 cm downstream in our study. This corresponds to a traveling distance/ring generator diameter of 7.5; therefore, it was quite reasonable to assume that the initial diameters of the rings entering into the interaction with the wall were constant.

The speed of the ring was also dependent on the head height of dye reservoir and solenoid opening time. Figure 2.5 shows a linear relationship between ring speed and valve opening time. The measured velocities were the averaged values during the first 15 cm downstream of the generator.

Different evolutions of vortex rings with concentrated vorticity were observed while the ring moved downstream without being perturbed by outer flow field. Within the first several ring diameters of traveling distance after the ring was released from the generator, the ring was coherent and remained the same oblate spheroid shape with well defined dyed boundary until it reached a certain position where an azimuthal waviness suddenly took place. The ring kept moving on with this wavy structure for a very short distance and then it went unstable completely and lost its vorticity concentration by turbulent diffu-

sion. Figures 2.6.a through 2.6.d show a series of evolutions of such a traveling ring with a Reynolds number of 1000 based on the ring diameter and the velocity of travel. Sometimes, a new ring was observed to emerge from this disorganized vorticity field. This newly formed vortex ring had a larger diameter and it moved slower than the original one did.

Figure 2.7 shows the effect of Reynolds number on the distance the rings travel before the onset of the wavy instability. In our study of the interaction between a vortex ring and a moving wall, we wanted to limit our investigation to initially stable rings impinging on the wall. So, we created rings with low Reynolds Number of about 400, This was combined with a limitation of about 17 cm traveling distance, which was short enough to keep the ring from going unstable while maintaines a constant size.

In this study, the constant head height of reservoir, the fairly accurate timer-solenoid valve, and devices to avoid compressible air and mechanical vibrations allow us to minimize the experimental perturbations, and to reproduce vortex rings with fairly close initial conditions.

2.1.2 Moving Belt

The "wall" upon which the vortex rings interacted with was actually a moving belt made of clear transparent

plastic which had a smooth surface. The two ends of the belt were joined together to form a loop, which circulated around two rollers as shown in figure 2.8.

The tension on the belt had to be high enough to prevent slipping between the belt and the rollers. The tension across the width of the belt was maintained constant so that the belt did not move laterally. The belt had a width of 25 cm and the test section was at 48 cm downstream from one of the rollers. This width/length ratio was sufficient to prevent the disturbances generated in the corners from reaching the center of the belt at the test section (this hypothesis was later confirmed using photochromic tracer technique). Therefore, the boundary layer flow on the moving belt could be considered two-dimensional.

One of the rollers was driven by an Dayton C25A512 1/100 HP DC motor controlled by a 0-50 VDC 1.5 A potentiometer. The speed of the belt was adjustable within the range from 1.5 cm/sec to 14cm/sec. The most important feature of the belt-motor device was that the belt reached a constant speed very soon (with a second) after power was turned on. This "hard-start" character allowed us to consider the belt to be impulsively started and to keep constant the velocity ratios between a ring and the belt during interactions of short delay time.

The ring generator was placed at various positions

above the belt. The ring moved in the direction of the belt movement with an angle of inclination between the initial line of flight of the ring and the belt. The test section was bounded by the generator at the upstream to 50 cm downstream. The height and the angle between the axis of the generator and the wall were all adjustable. Figure 2.8 shows the configuration of this set-up.

Since the azimuthal instability of the ring was critically dependent on the traveling distance of the ring, we kept the distance a constant, 17cm, in experiments with various angles of inclination by changing the height of the ring generator. The heights, measured from the center of generator to the belt surface, were 6.23 cm for the angle of 15°, 4.51 cm for 9°, and 2.73 cm for 3°.

As the belt moved, a boundary layer built up on the belt. A mixture of 2.5 ppm Rhodamime 6G fluorescent red dye and red food coloring was used to mark the boundary layer for visualization. A dye injecting pipe (refer to figure 2.9) was placed at the edge of the belt. An array of small holes, each with diameter of about 0.5 mm, were drilled along the pipe with spacing of 1 mm between each hole. When the valve (1) was opened and the belt was running, the dye in the reservoir would be ejected from these holes and attach to the belt to function as a boundary layer tracer. The orientation of the pipe and these holes were so arranged that the dye came out in a tangential

direction to the movement of the belt.

2.1.3 Timer

The opening duration time of the solenoid valve and the time delay between the onset of belt movement and release of the ring were all controlled by a 115 VAC/60 HZ timer which was designed and fabricated by R. Matthews from the College of Engineering. The timer had two working modes: In the first mode, the belt motor turned on, then the solenoid was triggered after a chosen delay time and it remained on for a specified valve opening time. In the second mode, the solenoid triggered first, then the belt motor turned on after a specified delay.

The valve opening time was accurate to 1/100 second and the delay accurate to 1/10 second. The diagram of the timer device is shown in figure 2.10.

2.2 Visualization Technique

Visual data were collected using both a videocasette recorder and a motion picture camera. The former was used to go through a wide range of experiments with different initial parameters and the latter was used to record several typical interactions and to study the fine datails involved.

A laser beam emitted from an 8 w Coherent CR-8 Super-graphite Argon Ion Laser was directed to 10 cm above the water tank. After being focussed down by a convex lens, it reached a cylindrical mirror which spreaded the beam into a light sheet. The sheet was perpendicular to the belt and was in the streamwise direction, as shown in figure 2.11.

The laser sheet covered the section from the ring generator to 30 cm downstream of the generator. Since only the portion of dye that was irradiated by the laser sheet was fluorescent, the vortex ring appeared as two roughly circular vortex cores rotating in the opposite directions as when viesed the tank from the side.

In order to record both the ring evolution in the laser sheet and the "footprint" of the interactions in the dye marked wall region simultaneously, we took split-field pictures containing both the side view and plan view. As shown in figure 2.12, one mirror was placed above the tank approximately 45° to the plane of the belt reflecting the plan view of the belt. Two additional mirrors were arranged to obtain the side view. The mirrors were positioned such that the distances from the camera to test section were the same for both views, thus the side and plan views were both in focus in the pictures. All mirrors were front-coated enhanced aluminum to avoid second surface images in the pictures.

Color separation technique was used to enable details of the differently dyed motions to be simultaneously photographed using the split field technique. The wall layer was dyed red, the ring was green, and the lighting from the back as well as from the bottom of the water tank were filtered with deep blue glass. Any two colors of red, blue and green are the components of the complementary color of the third one. For instance, the red and the green are components of the yellow which is the complementary color of the blue.

The blue has a power spectral distribution concentrated at short wave lengths; for the green, at intermediate wave lengths; for the red, at long wavelengths. The separation in the power spectral distributions allows us to distinguish between each color on the visualization data very easily.

Figure 2.13 showed how the pieces of filtering glass were arranged, and that a piece of white opaque glass was also used to diffuse the point light sources into uniform background lighting. Red lights coming down from the top of the tank were used to illuminate the red boundary layer dye on the belt.

The video camera system used to record the experiments were a Sony videocasette recorder, a JVC CV-0001 color video camera with F2.0/17-102 zoom lens, and Batamax video tapes.

A series of motion pictures were taken with a Photo-Sonics 35 mm motion picture camera and a 135 mm lens using a aperture of F/2.0. Filming speed was 120 frames/second and camera shutter opening angle was 144° which corresponded to a shutter speed of 1/500 sec. Films used were Eastman Kodak High Speed 5293 and 5294.

2.3 Photochromic Tracer Technique

2.3.1 Introduction

The theoretical thickness of boundary layer on a moving belt with finite length is very diffucult to obtain since the secondary flow effect and leading edge effect will begin to become important after the belt starts to move for some time. Experimentally, dyes or bubbles can be added to the fluid flow to mark the streamlines and indicate the velocity field. However, the marking materials injected into the flow can not have exactly the same properties as the fluid and the submerged solid bodies such as injection tubes or electrode wires in the fluid will disturb the flow stream. When these facts were combined with the difficulty of using the techniques near a moving surface, we employed a new technique which allowed us to measure the properties of the boundary layer without

disturbing the flow field.

To measure the boundary layer thicknesses, the photo-chromic tracer technique was applied in this study. Advantages of the technique were its non-disturbing property, its simplicity in application, and the fact that quantitative analysis can be easily performed from visualization data. The disadvantage was that the technique cannot be applied to experiments performed in water, the medium used for all other aspects of this investigation. Thus, knowledge concerning the dependence of boundary layer thickness on fluid properties was required to convert the results obtained.

Photochromism is attributed to atoms or molecules that are stable or metastable in two states which possess different molecular or electronic configurations. Certain external excitations can cause the atoms to shift between the two states. Popovich and Hummel (1967) first utilized this fact in an experiment in which such a chemical was disolved in a liquid and discolored under the irradiation light. Later researchers have used the technique in of measuring liquid flows whose velocity fields were difficult to obtain in other ways. In this study, the moving belt was submerged in kerosene with a photochromic chemical additive. An ultra violet laser was used to irradiate this organic solvent and to create colored time lines which marked the velocity profiles in the boundary layer on the belt. Pictures were taken to record these profiles. As the laser beam stopped flashing, the reverse reaction started to occur and dyed time lines faded away gradually. The details of the experimental apparatus are given below.

2.3.2 Ultra Violet Light Source

A Tachisto 800 XR excimer ultra violet laser was used with a gas lasing medium of XeF. The laser beam had a wavelength of 351 nm, a pulse duration of 20 nsec, and divergence of 6 mrad half angle. Maximum energy was 200 mJ/pulse and repetition rate was adjustable from 0.01 to 200 Hz. The beam had a size of 3.175 mm by 20 mm measured at the exit.

2.3.3 Test Fluid

Odorless kerosene (Shell-Sol 715) was used as the solvent. 4.3 ppm of the photochromic indicator 1,3,3-Trimethyl-8-Nitrospiro

(2H-1-Benzppyran-2,2-Indoline) was disolved in the solvent. Because the solvent was corrosive to Silicone rubber, the tank containing kerosene was sealed with Silastic 730RTV fluoresilicone sealant which was organic-solvent resistant.

When the laser pulses, a dark blue trace line was formed in the kerosene. Properties of the trace depend upon the laser energy and the concentrations of photochromic chemicals. Higher laser intensity results in a longer trace length and a darker trace color. Higher indicator concentration results in a shorter trace length, a longer trace life time, and also a darker trace color.

Since the test fluid had a low electrical conductivity, the electrostatic charging phenomenon due to the movement of the belt may possibly allow a discharging spark to cause an explosion of the fluid. To avoid this danger, an anti-static agent, 5 ppm Shell-Sol 71, was added to the kerosene to increase the conductivity of the fluid. The adding of the anti-static agent also increases the polarity of the test fluid and thus the equilibrium between the two molecular states was shifted toward the colored side. Therefore, the life time of traces increases with the concentration of the anti-static agent.

2.3.4 Optics and Illuminations and Photography

The experimental set-up is shown in figure 2.14. The convex lens (1) was a fused Silica lens, 38.2 mm in diameter, 500 mm in focal length, 5 mm in thickness, and with a transmission higher than 90% at 351 nm wavelength. The lens thinned the laser beam down to 0.32 mm (on the camera

side) at the focus, which was 1.5 cm above the belt. The divergence characters of the beam are shown in figure 2.15.

Mirror (2) was 50.8 mm in diameter, 9.53 mm in thickness and a reflecting surface of harden E-beam deposited dielectric coating, with a reflectance greater than 99% at 351 nm wavelength and 45° incident angle. The mirror was held by a mirror mount with the plane independently adjustable about both x and y axes with a resolution of 1 arc second.

A piece of yellow cellophane was put behind the tank as a background. The test section was illuminated by the lights from the front. Pictures were taken with a Nikon FM2 35 mm camera with a 55 mm f/2.8 microlens. The shutter speed used was 1/500 sec and the aperture was F/8. The films used were ISO 400 B/W Kodak Tri-X pan.

2.4 Data Reduction

2.4.1 Acquisition of Data for Vortex Ring/Wall Interactions

The interactions with different geometric configurations and initial conditions were first recorded as motion pictures. The first step of each experiment was to calibrate the speed of the moving belt. Because the chain, gears, bearings and other metal part of the belt system submerged in the water would be corrupted over a period of time between experiments, the belt speed could vary each time. Calibrations of belt speed were performed by measuring the time required for a specified point on the belt to move a distance of about 75 cm for a certain dial setting on the potentiometer. The speeds were calculated and a relationship between the settings on the potentiometer and the belt speed was established. A typical set of numbers is shown in table 1. Standard deviations of each measurement were always below 0.45 cm/sec.

Since the onset of the azimuthal instablity of vortex ring was dependent on the distance the ring had gone through as well as its speed. A major consideration in choosing the position of the ring generator was that the distance the ring had covered before the interaction occurred had to be less than the critical distance for the onset of the instability, and the same for different geometric configurations. Figure 2.16 shows three configurations with interaction angles of 3°, 9° and 15°. Assuming the ring path was a straight line, we could have the same traveling distance of 17 cm, which was shorter than the unstable distance in all three experiments.

To properly register the camera and split field mirror system, two pieces of plexiglass, one horizontal and the other vertical, were joined together as shown in figure 2.17. The plexiglass had tick marks on it and was placed on the still belt to function as a calibration ruler. This ruler was helpful in measuring the scales on the picture, in checking if the camera was looking straight into the side and down to the plane, and in checking if the two views were lined up with each other.

Motion picture data were then taken for different conditions. Six series of interactions are shown in figures 2.18 through 2.23. Initial conditions are listed in table 2. The delay time was defined as the time between the start of the belt and the release of the vortex ring.

The high resolution of motion picture data enabled us to get the detailed information on the vortex ring/moving wall interactions. However, the time required for the films to be processed and for results to be fed back to choose new conditions for another experiment was much too long to allow us to cover the parameters that determined the wide range of evolutions observed. In order to solve this problem, the video camera-recorder system was used. The disadvantages of using video recorder were its resolution, distortion and instability of pictures. therefore limited qualitative observations. to Experimental data were taken by video recorder over a wide range of initial parameters. Based on these data, stability maps were plotted. These are discussed in Chapter 3.

2.4.2 Acquisition of Data for Boundary Layer Thickness

A tank was filled with Shell-Sol 715 (kerosene) solution described in section 2.3.3. The distance from the surface of solution to the surface of the moving belt was 10 cm, which was significantly greater than the boundary layer thickness approximately evaluated from Stokes' equation for an implusively started plate: $3.64\sqrt{\nu t}$, and was shorter than the trace length obtained from using an ultra violet laser with the energy of 115 mJ/pulse and an indicator concentration of 4.3 ppm, The irradiated trace can therefore penetrate all the way down to the belt.

To measure the layer thickness at T second after the belt started to move with a speed of V, we impulsively started the belt, pulsed the UV laser at a short time (about 1/2 to 1 sec) before T sec was reached and continued to flash the laser till time T when a picture was taken. Figures 2.24.a through 2.24.d show the data taken at T=8, 12, 16, and 20 sec respectively. The laser was pulsing at a frequency of 2 Hz. The laser beam came from the top and the black area on the bottom was the belt moving from right to left at a speed of 1.35 cm/sec. Figures 2.25.a through 2.25.d shows the series at T=220, 220, 230, and 240 sec and V=2.68 cm/sec.

The belt velocity was obtained by measuring the spacing between the intersections of any two traces with the belt and multiply it with the frequency of laser pulsestraces with the belt and multiplying it with the frequency of laser pluses. The laser frequency was re-checked with an oscilloscope while experiments were in process and was shown to be stable and accurate. The traces themselves had thicknesses of 0.35 mm, which introduced some errors in the measurements. For instance, if the spacing between intersections of traces with the belt was 6 mm, the error introduced by the thickness of the trace in measuring the belt speed would be 5.8%. The fact that the belt speed was constant can be checked by the data in each picture, which shows that all the traces are equally spaced where they intersect with the belt.

The velocity profile was obtained as follows: measuring the spacing between two points of the line pair most recently created at a certain height above the belt, then multiplying it with the laser frequency gave us the velocity at that particular height. Following the procedure for different heights and plotting out the velocity field gave the velocity profile at that specified time T sec. Figure 2.26 shows a typical velocity profile on the moving belt at V=1.35 cm/second and T=10 sec. The velocities were measured at 7 different heights.

Since the velocity measurements had errors greater than 1% which is the deviation between layer edge velocity and free stream velocity in the definition of δ_{99} , in this study, the edge of boundary layer was simply defined

as the point where two adjacent lines can not be distinguished. Boundary layer thicknesses were measured for different belt speeds ranging from 1.35 cm/sec to 19.2 cm/sec and at different time durations for each speed. Table 3 list the thickness data under different conditions. Figures 2.27 through 2.33 show the relationship between the thickness and time duration for various belt speeds.

CHAPTER 3

RESULTS

With different geometric configurations and initial conditions, interactions between an impinging vortex ring and a moving wall can have various types of evolution. In our investigations, most of the evolutions were found to fall into two major categories, namely the stable interaction and the unstable interaction. In this chapter, features characterizing each type of evolution are studied in detail. Critical parameters governing the stability of interaction are found to be the angle of interaction, the velocity ratio between the ring and the wall, and the boundary layer thickness. The dependences of the stability upon these governing parameters are quantatively described through stability maps.

3.1 Features of Different Evolutions

Motion picture data were qualitatively analyzed over various initial parameters, which include height and inclination angle of the ring generator, ring speed, belt speed, and delay time. Two typical series of evolutions are shown in figures 2.18 and 2.19: details are discussed in the following sections.

3.1.1 Unstable Interaction

The series shown in pictures 3.1 was an experiment run with the ring generator angle of 15°, the speed ratio of ring to belt of 0.8, and a delay time of 10 sec. The wall was moving from left to right at the bottom of the side view, in which the impinging vortex ring appeared as two lobes in the laser sheet. The interaction is divided into four continuous stages each possessing distinguishable features.

Before the interaction occurs, wall layer marking lines were seen from the plan view to be straight and equally spaced. The two lobes of the vortex ring were of the same sizes and were both coherent.

The first stage of evolution started when the ring's stagnation point reached a height of about two ring core diameters above the wall. The wall layer marker was moved laterally (i.e. Z direction) away from the center of the interaction region. In the mean time, marker at the downstream end (+X direction) of the ring was gathered together. Viewing from the side view, we observed no Y-directional motion of the wall fluid up to this point.

During stage two, marker on the wall was pushed sideways from the center. The curled marking lines formed into two clear boundaries of this interaction region with the shape of a "pocket" (This terminology is given based on the similarities between this structure and the pocket structure observed in the viscous sublayer of a turbulent boundary layer, which is to be discussed in Chapter 4). This pocket pattern grew in size as it was convected downstream. In the mean time, marking lines gathered together at the downstream end of the ring were seen to be lifted up from the wall. This rising fluid was coherent at this point and had a vorticity with the opposite sign of the mean flow. The impinging vortex ring at this moment was still quite stable with clear spiral structures in both lobes.

During the third stage, the scale of the pocket pattern grew to about three times the ring core diameter. Other visualization records, like the one shown in figure 3.1, indicated that there was fluid rising from the wall It had a vortex sign the same as the mean shear (+Z) and it occurred at the upstream end of the pocket and quickly went back to the wall. However, this rising fluid is not clearly seen in this series shown in figure 2.18. On the other hand, the lifted wall fluid at the downstream side of the interaction went higher and then a large fraction of it was ingested into the lower lobe of the ring which came close to the wall. The lower lobe was observed to become smaller in size and the vorticity contained in was stretched and amplified during the ingesting pro-The ingested fluid went upstream to a position close to the ring's stagnation point and broke down into two parts: one which went down to the wall and the other which went up into the top lobe of the ring. Both movements were Y-directional and Z-directional. The fraction of the lifted fluid at the downstream that was not ingested into the ring stayed at a certain height and also broke down into two parts: one on the right and other on the left (as seen in the plan view). The two parts were then moving away from each other. At the downstream end of the pocket, wall layer marking lines were pushed away from the center and thus a "secondary pocket" formed. It was narrower in shape and smaller in size than the main one. In the mean while, the upstream boundary of the main pocket started to be diffused and to lose its coherence.

During the last stage (stage five), the lower lobe of the vortex ring was highly stretched and intensified while the upper ring lobe was seen to show the onset of in its structure. More of the lifted wall bility dye, "ejected" from the wall region, got into the upper lobe and broke up into smaller and smaller scale motions with an extremely strong mixing effect. Part of the rising fluid which origionally did not get ingested by the ring kept risinging slowly to a height lower than the mixed fluid, and it stayed somewhat coherent without breaking up. It showed little evidence of fine scale mix-The upstream boundary of the main pocket was ing. diffused and difficult to define. Because of the velocity gradient across the wall region, the secondary pocket now took over the relative position of the main pocket with respect to the mixed fluid. It grew in scale and gradually diffused away and brought an end to the sequence of this interaction.

3.1.2 Stable Interaction

Figure 2.19 shows another type of evolution with a ring generator angle of 15°, a speed ratio (ring to belt) of 0.5, and a delay time of 10 cm/sec. That is, the initial parameters were the same as the previously described experiment except for the lower speed ratio. The present interaction is also divided into four stages as discussed below.

During the first stage, the wall layer marking lines on the center laser sheet were not observed to move laterally. However, lines that were originally out of the center laser sheet (up to three ring diameters away as seen in the plan view) were bent toward the center and joined with traces from the other side at the downstream end of the in-coming ring (refer to figure 2.19.a). Wall fluid at this joining spot then was lifted up and away from the wall. The ring was coherent and its spiral structure was clearly seen.

During the second stage, the wall layer marker in the

center of the interaction region started to be pushed sideways. A pocket of marker-free fluid began to show up in the wall region. The upstream boundary of this pocket was recognizable, while the downstream boundary was extremely clear. The lifted wall fluid then split into right and left moving parts with respect to the center laser sheet and they kept moving away from the center and going up higher away from the wall. The ring kept coming closer to the wall without losing its stability. The vortex stretching phenomenum which would decrease the size of the lower lobe, was not apparent.

During the third stage, the ring changed its direction of flight and moved away from the wall. Its basic structure and coherence stayed unchanged. The lifted fluid at the downstream end of the pocket was not ingested into the ring, and it moved to two sides. The scale of pocket pattern became larger and its front boundaries started to be diffused. No secondary pocket was observed and no wall fluid dye was ever ingested into the ring.

At the final stage, the ring left the wall region essentially intact. The instability described above was never initiated. The lifted wall fluid which was left behind by the ring remained at a certain height above the belt and was observed to undergo some additional weak evolution. Boundaries of the pocket became diffused and undefinable.

In general, the possible evolutions that vortex ring/moving wall interactions can have include:

- (1) the interaction in which the entire ring as well as the wall fluid that interacted with the ring become completely unstable and a strong mixing effect occurs.
- (2) the interaction in which the lifted wall fluid is ingested into the vortex ring before the ring changes its direction of flight, the lower lobe of ring breaks up and the upper lobe stays coherent while the ring leaves the wall region. This kind of evolution gives one the impression that a single vortex is rising up from the wall.
- (3) the lifted wall fluid is not ingested, but is rolled up into a "hairpin" which may undergo secondary distortions. The vortex ring remains coherent throught the interaction.
- (4) the lifted wall fulid is not ingested and does not get far from the wall region, and does not break up into smaller scale motions after the interaction. The vortex ring maintains the same coherent structure throughout the interaction.

The two interactions studied above can be categorized as the first and the third types respectively. However, the first and the second types can be further incorporated into one type, called the unstable interactions while the third and the fourth are united as the stable interactions. The evolutions in both interactions,

stable and unstable, have some features in common: wall layer vorticity is all redistributed in ways that result in wall fluid being lifted up by the induction of the external vorticity field of the ring which interacts with the boundary layer, and pocket patterns are created in each case as the marks or footprints of the interactions between a vortex ring and wall.

Characteristics differentiating the two different types of interaction are as follows:

- 1. The vortex rings, which are initially coherent, will become completely distorted and unstable after the first type of interaction, but they will maintain their initial structure and stability throughout the second type of interaction.
- 2. In an unstable interaction, the secondary pocket structure with well-defined boundaries is created behind the main pocket which has a larger scale and occurs earlier. However, in a stable interaction, only the main pocket forms; the secondary structure is missing.
- 3. Whether the rising wall fluid can be ingested into the ring or not depends on the type of interaction that occurs. In an unstable interaction, the ingestion occurs and the wall fluid acquires a vortex whose sign is opposite to the mean shear layer. In a stable interaction, lifted fluid does not get into the ring. It moves downstream towards the wall and has the appearance of a

Theordosen hairpin vortex with the same sign as the mean flow.

- 4. Fine scale motions and strong mixing effects characterize the last stage in an unstable interaction. But in a stable interaction, the rising wall fluid does not lose its coherence completely. The ring stays laminar throughout the whole evolution, and no severe mixing ever happens.
- 5. The height above wall, that the lifted wall fluid can reach, varies with different types of interaction. At the final stage of an unstable interaction, the wall layer fluid, mixed with the disorganized vortex ring, is convected from the wall region to at least four ring core diameters above the wall. In a stable interaction, the lifted wall fluid does not go any higher than one to two ring diameters above the wall.
- 6. The scales and the shapes of pocket structures are different in the two types of interaction. In stable interactions under various conditions, the streamwise dimensions of the pocket pattern are 1 to 1.9 times the spanwise dimensions, and it ranges from 3.5 to 6.4 times the ring core diameter. In unstable interactions, the streamwise dimensions are somewhat shorter than the spanwise one. The ratio is between 0.8 and 1.0. Besides, the whole scale of the structures are smaller than those observed in stable interactions. The ratios of the

streamwise dimension to ring diameter were between 2.0 and 3.5.

3.2 Stability Maps

3.2.1 Governing Parameters

Vortex ring/moving wall interactions can have evolutions which are either stable or unstable as discussed before. However, in order to precisely distinguish the two types of evolution, we need a solid definition to verify the stability of interactions. Some of the features observed during the interactions could be chosen to characterize different evolutions. For example, does the lift-up at the downstream end of the interaction get ingested into ring? If yes, does this ingestion occur before the ring changes direction and moves away from the wall region? If no, does the lifted wall fluid break up later? Does the lower lobe, or the upper lobe, or both the lobes of the vortex ring become unstable? In this study, interactions were divided into two types, namely the stable interaction and the unstable interaction. The second question mentioned above was chosen to be the basis of a criterion which defined the stability of the interac-In other words, if a vortex ring coming towards a tions.

wall ingests wall fluid into its vortex field before it changes its path of flight to an upwards direction, the interaction is defined as unstable; if the ring ingests wall fluid after its path of flight changes to an upward direction, or the ingestion never occurs, the interaction is defined to be stable.

Based on this definition, data which was collected with a viedorecorder system for interactions which occurred over a wide range of initial conditions. These were classified into two categories, and the parameters that effect the evolutions of interactions were studied. The thickness of the boundary layer on the moving wall, the speed ratio between the ring and the moving wall, and the angle of interactions are found to be the dominating factors for the vortex ring/moving wall interactions.

According to the Stokes' solution for the boundary layer flow on an infinitely long plate in motion, the boundary layer thickness & is proportional to the square root of the time interval T. To investigate the dependence of the interactions upon the wall layer thickness, experiments were performed with delay times ranging from 0 to 150 seconds (defined as the time duration between when the wall is started and the ring is released) while other parameters were kept constant. The upper limit of delay time in this study came from the fact that a thick boundary layer would interact with the ring gen-

erator and bring about a wake flow downstream of the ring generator thus disturbing the flow field.

Results indicated that with a thicker boundary layer on the moving belt, the interaction was more stable. In other words, with less vorticity concentrated near the wall, it is more likely that the lift-ups of the wall layer fluid are not ingested into the ring. In this case the pocket structure created on the wall are of larger scales, and the vorticity distribution within the impinging vortex ring is not drastically rearranged.

The importance of the speed of the ring was first studied using two different ring velocities, 5.50 cm/sec and 6.42 cm/sec respectively, while all other conditions were kept the same. Figure 3.4 and Figure 3.5 showed the data of experiments. The stability map using wall layer thicknesses as the ordinates is shown in figure 3.8. data for the two different ring speeds fall onto the same curve, which suggested that the absolute velocity of the ring was not an important factor to the stability of interactions. However, by performing the experiments over a wide range of conditions, we found that the velocity ratio of ring to belt, which is physically the convective velocity of the ring compared with the mean flow, was one the critical parameters. With higher convective velocities of the ring, and the same amount of circulation being put into the wall region, we observed greater

effects in perturbing the vorticity field near the wall.

Results showed that the effect of an shallower angle is to shift the evolutions toward the stable Qualitative descriptions concerning the amount of shifting are given in section 3.2.3 where the stability maps are presented. Differences in evolution resulting variations in interaction angles were observed to be the following: (1) In unstable cases with shallower angles, the diameter of the ring became smaller before going unstable and the vorticity contained in it was stretched and intensified more drastically than those with larger interaction angles. Since vortex stretching is three-dimensional phenomenon, it suggested that three-dimensional effects were more important in interaction with a smaller angle. (2) With a shallower angle, the lift-ups of wall fluid occurred at the ends of two side-boundaries of the pocket pattern rather than at the downstream center. (3) With shallower angles, trajectory of the impinging ring was flatter and longer in the wall region than those with larger interaction angles. With shallower angles, the streamwise dimensions of the pockets were closer to the spanwise dimensions, thus the pockets themselves possessed more roundish shapes than those under larger interaction angles. Interactions with shallower angles are shown in figures 2.20 through 2.23 with angles of 9° and 3° respectively.

3.2.2 The Boundary Layer on the Wall

The boundary layer building up on the moving wall was investigated because of the important role it played in the evolution of interactions between a wall and an incoming vortex ring. The velocity distributions in the wall region and the thicknesses of boundary layer were measured photochromic tracer technique. using Figures 2.24.a through 2.24.d show a sequence of experiments with a belt speed of 1.35 cm/sec and durations of belt movement of 8 sec, 12 sec, 16 sec, and 20 sec respectively. 2.25.a through 2.25.d show the series with a belt speed of 2.68 cm/sec, and for durations of 210 sec, 220 sec, 230 sec, and 240 sec. The black region at the bottom of each picture is the belt which was moving from right to left. Time lines were created by pulsing ultra violet laser at a frequency of 2 Hz. As we measure the distance between each time line, the error introduced by the thickness of lines is about 3 to 5% at the belt surface when picture data was projected on an NAC KS-1870 film motion analyzer which enlarges a 35mm frame to a 17.7 cm by 38.4 cm pic-This error can be reduced by using a smaller laser pulsing frequency which leads to wider spacings between However, the velocity obtained with a smaller lines. laser frequency would be an averaged value over a larger window size, thus we lose the capability to measure the instantaneous velocity distribution in the wall region.

The belt surface was seen as a line from the camera being placed in front of the kerosene tank. The portion of belt that was closer to the camera was out of focus and thus blurred the surface line to some extent. The error associated with it is approximately 0.02 cm in measuring the boundary layer thicknesses which is in the order of 1% at a layer thicknesses of 3 cm. A sketch of the error associated with the thicknesses of trace and belt is shown in figure 3.3.

The distances between every two adjacent end points of traces on the belt were measured over the whole range of duration times. The variations did not exceed 3% which was not more than the error introduced by the trace thickness itself. Thus, the belt speed can be considered constant throughout the experiments.

The tracers all stayed in the y-x plane and no lateral motion was observed to occur in the test section. This indicated that the disturbances originating at the two edges of the belt had no effect on the flow at the belt center over the portion in which the interaction occurred. Thus the boundary layer was two-dimensional.

Figure 2.26 shows a velocity profile in the boundary layer at a belt speed of 1.35 cm/sec and the delay time of 10 sec, using measured data points at 7 different heights. The thicknesses of the traces result in the error in velocity measurement, and both the baseline thickness and the

trace thickness result in the error in height measurement. The velocity distribution calculated from the Stokes' solution is also plotted for comparison. It shows that the experimental velocity distribution agrees well with the analytical solution for the velocity profile in a boundary layer on a wall impulsively set to motion. This conclusion confirms our design expectations since the test section is 48 cm down stream of the belt leading edge and 10 sec is too short a time for the information from the leading edge to be convected to the test section.

We attempted to define the boundary layer thickness 8. as the positon where the velocity decayed to 1% of the wall speed. In this experiment the measured velocities at various heights have errors greater than 1% of the velocity. Because of this error, we chose to define the edge of boundary layer to be located at the point where two adjacent lines can not be distinguished from each other. belt speeds between 1.35 cm/sec to 19.2 cm/sec, boundary layer thicknesses were measured for durations of movement ranging from 0 sec to 150 sec. But, for belt speeds higher than 9.84 cm/sec, inflectional trace lines were observed in the boundary layer after a duration of 50 sec. This indicated that there existed a secondary flow field moving in the same direction as the boundary layer flow. The inflectional zone resulting from the secondary flow hindered us from measuring $\delta_{s,s}$ accurately, thus the data were taken up to the durations of 30 sec to 50 sec over that high belt speed range.

Theoretically, the boundary layer thickness is equal to $3.64\sqrt{\nu t}$ for an infinitely long plate moving in still ambient fluid (Stokes' flow), while the layer thickness equals to $4.6\sqrt{\frac{\nu x}{U_w}}$ for flow over a flat plate with a leading edge (Blasius' flow). In this study, by dividing the wall layer thickness measured in the kerosene solution by the square root of kinematic viscosity ratio of kerosene to water, we converted the measured thickness into the thickness in water under various conditions. The growth of boundary layer thickness with respect to time at various belt speed was shown in figures 2.27 through figure 2.33. Results are comparied with analytical solutions of both Stokes' flow and Blasius'flow.

Results allowed us to measure the growth of vortical region from the vicinity of the wall after the movement of the belt was initiated. However, after t=40 to 50 seconds, the vorticity stop diffusing with time, the boundary layer reached a fully-developed steady-state condition, and the thickness stayed at a constant value throughout the remainder of the experiment.

In a Stokes' flow, the vortical layer would continue to diffuse outwards as time goes on, and would never come to steady-state equilibrium. In this study, the effect of the leading edge was convected downstream to the test section and resulted in the fact that the experimental thicknesses are less than those of the Stoke's flow and eventually approach a fully-developed, thev time-independent status which qualitatively resembles the behavior of Blasius' boundary layer. However, the strong velocity-dependence of boundary thicknesses in a Blasius' flow is not observed in the experimental data. This character may be due to the round shape of the leading edge instead of a sharp one assumed in the exact solution, the local curvature near the edge, and presence of the boundary layer dye injector.

These phenominun suggest that after the boundary layer is fully developed, the evolutions of vortex ring/moving wall interaction become independent of the delay time of the belt movement.

3.2.3 Stability Maps

To qualitatively describe the sensitivity of the evolution to the three parameters discussed in section 3.2.1, we first construct the stability map with speed ratio of ring to belt as the abscissa and the delay time as the coordinate. All the data collected were then plotted onto the maps for different angles, figure 3.5 through 3.7, which show the maps of angles for 15°, 9°, and 3° respectively. On each map, there are two regions: one on the

right and one on the left. The interactions which occur when their initial parameters fall in the left region will have stable evolutions, while those with parameters located in the right region will have unstable evolutions. The two regions are separated by a rather smooth band which has the shape of an increasing function.

The points farther away from the band have more clear features of either the stable or unstable evolutions than those closer to the band. That is, cases located in the stable region, which are far away from the band have very weak redistributions of the wall vorticity and very little change in the coherent structure of the vortex ring throughout the interaction. Cases located in the unstable region show strong interactions associated with the breaking up of the ring and violent mixing effects. Cases the vicinity of the band have characteristics partially belonging to stable interactions and partially belonging unstable ones, therefore it is difficult to classify them into either of the two types. Furthermore, the stability of interactions near the band is rather sensitive to experimental perturbations such as temperature differences, mechanical vibrations, or irregularities in the flow field. Thus the reproducibility of cases farther away from the sensitivity band is greater than those closer to it.

In the stability map for interactions with initial

angles of 15°, the curve of the band is flatten out over the region where speed ratios of ring to belt is less than 0.5. It says that a small amount of change in the delay time would lead to a drastic change in the evolution of interaction. On the other hand, the curve becomes extremely steep over the range of speed ratio between 0.6 and 0.74, which suggests that the stability is independent on the delay time and all the interactions that take place at speed ratios higher than 0.8 will be unstable. In the region where speed ratio is between 0.5 to 0.6, both the delay time and the speed ratio are important since the solpe of the band is about 1 over this region. After the conversion from delay time to boundary layer thickness as the coordinate, which is to be discussed later in this section, it is clear that the delay time is not a good representative parameter of the physics involved.

Comparing the data of 15° with that of 9° and 3°, (refer to figures 3.5 to 3.7), one can get the impression that the bands in these stability maps all have the shape of an increasing function which consists of two boundaries and a knee. However, with a shallower interaction angle, the stability band is shifted toward the unstable side, thus stable interactions occur over a larger region of both speed ratio and delay time. This implies that for vortex rings with the same convective velocities and the

same amount of vorticity with respect to the vorticity in the wall layer, evolutions of their interactions with a wall can be shifted from an unstable type to a stable type by just changing the angle of approach to a smaller angle. If an analogue to the turbulence production process in a turbulent shear layer can be made, it further suggests that the larger the angle with which a coherent eddy comes into the viscous sublayer the better the possibility for new turbulence to occur from the interaction.

Based on the boundary layer data acquired from the photochromic tracer measurements, the delay time can be converted into boundary layer thickness. Linear interpolations were applied to enable the conversions to be made for those cases of belt velocities not directly measured by experiments. The stability maps for different angles were then replotted using the ratio between the boundary layer thickness and the ring diameter (used to nondimensionalize the length scale) as the ordinate. Results are shown as figure 3.8 to 3.10.

In the stability map for the angle of 15°, interactions with parameters on the right hand side of the stability curve are all stable, while those on the left hand side are unstable. Regions for speed ratios lower than 0.4 and non-dimensional boundary layer thicknesses greater than 0.8 were not investigated because of experimental limitations (as discussed in section 3.2.1).

Boundary layer on the moving belt was observed to become turbulent (which is a condition beyond the scope of this study) at speed ratio of ring to belt lower than 0.4 while ring speed is 6.42 cm/sec. The boundary layer in the test section asymtotically reaches an steady-state value of not more than 2.3 cm which restricts the nondimensional thickness to be less than 0.8.

The importance of each parameter is shown by the slope of the stability curve. Over the range of speed ratio (between ring and wall) of 0.45-0.65, the speed ratio between ring and belt plays a very important role in the stability of interactions. However, in the region where speed ratio ranges from 0.7 to 0.74, the slope of the curve is nearly flat, thus an extremely strong dependence of the evolution on the non-dimensional boundary layer thickness exists. It suggests that when a ring is larger than 1.25 times the wall layer thickness comes to a wall with a velocity greater than 0.7 times the belt speed and an angle larger than 15°, an unstable interaction will take place. When a ring which is smaller than 5.6 times the layer thickness moves with a speed lower than 0.45 times the belt speed into the wall region, a weak interaction can be expected.

Over the region of speed ratio from 0.6 to 0.74, the strong dependence of evolutions on the speed ratio observed in the stability map drawn with delay time

against speed ratio was shown to be overexaggerated. Since the wall layer thickness reaches a steady state and is insensitive to time after it is fully developed, the dependence on boundary layer thickness in the range of speed ratios between 0.7 to 0.74 can not be detected.

In the stability map for 9°, the stability curve is shifted toward the unstable side from that in the map for 15° by approximately 40% of speed ratio. In the region where speed ratio is around 0.98, There exists a knee connecting the horizontal and vertical boundaries. For speed ratios between 0.92 and 0.98, the evolutions of interaction are obviously speed-ratio-dependent. For speed ratios higher than 0.98 and up to 1.12, the boundary layer thickness completely dominates the evolution.

In the map for 3°, the flat slope region is not obviously seen from the data acquired. The curve is again shifted 30% toward the unstable side compared with that for 9°, thus an even larger region is created for stable interactions to happen. If we think of the interaction as a model of the turbulence production process, it suggests that all the typical eddies that interact with a wall with an angle shallower than 3° will not be able to generate new turbulence.

CHAPTER 4

DISCUSSION

The major outcome of this experimental study has been the quantification of the different types of evolutions that can take place when a vortex ring comes into contact with a moving wall. These evolutions can be grouped into two major categories: stable interactions and unstable interactions. Features observed in an unstable interaction are: lateral motions of the wall fluid which lead to a "pocket structure", a lift-up of wall fluid at the downstream end of this pocket, the ingestion of this lifted fluid into the vorticity field of the impinging ring before the ring changes its direction of flight, the onset interaction instability characterized by the breaking up of the vortex ring structure and the ingested wall fluid, the presence of fine scale motions and a strong effect of mixing. The features observed in a stable interaction are: pocket structure is created in the a wall region, lifted wall layer fluid at the downstream end of the pocket has its vorticity stretched and amplified so that it rolls into a vortex with sign of rotation the same as the mean flow, and the ring leaves the wall region with structure and stability essentially unchanged. Neither ingestion of the lifted wall fluid into the vortex ring nor strong mixing occurs. Those interactions which have evolutions which range between the above two can be classified into either of the two categories based on whether or not the ingestion of wall fluid into the vortex ring occurs after the ring alters its direction of flight to move away from the wall. If ingestion occurs before the ring changes direction, the interaction is unstable. If the ingestion never happens, or it happens while the ring is moving away from the wall, the interaction is stable.

The stability of interactions is governed by three parameters: the angle with which the vortex ring comes into the wall, the velocity ratio of the vortex ring to the moving wall, and the ratio between the boundary layer thickness and the ring core diameter. The effect of a shallower interaction angle, or a slower speed of the traveling ring with respect to the moving wall, or a thicker boundary layer on the moving wall is to reduce the effect of the impinging vortex ring on the vorticity distribution near the wall, and to shift the evolutions of interaction toward the stable side.

The properties of the boundary layer on the moving wall were quantitatively measured using the photochromic tracer technique. The velocity profiles across the boundary layer at the beginning stage of the wall movement were verified to be well matched with the Stokes' exact

solution for a flow field created by the movement of an infinitively long plate in fluid. However, after duration of wall movement, the vortical layer seconds stops diffusing outwards and it reached a constant value laver thickness. The property that this wall layer asymptotically approaches a fully developed, steady state condition qualitatively resembling the behavior of a Blasius' boundary layer. However, data taken at different wall velocities show that there is no apparent relationship between the boundary layer thickness and the wall The boundary layer thickness described by Blavelocity. sius' solution is inversely proportional to the square of free stream velocity. Experimental data at the root wall velocity of 5.01 cm/sec are the closest to the Blasius' solution. Data with velocities that are much higher or lower than that are inconsistant with the Blasius' solution. This experimentally detected behavior of the wall layer is possibily attributed to the errors in measurements caused by the thickness of the trace lines, or the wall surfaces on the picture data, or to the difference between the sharp leading edge hypothesis in Blasius' solution and the round edge in our actual experiments with local curvature and a dye injector placed close to it. definitive explanation for However, no the velocity-independence property of the layer thicknesses can be put forward at this point.

Raw data of interaction stabilities under various governing parameters can be plotted onto the stability maps. Furthermore, the time durations of wall movement can be converted into boundary layer thicknesses using the data acquired by photochromic technique provided that the layer thickness is proportional to the square root of the fluid's kinematic viscosity. Stability maps replotted using velocity ratios between ring and belt as the and. boundary layer x-coordinates, thicknesses non-dimensionalized the ring diameters by as the y-coordinates indicate that when a boundary layer is 0.8 times as thick as the diameter of the impinging vortex ring, and when a velocity ratio is between 0.7 and 0.75 at angle of 15°, or between 0.98 and 1.11 at 9°, a slight increase in the layer thickness will lead to a stable interaction while a small decrease in the thickness will result in an unstable interaction. On the other hand, when the ratio of boundary layer thickness to ring diameter ranges from 0.3 to 0.7, the stability is sensitive to velocity ratio between the ring and the belt. However, with governing parameters other than those stated above, the stability of interactions close to the stability band is critically sensitive to all of the parameters, thus, a small error associated with calibration of these parameters or any unexpected disturbance could appear to make the evolutions to happen differently from the way they are predicated from the stability maps. So, the data farther away from the band are more reliable in terms of predicting which type of evolution the interaction, under specified initial conditions, will go through.

The visualization data acquired using the laser illumination/dyed fluid technique allow us to obtain detailed qualitative descriptions of the interactions that occur. However, quantivative information such as the distribution of velocity and vorticity in the flow field can not be detected from this technique. In order to quantitatively measure the flow field, a further study is suggested in which one may use the photochromic tracer technique by splitting the ultra violet laser beam into several lines, and pulsing these lines from two orthogonal directions so that colored grids, instead of the single time-line in this study, can be created in the organic solvant. The vorticity and velocity field can then be marked out in the test section throughout the whole process of the vortex ring/moving wall interactions.

A comparison with the mechanism of turbulence production in the wall region of a turbulent boundary layer can be made. This mechanism was synthesized by Falco (1979) based on experimental data obtained from combined simultaneous flow visualization and hot-wire annemometry in a wind tunnel. The mechanism involves a well defined sequence of events, called the "pocket flow module",

which is essentially the interaction between vortex-ring-like "typical eddies" of the outer region, which moves toward the wall, with the wall region flow. Faloc broke down the evolutions into five stages, and each of them was characterized by the dominance of one of the Reynold stress causing events. During stage 1, a wallward moving high speed fluid (defined as a "sweep") created a roundish hole, which was called pocket, in the smoke-marked wall region. Stage two was characterized by the formation of a characteristic crescent shape on the wall, a lift-up of sublayer fluid at the upstream end of the pocket, and its rapid return back to the wall. During the third stage, a pair of counter-rotating streamwise vortices being joined around the upstream end of the pocket pattern were formed and another lift-up of sublayer fluid had been initiated in the downstream portion. During the fourth stage, lift-up from the downstream end of the pocket continued to move outward beyond the buffer zone and was called an "ejection". The main features for stage 5 was that the pocket pattern had diffused and the lifted fluid appeared to have broken down into a range of small and large scale motions.

Similarities between the vortex ring/moving wall interactions and the turbulence production mechanism near walls were studied. Using a Galilean transformation, the wall moving in a still ambient fluid can be considered as

the case of a flow passing over a flat plate, and the laminar boundary layer building up on the moving wall corresponds to the viscous sublayer in an actual turbulent The geometric arrangements of which an boundary layer. impinging vortex ring with a velocity of the same smaller magnitude as the moving wall, (that is the case when the speed ratio of ring to belt is positive is less than one), parallels the situation in which a typical eddy is being convected down stream with an absolute velocity lower than the mean flow. On the other hand, the case of rings with velocities higher than the moving wall, that is when speed ratios of ring to belt are greater than one, corresponded to situations in which a typical eddy is traveling upstream with respect to a stationary coordinate, while the main flow moves stream. (This is very unlikely to happen in actual boundary layers.) Furthermore, the typical eddies observed using laser sheet/flood light technique (1977) Thus, the interactions had the shapes of vortex rings. between these Taylor microscaled typical eddies and the viscous sublayer in a turbulent bounded shear flow can modelled by the sequence of events that take place when vortex rings come into contact with laminar wall layers.

Characteristic features observed in a turbulent boundary layer may not all fit into any single type of vortex ring/moving wall interaction. Both stable interactions

and unstable interactions, as well as other interactions in between the extreme cases, all have similarities with the qualitative impressions of the turbulence production process observed near a wall. The way that the wall smoke pushed away from the center of was convecting pocket pattern in a turbulent voundary is very similar to the pocket structure observed in this study of vortex ring/moving wall interactions. The pair streamwise vortices found in the turbulent boundary layer can be modelled by the vorticity field due to a ring with a portion lying down on the wall inducing wall fluid away and then back toward the wall.

In a turbulent boundary layer, the "hairpin" vortex which was seen at the downstream end of the pocket could be either a lift-up of boundary layer fluid that is not ingested into the ring during the interaction, or the lift-up of boundary layer fluid at the upstream of the impinging ring, or a vortex ring with its lower lobe broken up and attached to the wall while its upper lobe is still coherent. The ejection of fluid from wall region and the breaking up of the lifted fluid into both small and large scales motion looks very much like the case of an unstable interaction in which strong mixing ensues.

The convective velocity of the pocket pattern with respect to the mean turbulent flow (i.e. pocket velocity/mean flow velocity) was about 0.6 (Falco and

Lovett, 1982). In the study of vortex ring/moving wall interactions, the convective velocities of the pockets with respect to the moving belt were measured to be in the range of 0.4 to 0.95, depending on the interaction angles and the speed ratios of ring to belt.

These similarities indicate that the viscous and inviscid instabilities that vortex rings undergo when they interact with a boundary layer can qualitatively explain some of the physics associated with the turbulence generation process near walls.

CHAPTER 5

CONCLUSIONS

The interactions between a vortex ring and a moving wall are observed to have a wide range of evolutions, from the cases in which an impinging ring redistributes the wall layer vorticity, ingests wall fluid into it, and drastically breaks up, to the cases in which the ring emerges from the interaction essentially intact.

The critical parameters dominating the evolution of interaction are the angle of interaction, the thickness of boundary layer on the wall, and the velocity ratio between the ring and the moving wall. Flow visualization data combined with the boundary layer thickness data acquired using the photochromic technique allowed us to plot the stability maps using these parameters properly non-dimensionalized as coordinates. The maps suggest that:

- (1) When the boundary layer thickness is 0.8 times the ring core diameter, the stability of the interaction critically depends on the boundary layer thickness while: a. velocity ratio of ring to wall is between 0.7 to 0.75, at an interaction angle of 15°. b. velocity ratio is between 0.98 to 1.1 at an angle of 9°.
 - (2) For boundary layer thicknesses/ring core diameter

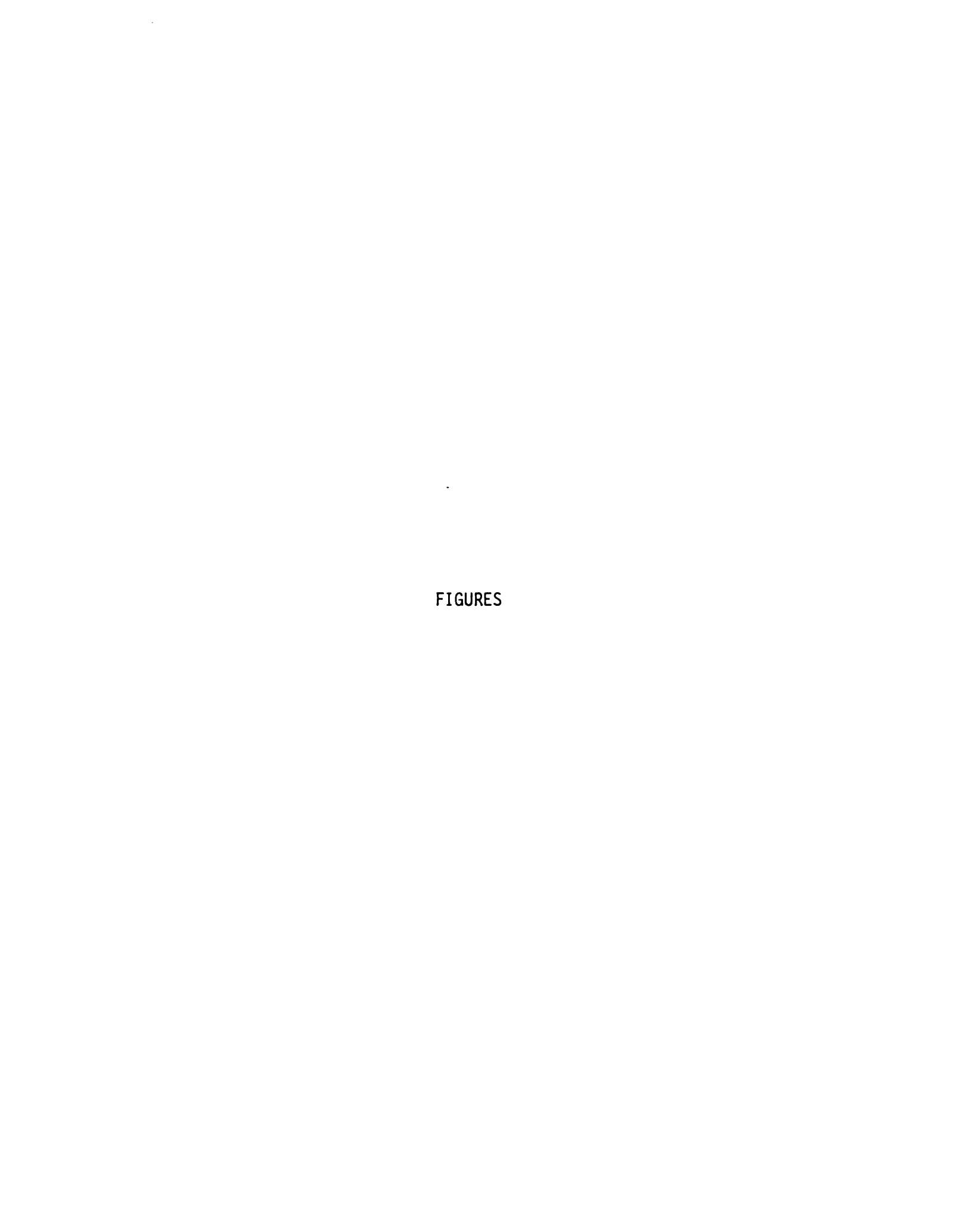
ranging from 0.3 to 0.7, the stability is sensivitive to the velocity ratio at: a. velocity ratio between 0.45 and 0.65 and an interaction angle of 15° . b. velocity ratio between 0.92 and 0.98 and an angle of 9° . c. velocity ratio between 1.24 and 1.30 and an angle of 3° .

The evolutions of vortex ring/moving wall interactions have similarities with the turbulence generation process observed in turbulent boundary layers. If these interactions can model the mechanism of turbulence production near walls, it suggests that the generation of new turbulence will be critically dependent on the instantaneous thickness of the viscous sublayer, the convective velocity of the coherent eddies, and the angle of interaction of these eddies with the wall. Furthermore, indicates that larger diameters and slower convective velocities of the coherent eddies, and larger interaction angle with which these eddies enter into the sublayer of a turbulent boundary layer will provide better possibilities for new turbulence to be generated.

REFERENCES

- 1. Batchelor, G. K. 1967. An Introduction to Fluid Dynamics
- 2. Borner, H., Schmeling, T. and Schmidt, D. W. 1983 Experiments on the Circulation and Propagation of Large-Scsle Vortex Rings in He II Physics of Fluids 26 (6)
- 3. Brodkey, R. S. 1967 The Phenomena of Fluid Motions
- 4. Falco, R. E. 1977 Coherent Motions in the Outer Region of Turbulent Boundary Layers. Physics of Fluids, vol 20, no 10, pt 11
- 5. Falco, R. E. 1978. 16mm movie, Vortex Rings/wall interactions
- 6. Falco, R. E. 1978. The Role of Outer Flow Coherent Motions in the Production of Turbulence Near a Wall. AFOSR/Leigh
- 7. Falco, R. E. and Wiggert, D. C. 1980. Effects of Dilute Polymer Solutions on Vortex Ring/Wall Interactions-A Mechanism for Drag Reduction. Progress in Astronautics and Aeronautics, vol 72
- 8. Falco, R. E. 1980. The Production of Turbulence Near a Wall. AIAA 13th Fluid & Plasma Dynamics Conference
- 9. Falco, R. E. 1982. A Synthesis and Model of Turbulence Structure in the Wall Region. ICHMT/IUTAM Conference on the Structure of Turbulence. Heat & Mass Transfer
- 10. Falco, R. E. 1983. New Results, a Review and Synthesis of the Mechanism of Turbulence Production in Boundary Layer and its Modification. AIAA 21st Aerospace Sciences Meeting
- 11. Frantisak, F. A., Palade de Iribarne, Smith, J. W., and Hummel, R. L. 1969. Nondisturbind Tracer Technique for Quantitative Measurements in Trubulent Flow. I & EC Fund., 8, 160
- 12. Lamb, H. 1945. Hydrodynamics
- 13. Linden, P. F. 1973. The Interaction of a Vortex Ring with a Sharp Density Interface: a Model for Turbulent Entrainment. J. of Fluid Mechanics, vol 60, part 3,

- 14. Maxworthy, T. 1972. The Structure and Stability of Vortex Rings. J. of Fluid Mechanics, vol 51, part 1
- 15. Maxworthy, T. Some Experimental Studies of Vortex Rings. J. of Fluid Mechanics, vol 81, part 3
- 16. Naoyuki Tokuda, 1968. On the Implusive Motion of a Flat Plate in a Viscous Fluid. J. of Fluid Mechanics, vol 33, part 4
- 17. Seeley, L. E. 1972. Ph.D. thesis, Chem. Engineering Dept., University of Toronto
- 18. Seeley, L. E., Hummel, R. L. and Smith, J. W. 1974. Experimental Velocity Profiles in Laminar Flow Aroundheres at Intermediate Reynolds Numbers. J. of Fluid Mechanics, vol 68, part 3
- 19. Sommerfeld, A. 1950. Mechanics of Deformable Bodies



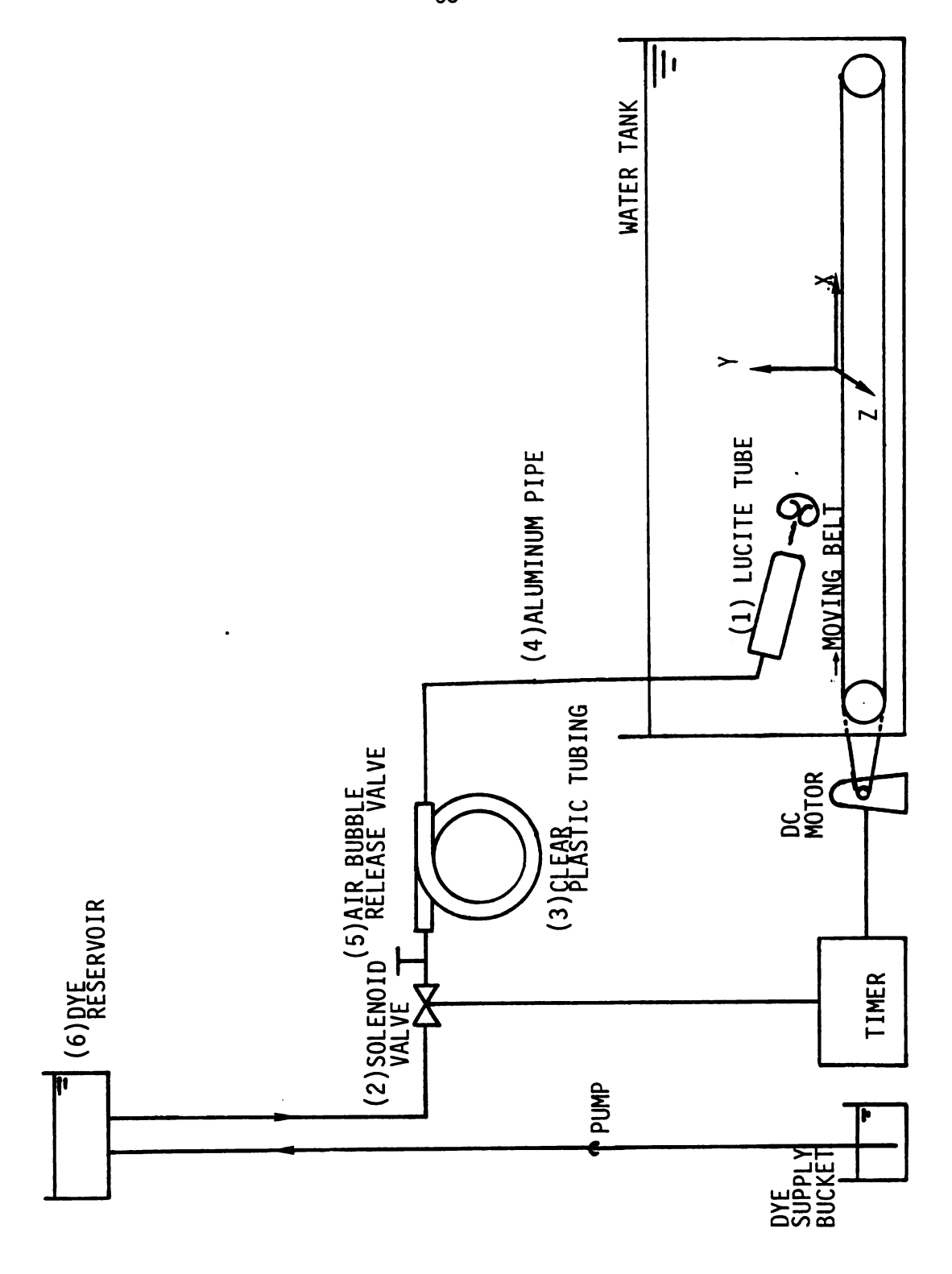


Figure 2.1 Vortex Ring Generating System

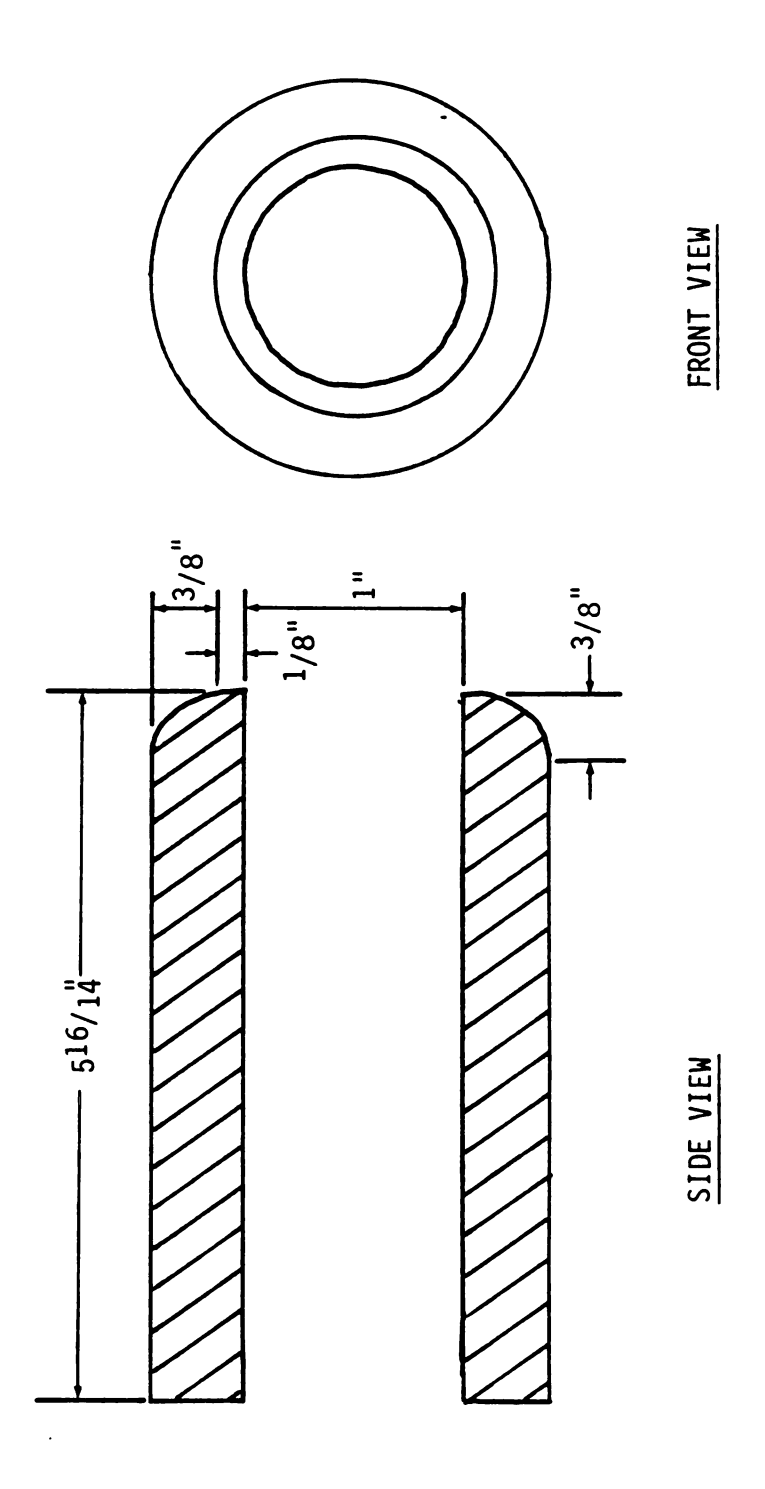


Figure 2.2 Dimensions of Ring Generator

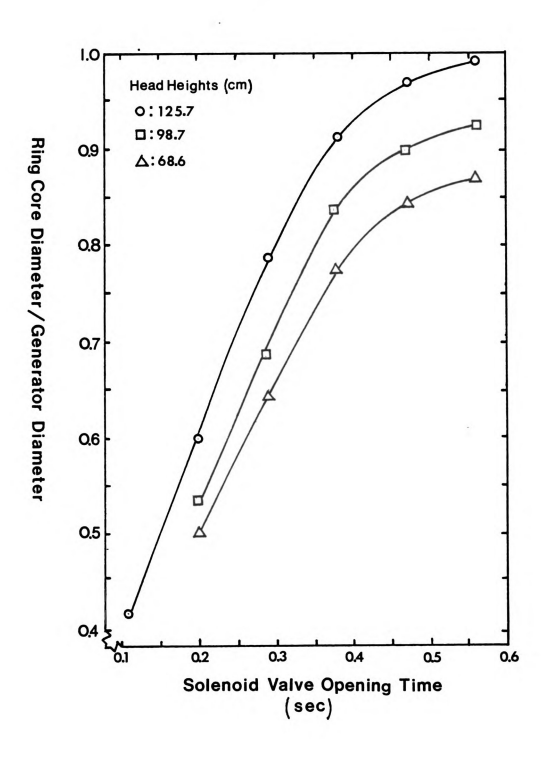


Figure 2.3 Ring Core Diameter for Various Soleniod Valve Opening Times and Head Heights of Dye Reservoir $\,$

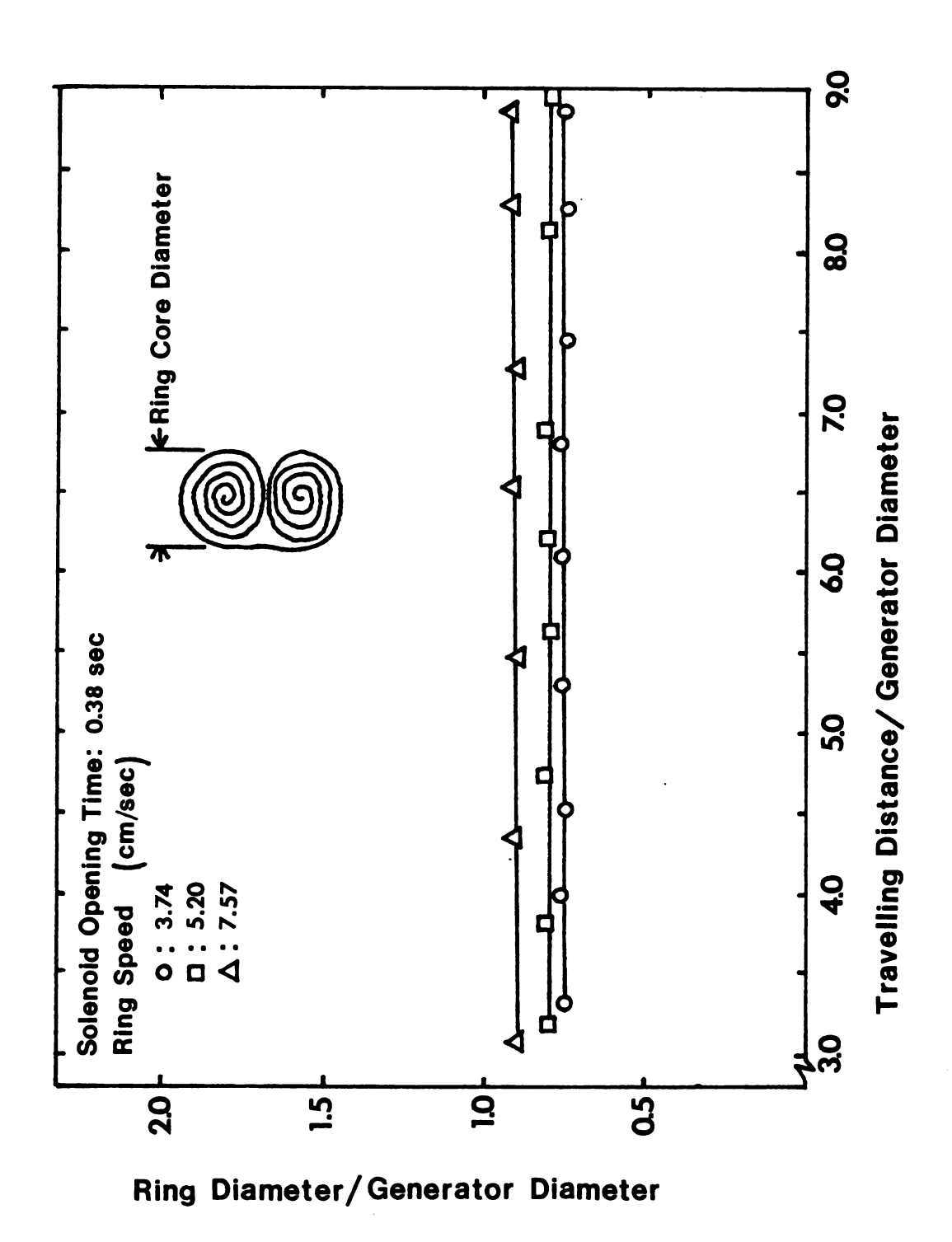


Figure 2.4 Ring Core Diameter for Various Ring Speeds and Traveling Distances $% \left(1\right) =\left(1\right) +\left(1$

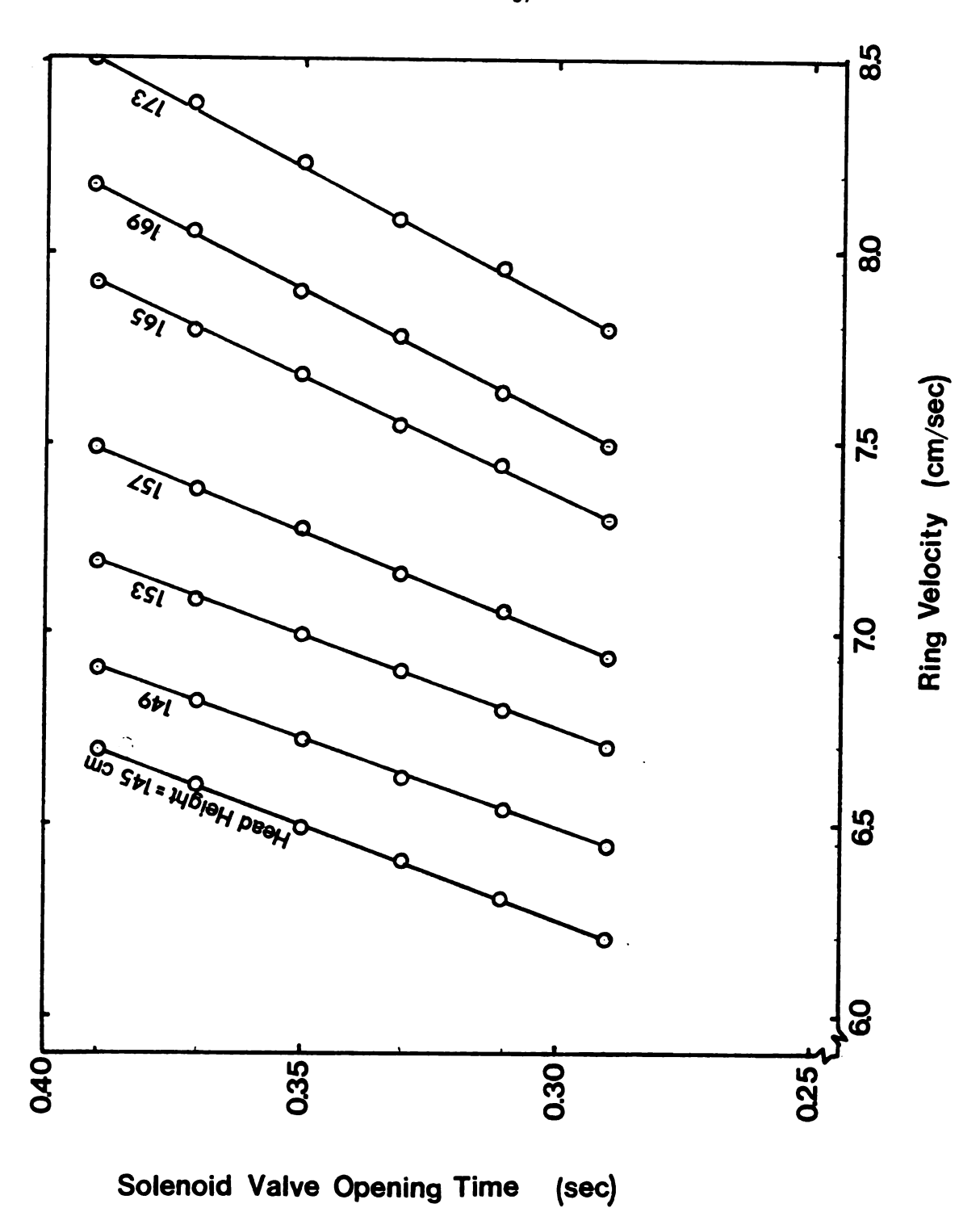


Figure 2.5 Ring Speed for Various Solenoid Valve Opening Times and Head Heights of Dye Reservoir

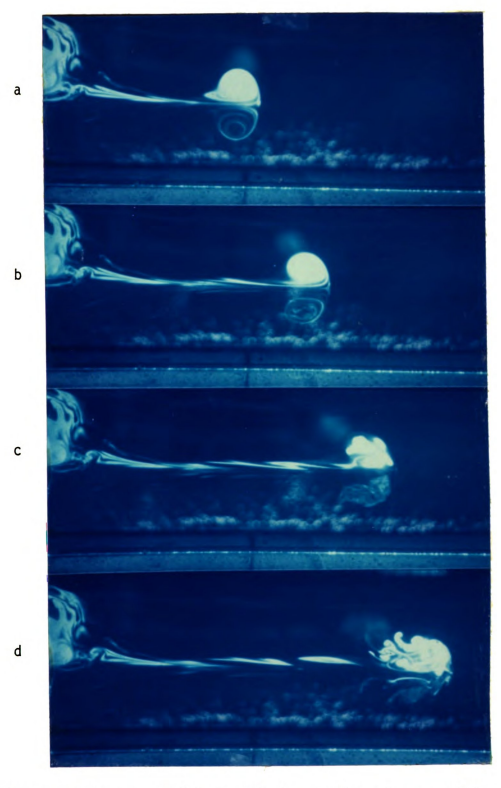


Figure 2.6 The onset of Azimuthal Instability of a travelling vortex ring $% \left(1\right) =\left(1\right) \left(1\right)$

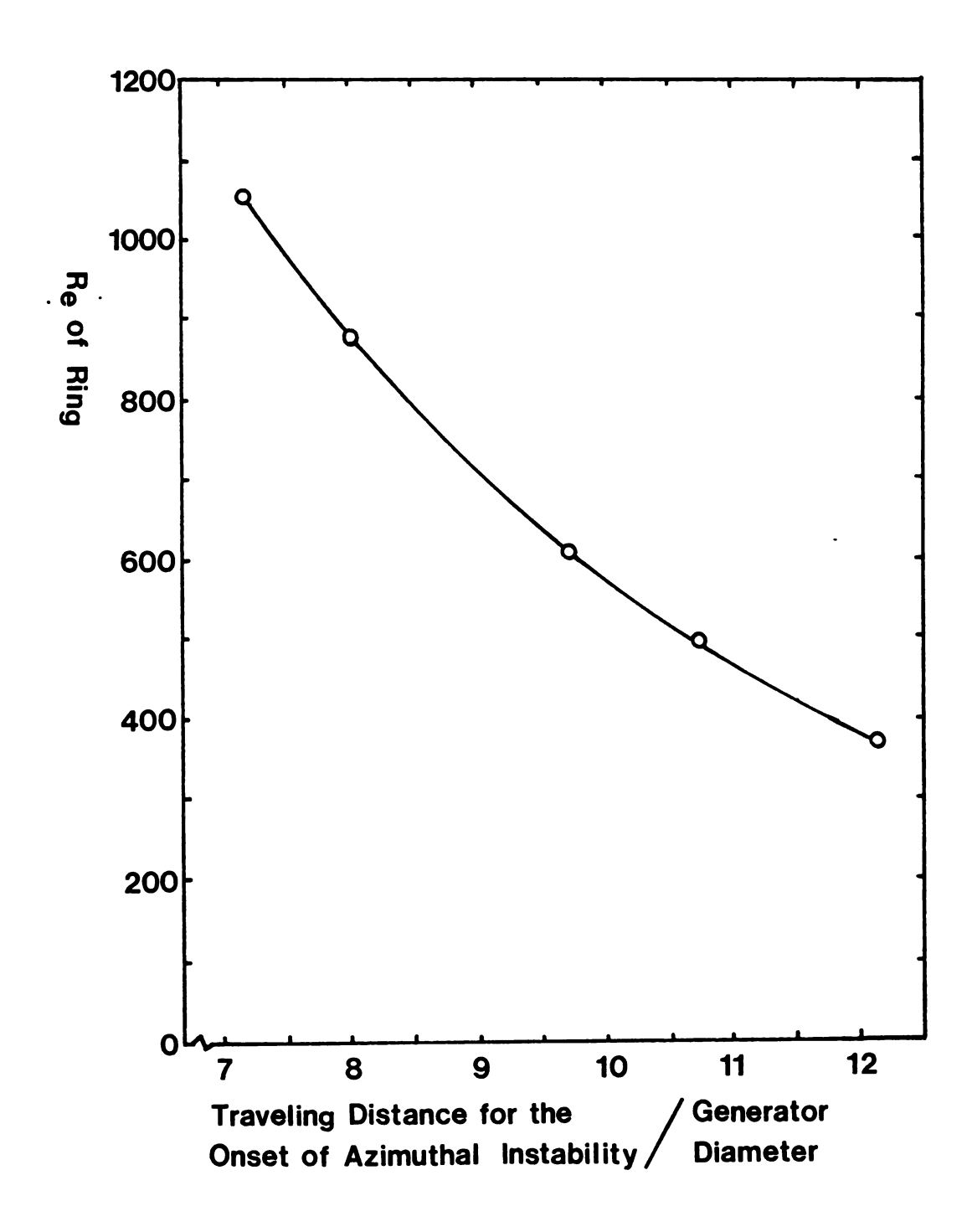


Figure 2.7 Travelling Distance for the onset of Azimuthal Instability of Vortex Rings of Various Reynolds Numbers

à.

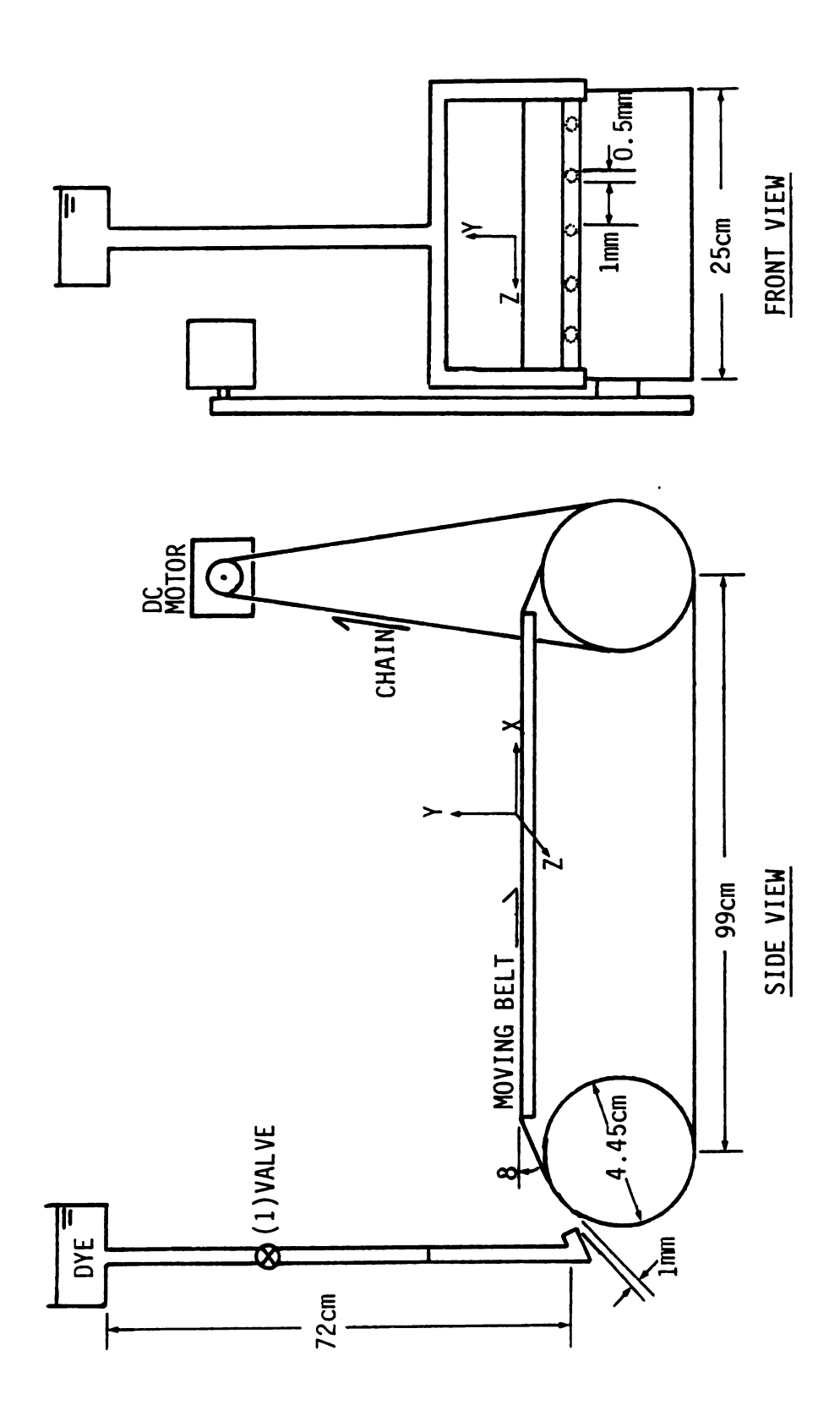


Figure 2.8 Moving Belt System

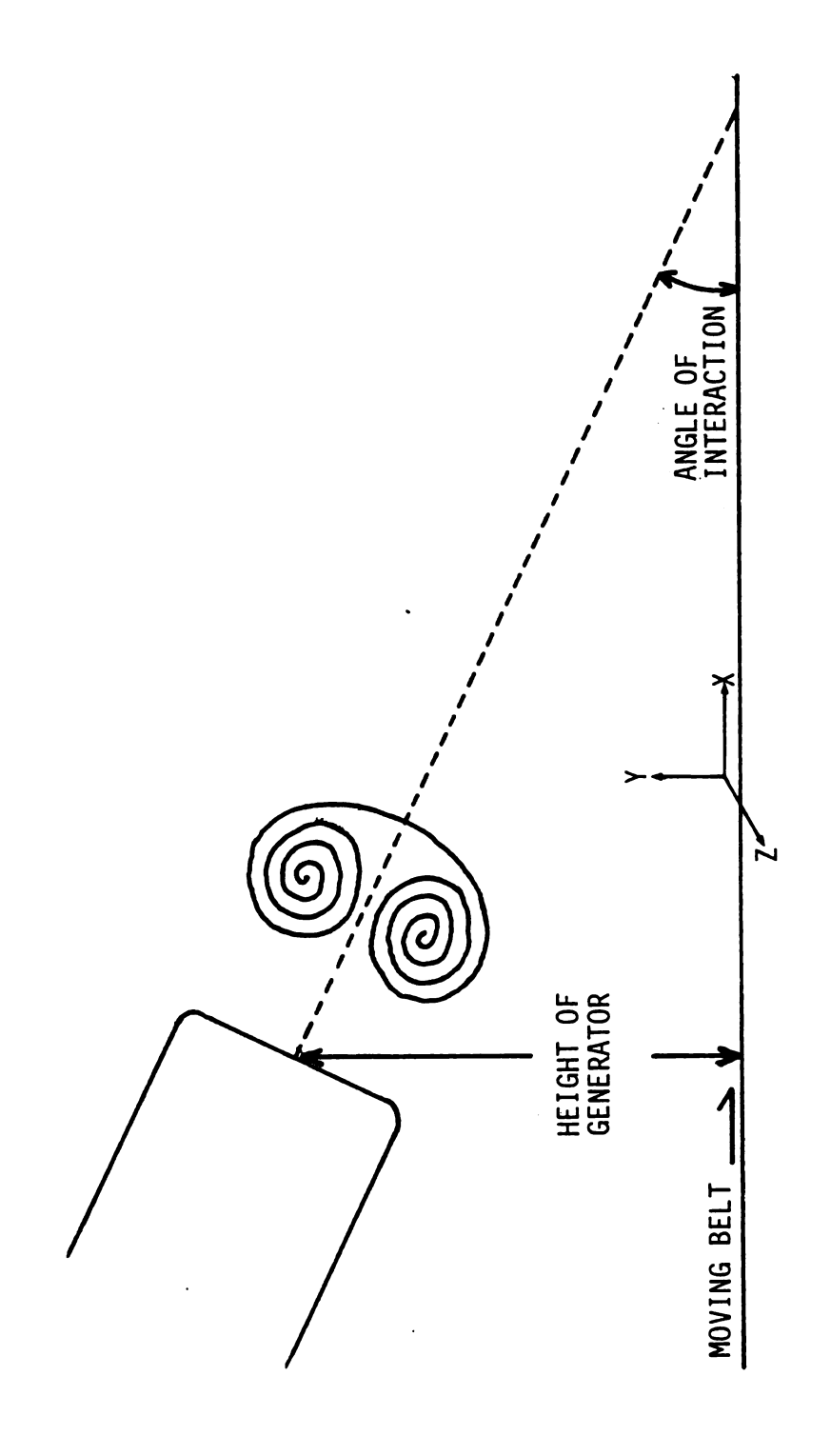


Figure 2.9 Test Section for Vortex Ring/Moving Wall Interactions

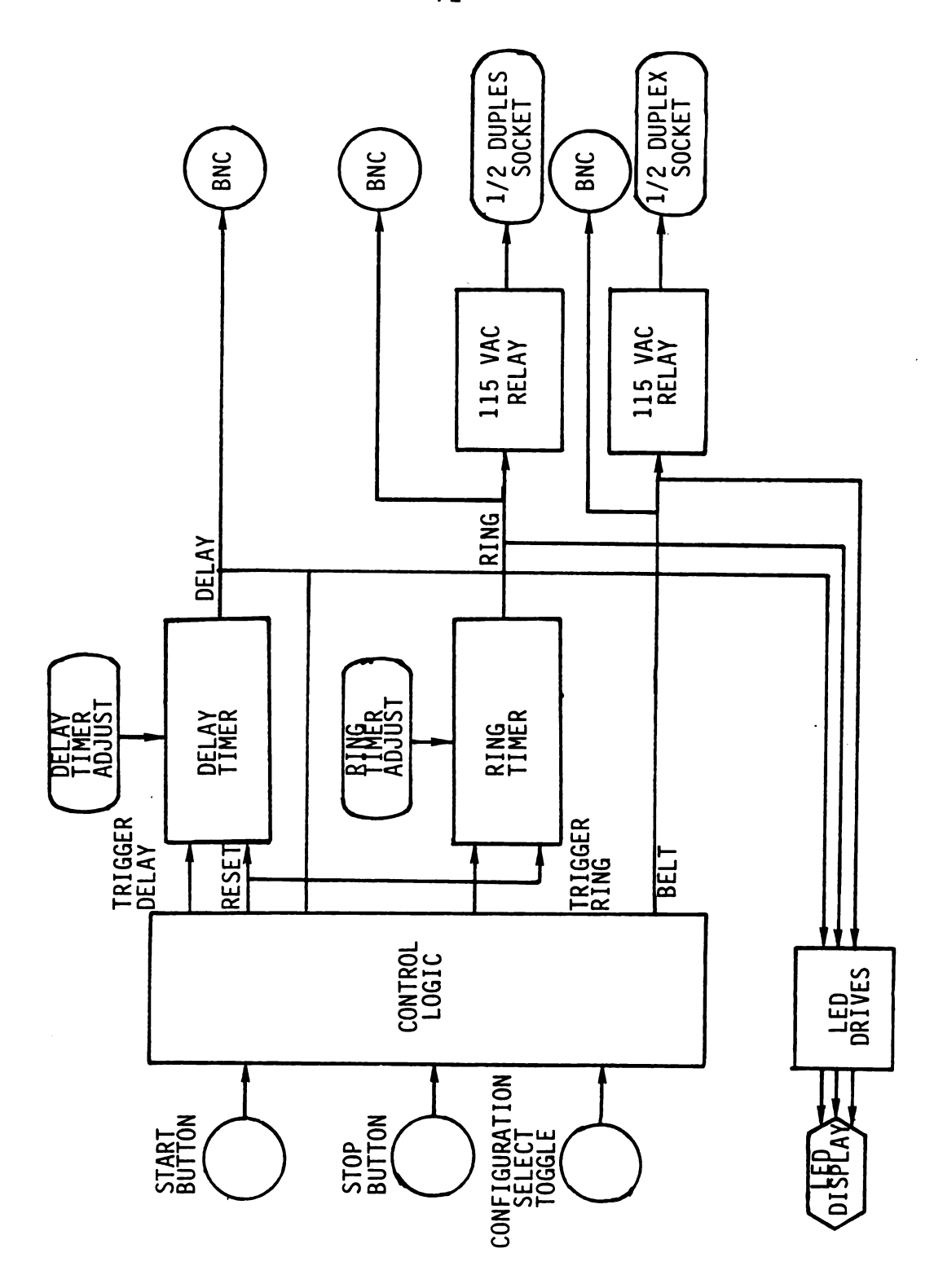


Figure 2.10 Block Diagram of the Timer

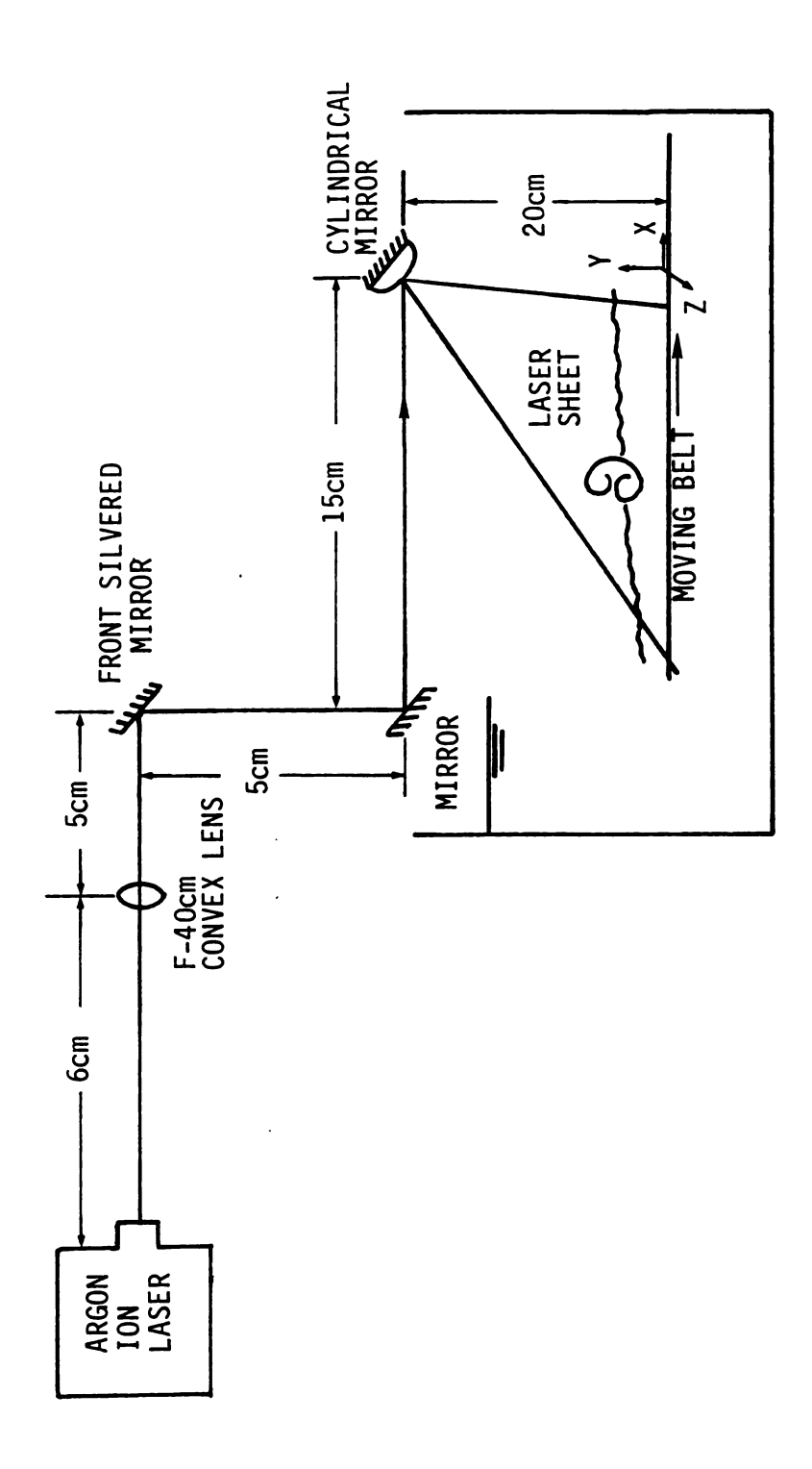


Figure 2.11 Laser Illumination System

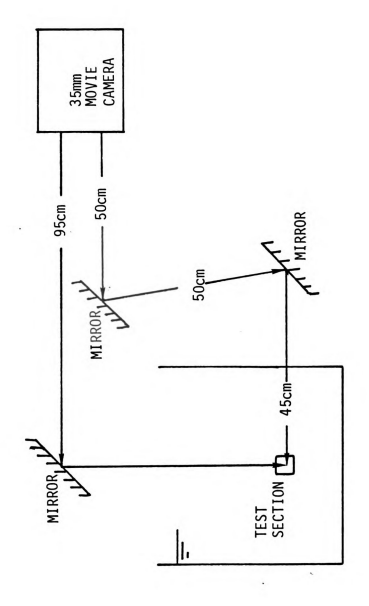


Figure 2.12 Arrangement for Split-Field Photography

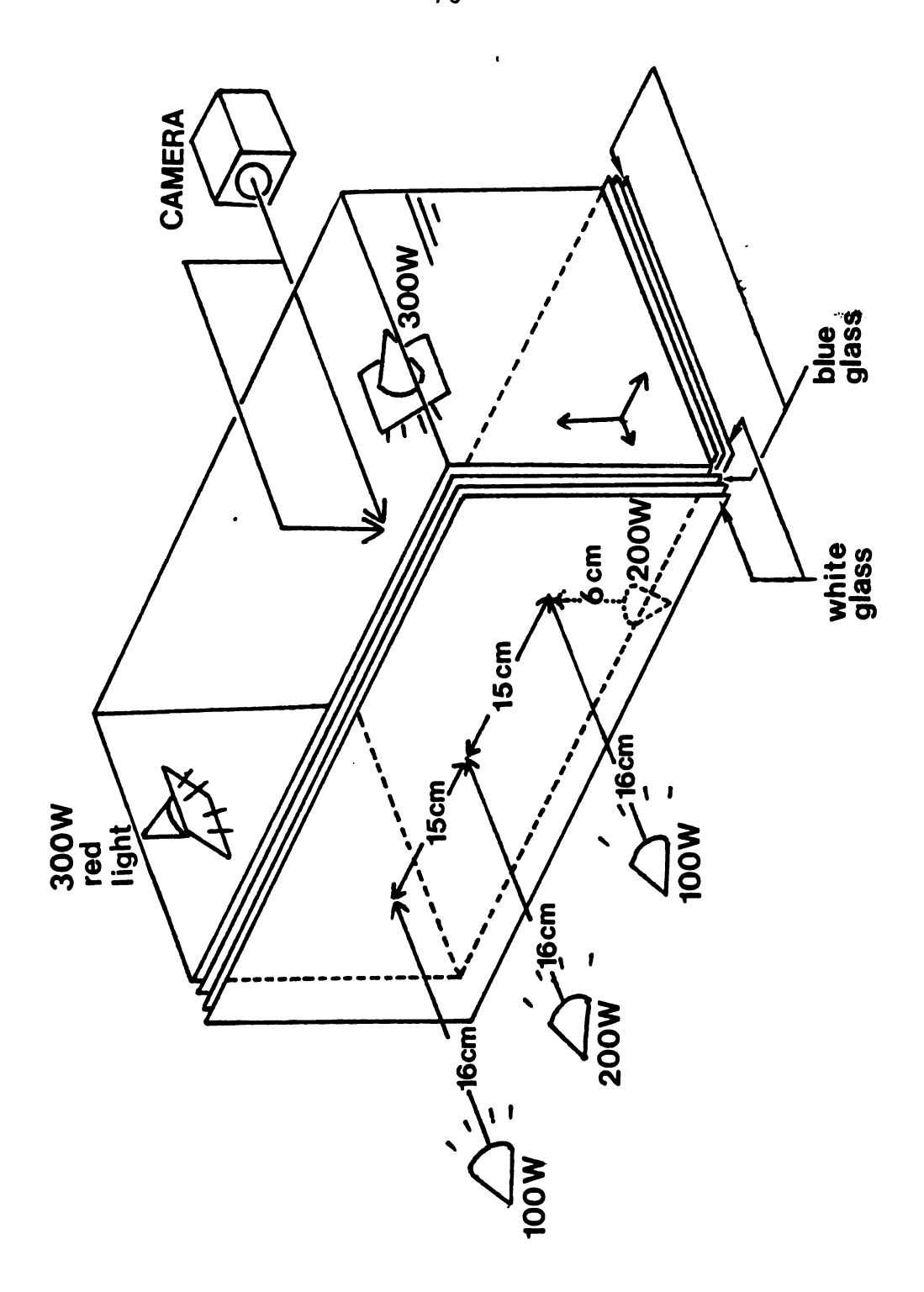


Figure 2.13 Background Lighting and Filter Arrangement

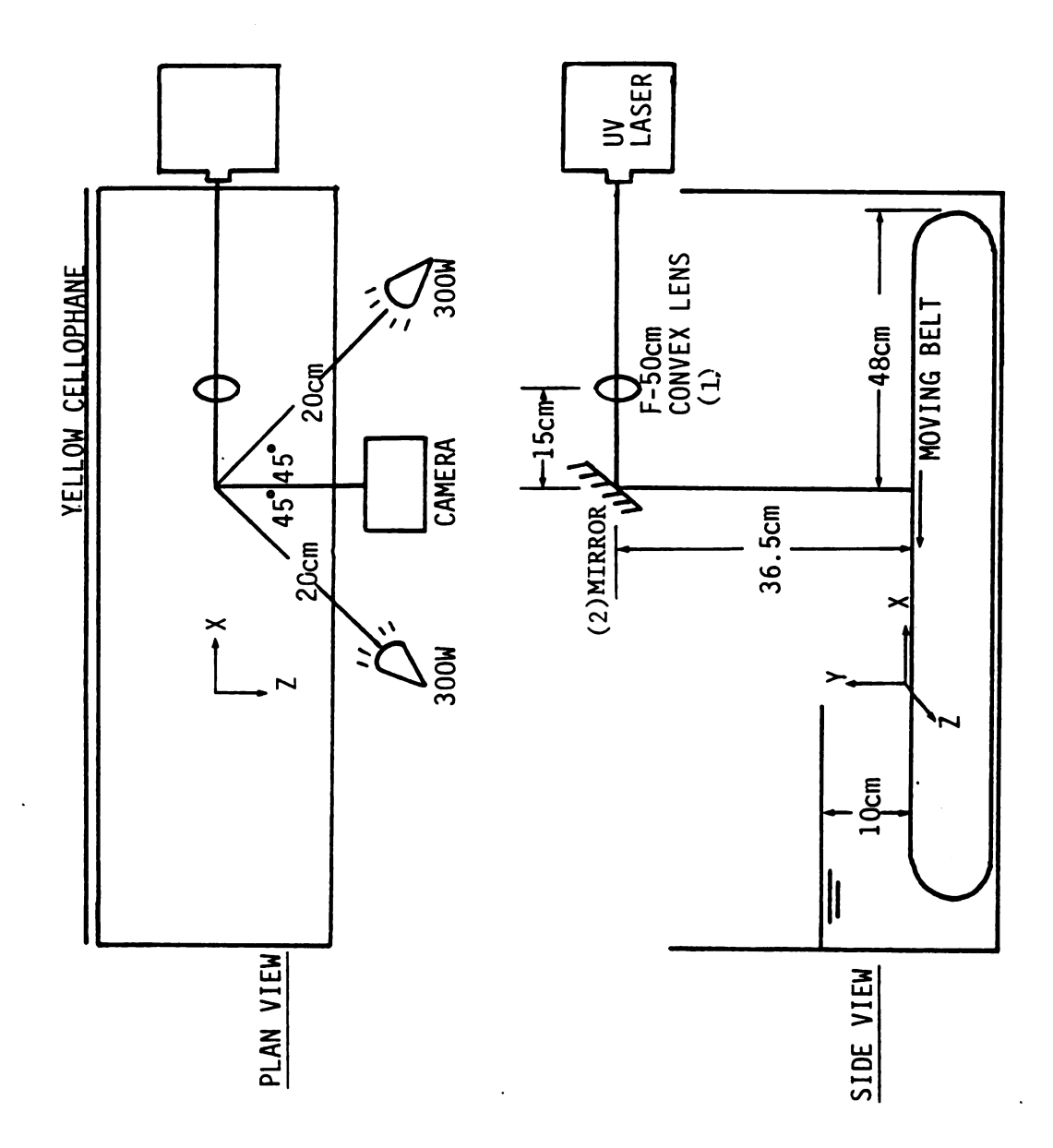


Figure 2.14 Arrangement for Photochromic Tracer Technique

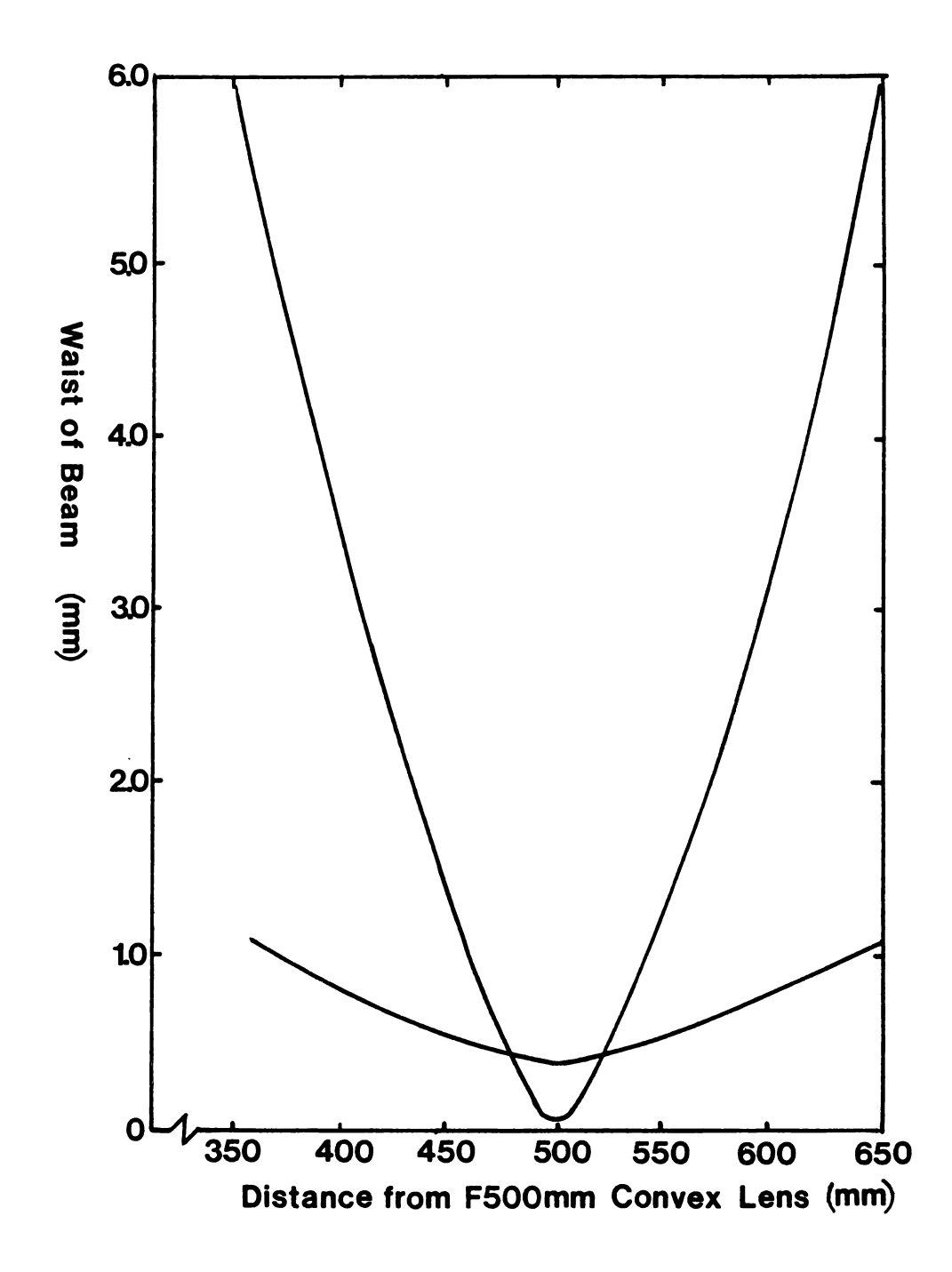
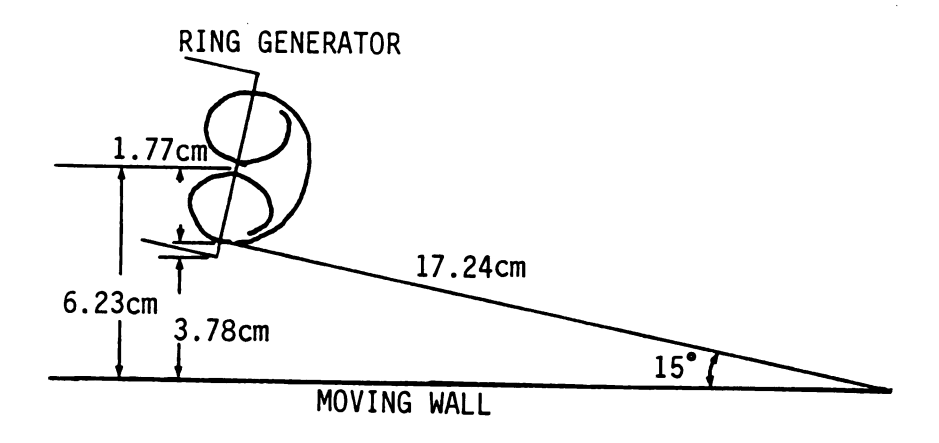
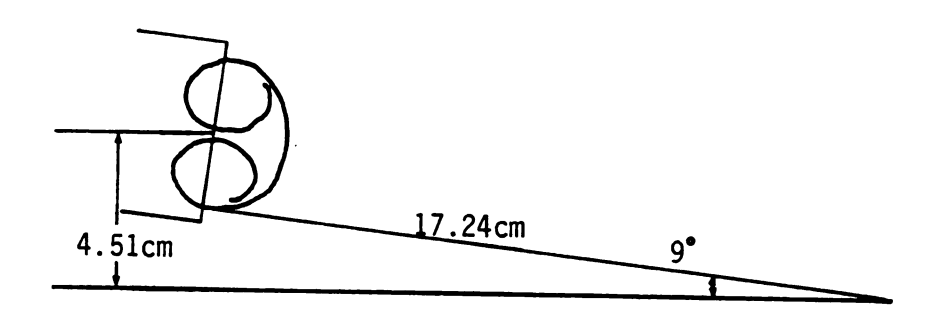


Figure 2.15 Divergence of Laser Beam after a F-500mm Convex Lens (Based on Tachisto Co.' formula:

Waist=1.27x focal lengthx5xwave length initial beam diameter





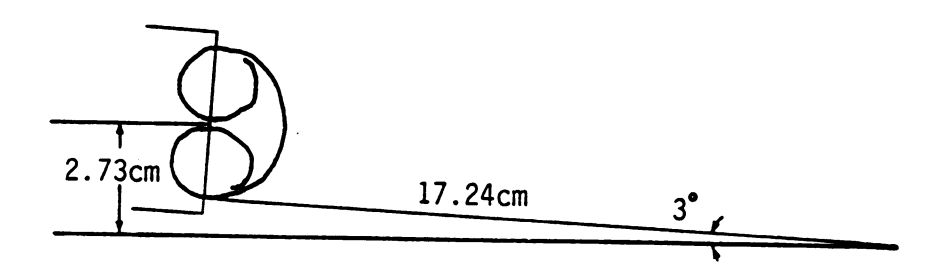


Figure 2.16 Arrangement to Maintain the Same Ring Traveling Distance for Different Generator Angles

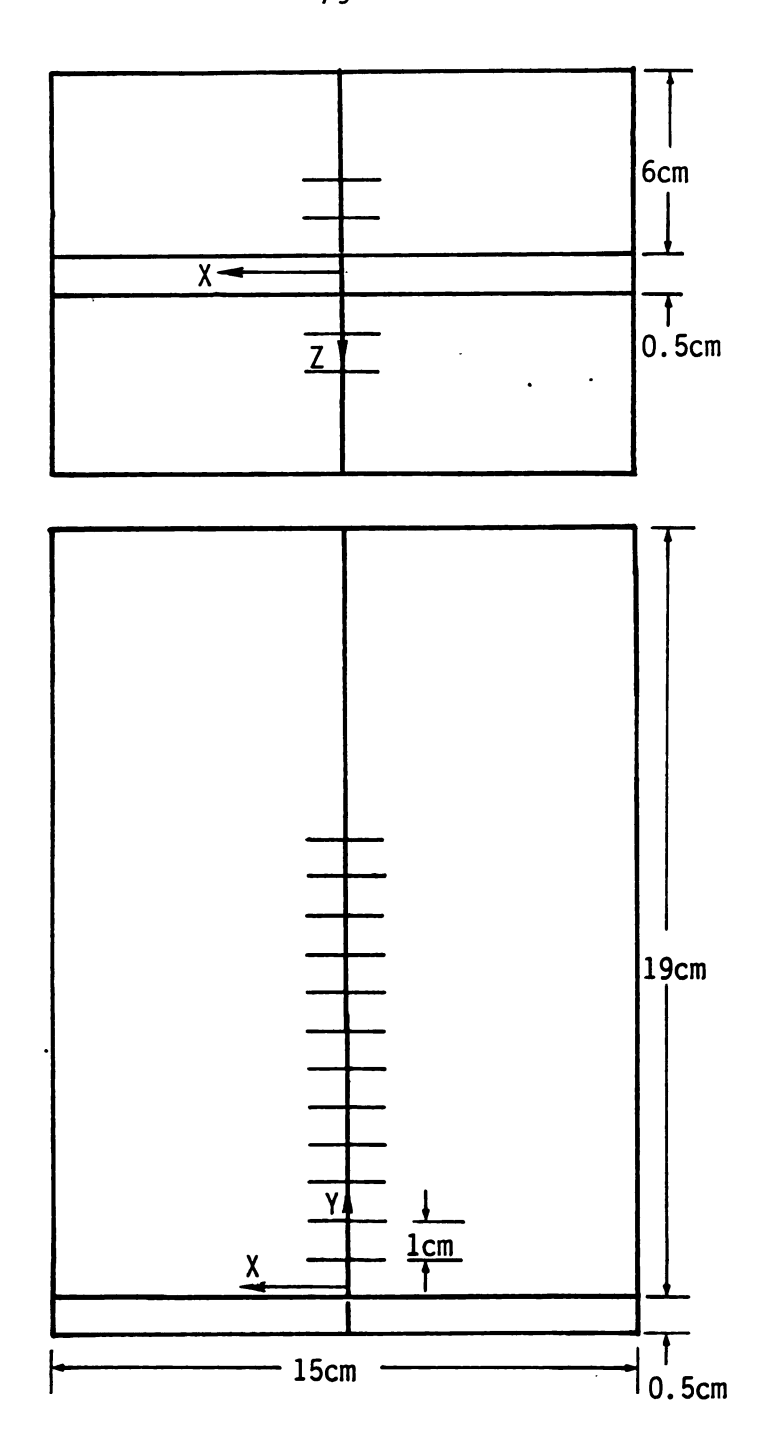


Figure 2.17 Calibration Ruler

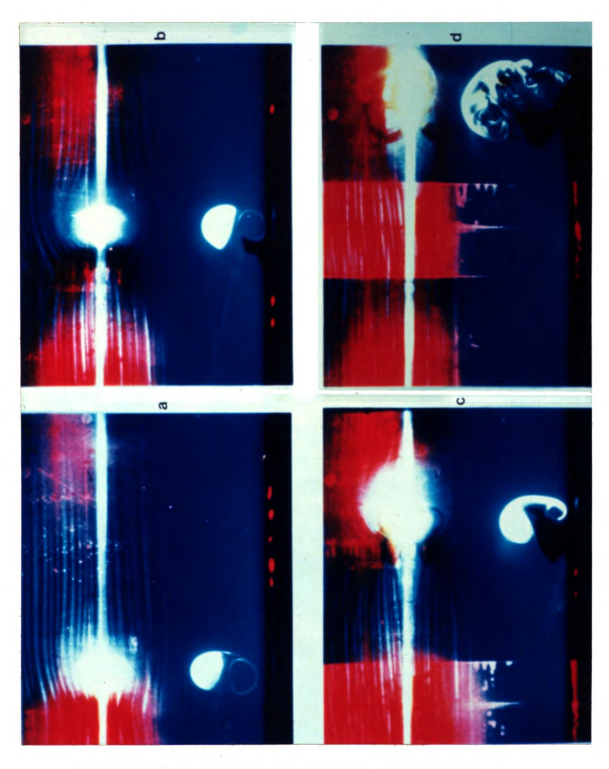


Figure 2.18 An Unstable Interaction at 15 Degrees (Refer to Table 2 for Initial Conditions)

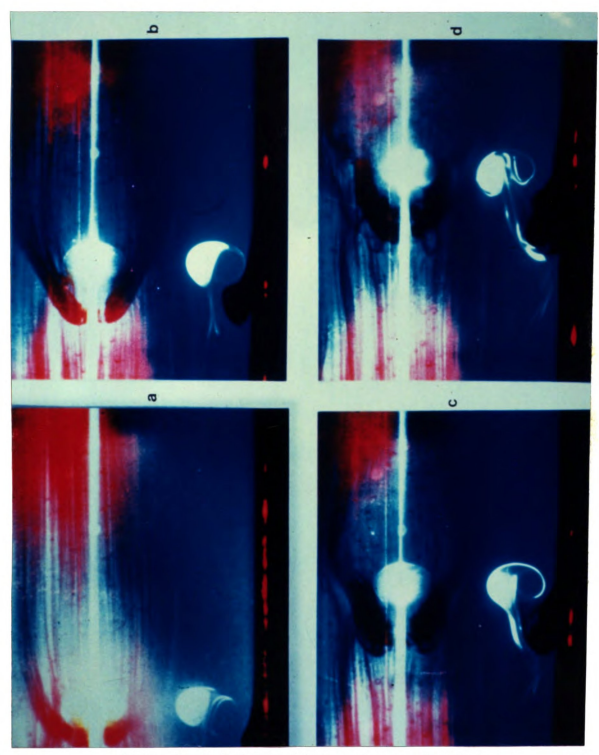


Figure 2.19 A Stable Interaction at 15 Degrees (Refer to Table 2 for Initial Conditions)

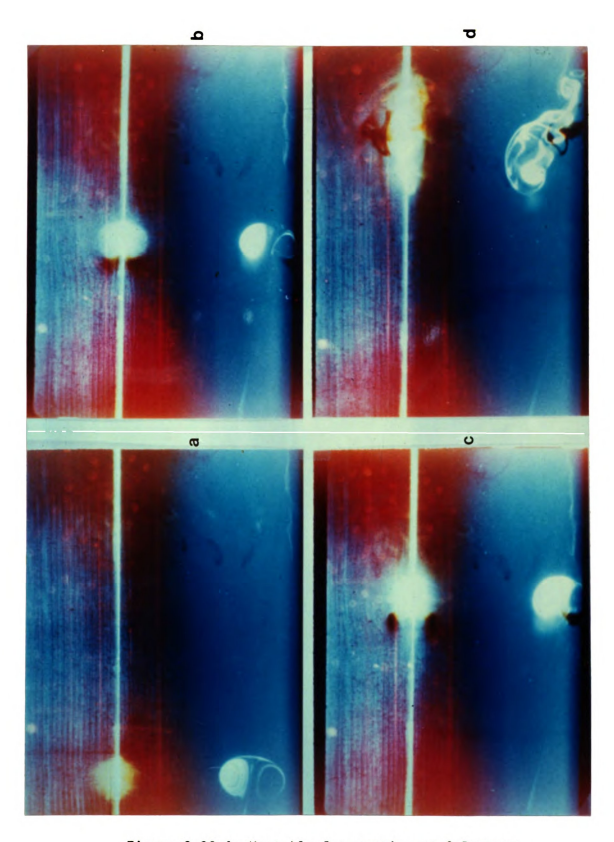


Figure 2.20 An Unstable Interaction at 9 Degrees (Refer to Table 2 for Initial Conditions)

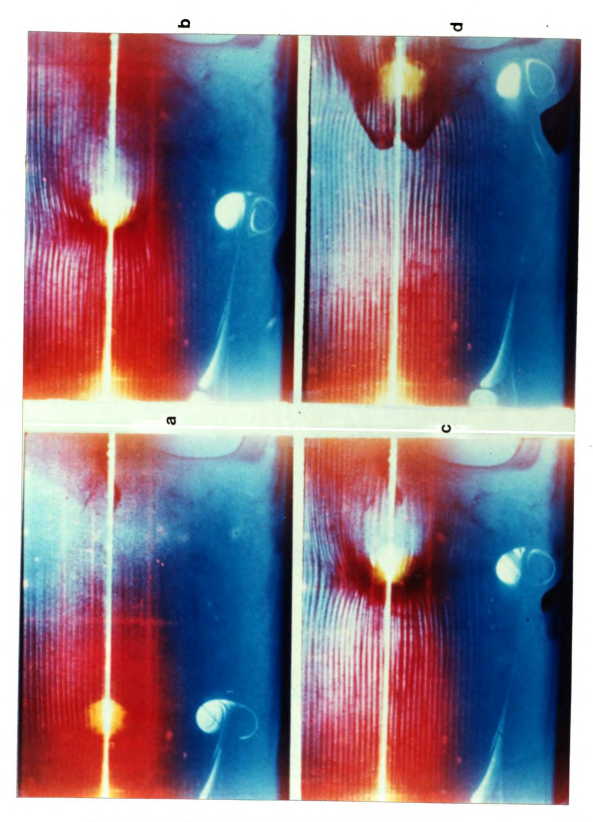


Figure 2.21 A Stable Interaction at 9 Degrees (Refer to Table 2 for Initial Conditions)

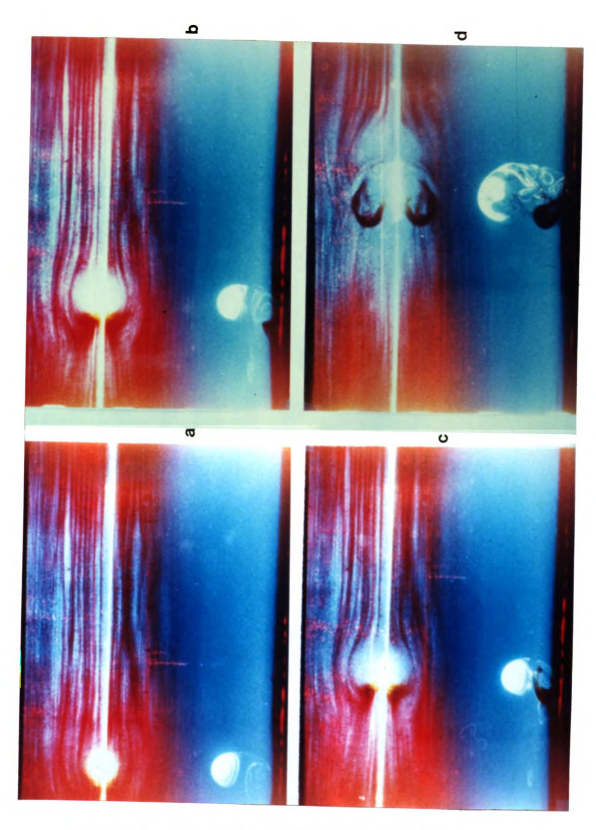


Figure 2.22 An Unstable Interaction at 3 Degrees (Refer to Table 2 for Initial Conditions)

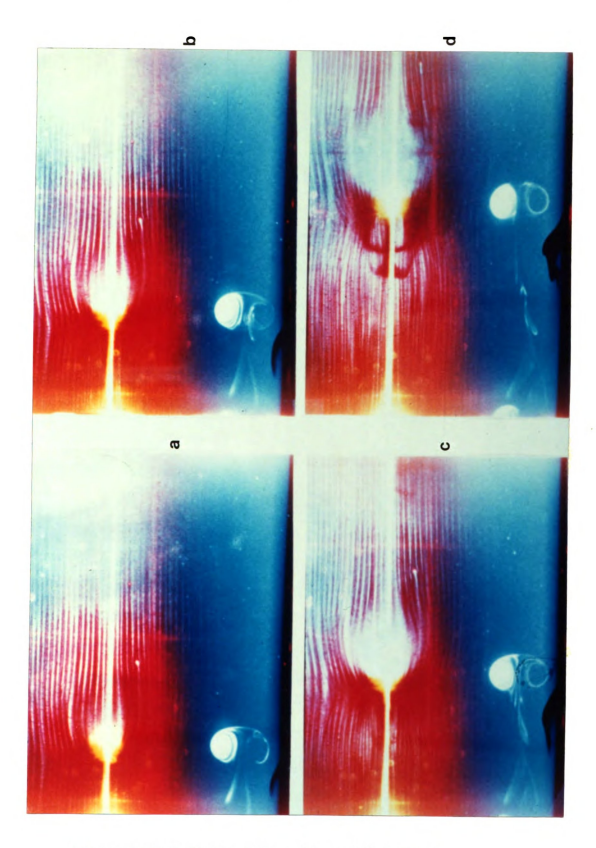


Figure 2.23 A Stable Interaction at 3 Degrees (Refer to Table 2 for Initial Conditions)

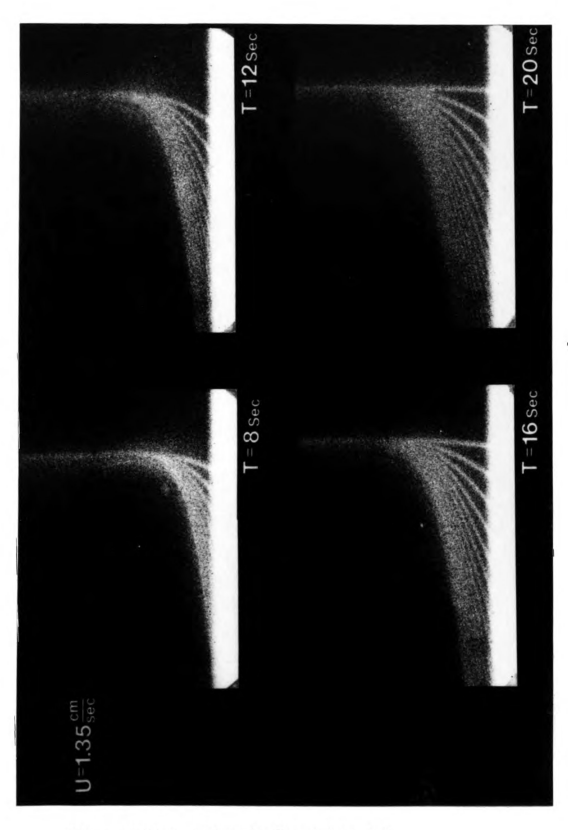


Figure 2.24 Photochromic Time Lines (1)

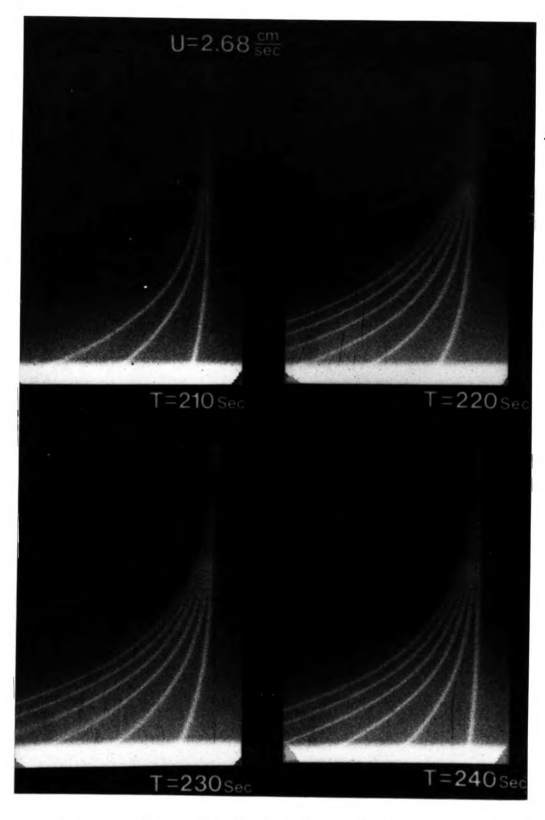


Figure 2.25 Photochromic Time Lines (2)

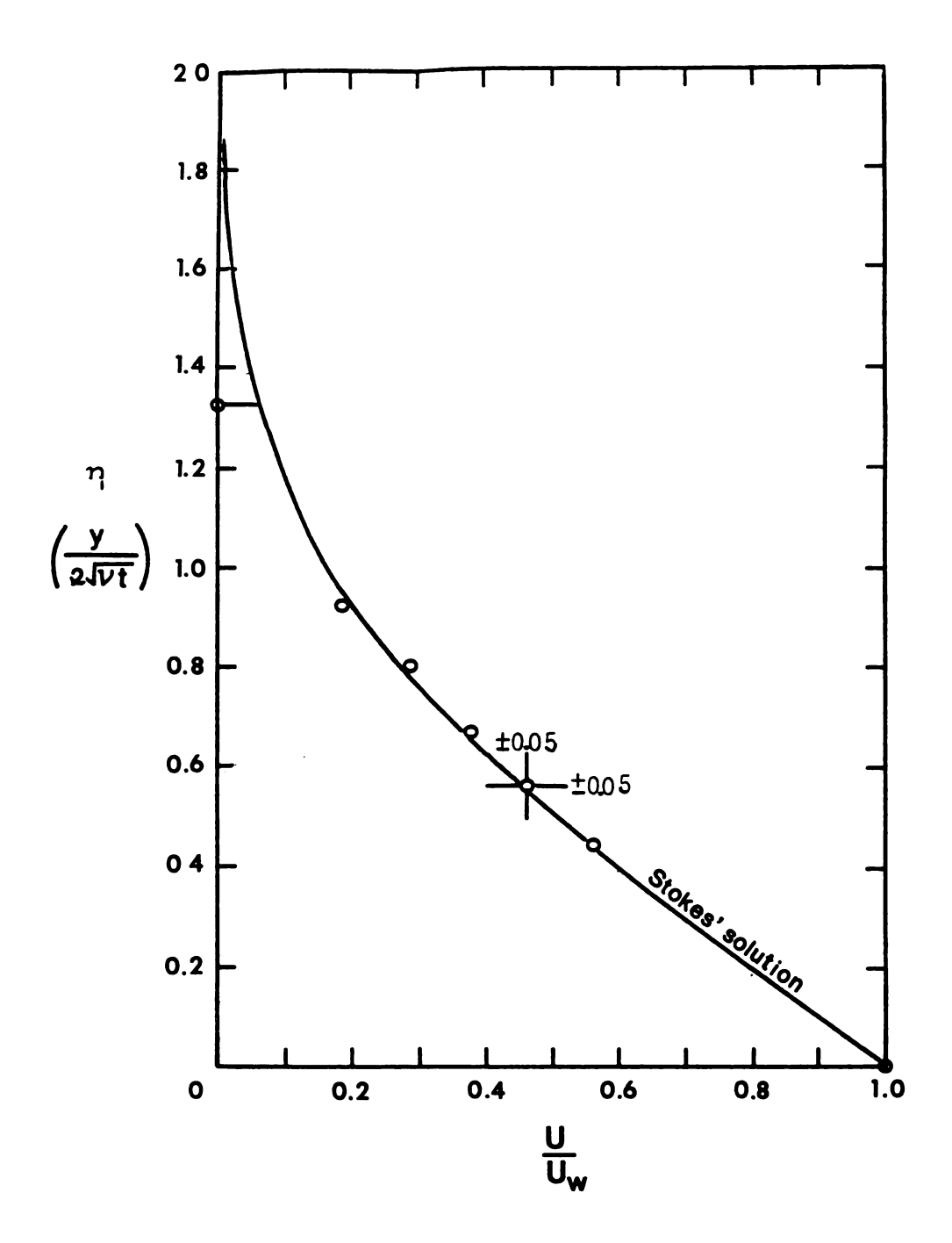


Figure 2.26 Velocity Profile in the boundary layer on the moving belt. o denote experimental data. Solid line is a Stokes' solution plotted for comparison. Belt velocity is 1.35 cm/sec. Time duration is 10 sec. Error in U/U_W is estimated from $0.06\times2/1.35$. Error in η is $(0.06+0.02)/2\times2\sqrt{0.017\times10}$.

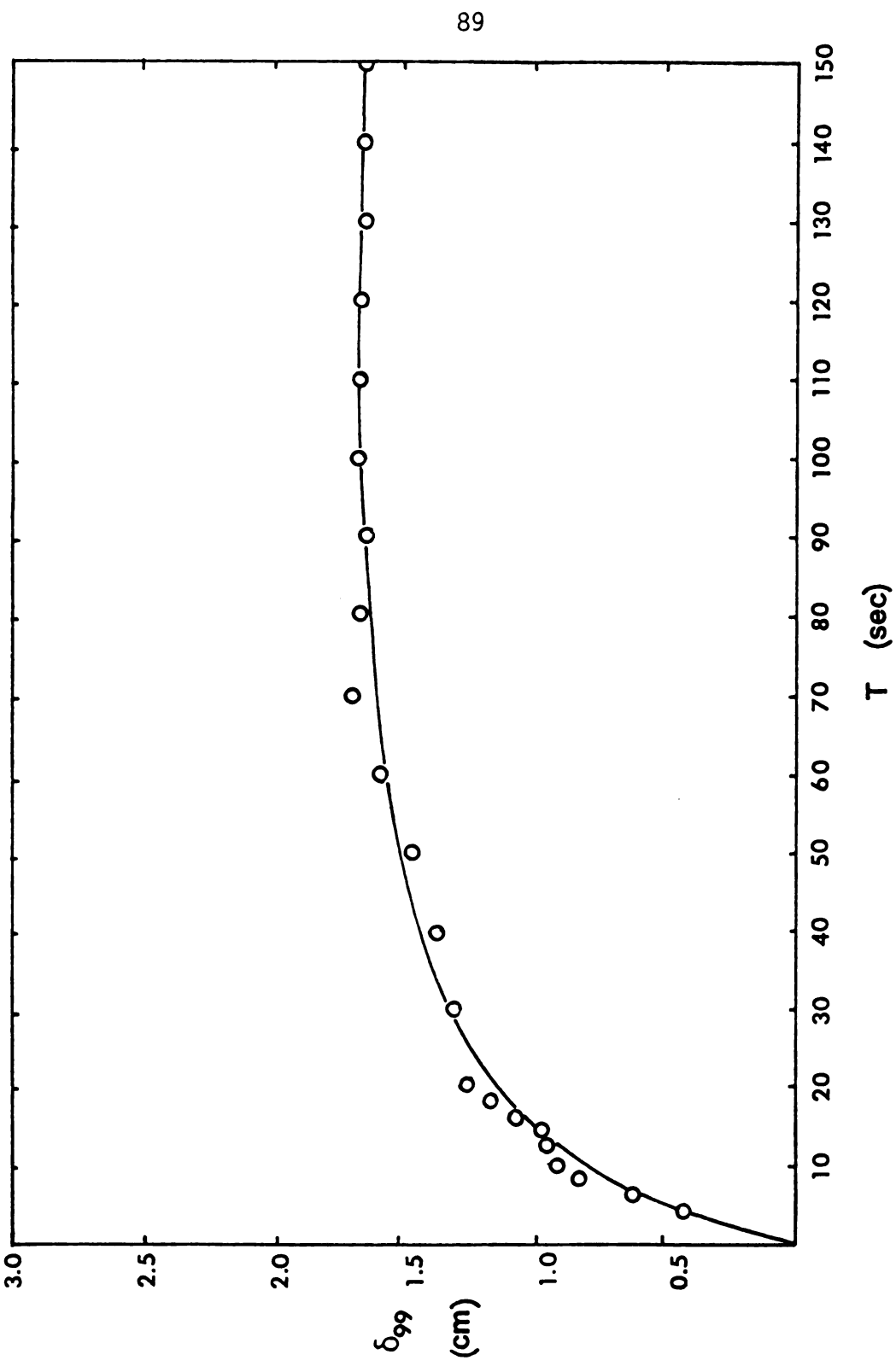


Figure 2.27 Boundary Layer Thickness at U_W =1.35 cm/sec

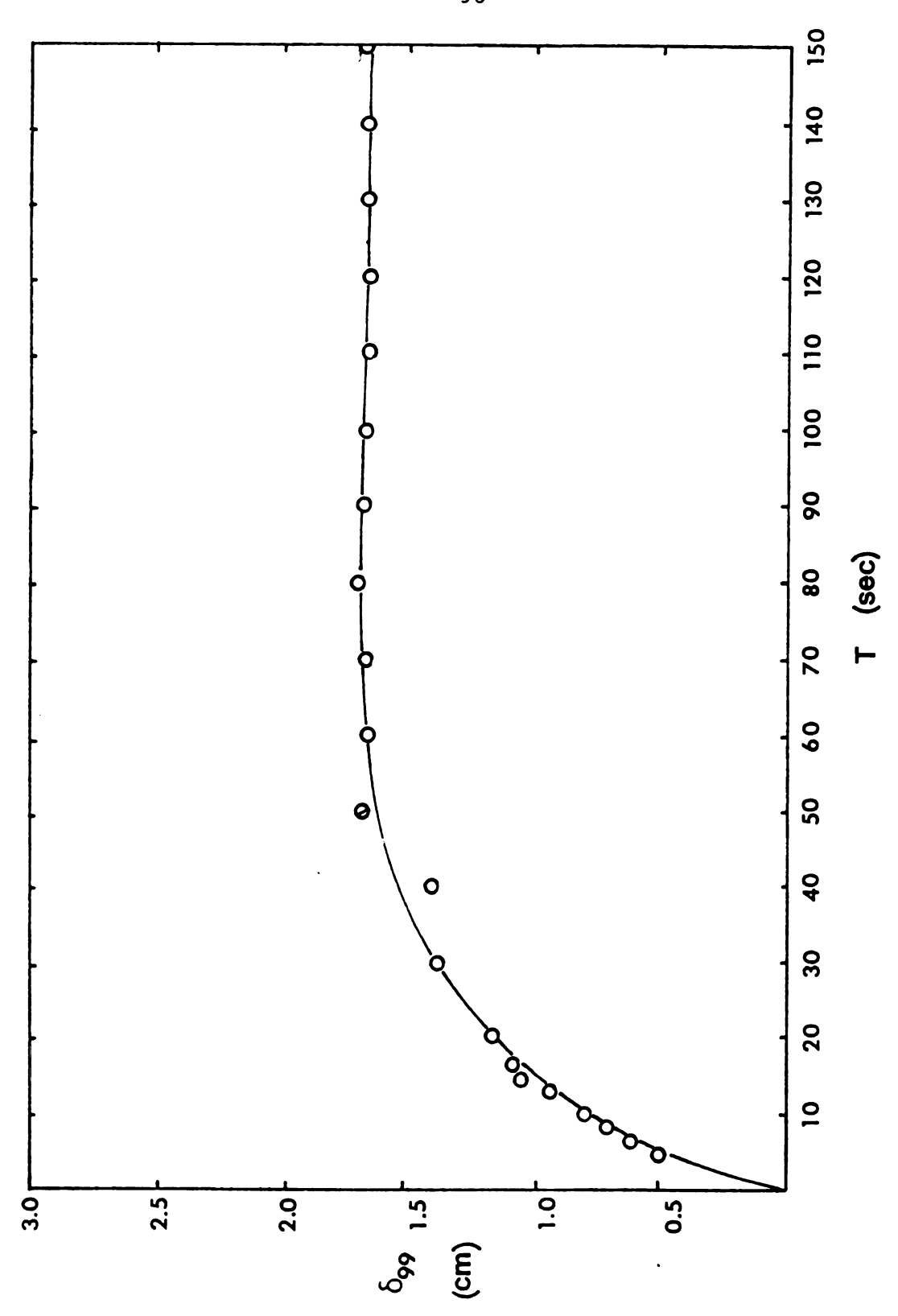


Figure 2.28 Boundary Layer Thickness at $\rm U_W$ =2.68 cm/sec

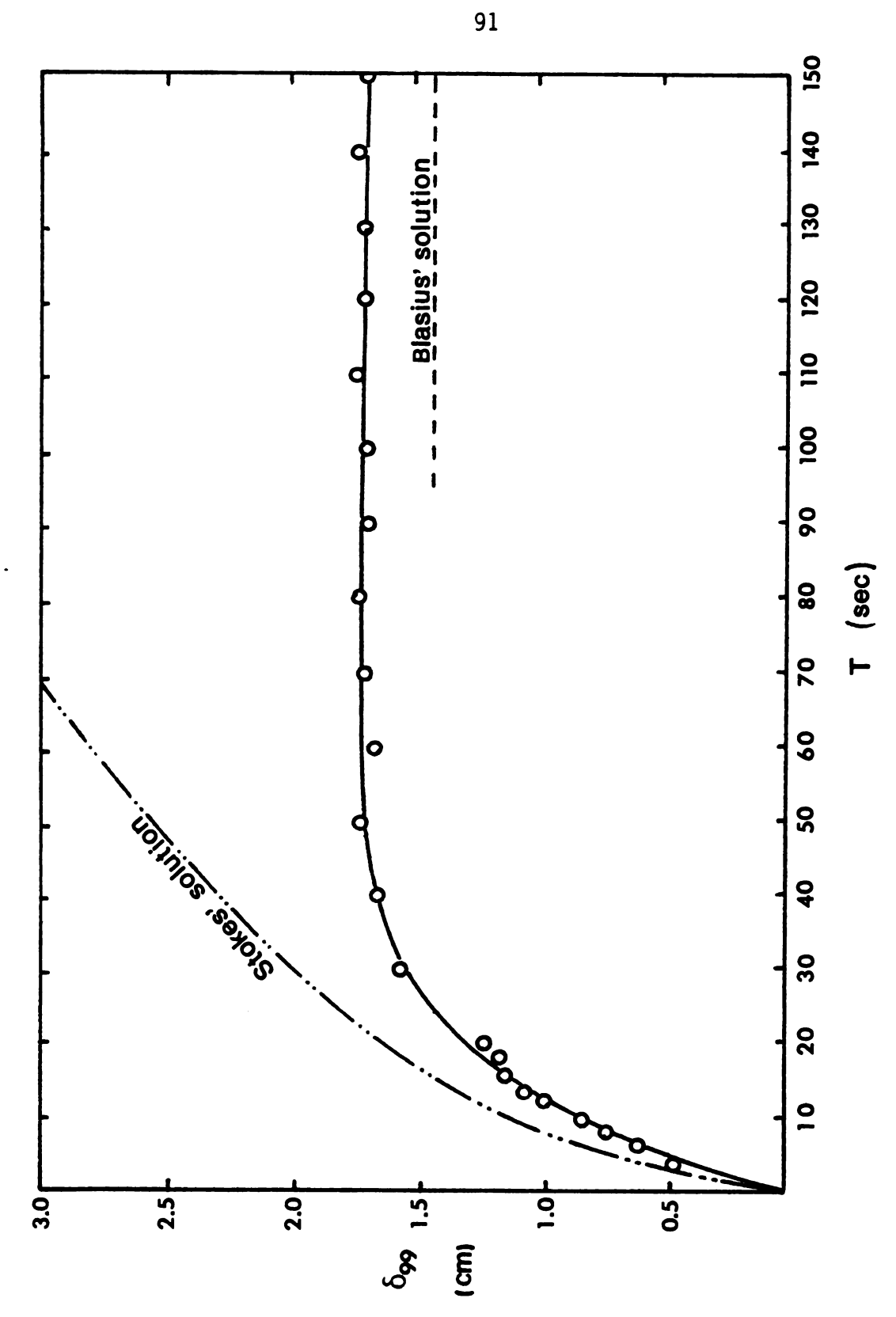


Figure 2.29 Boundary Layer Thickness at U_{W} =5.01 cm/sec

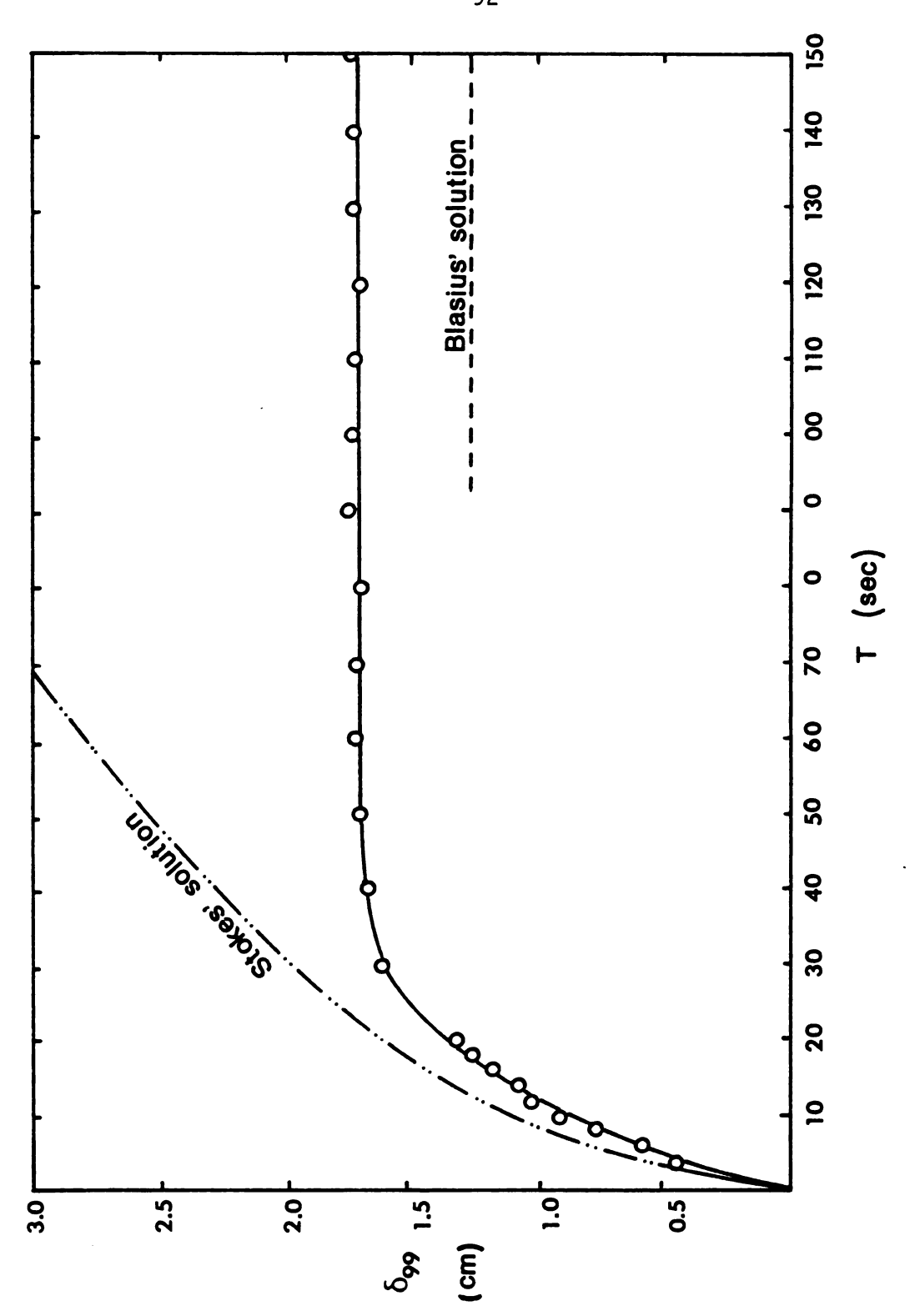


Figure 2.30 Boundary Layer Thickness at $U_{\mbox{W}}$ =6.57 cm/sec

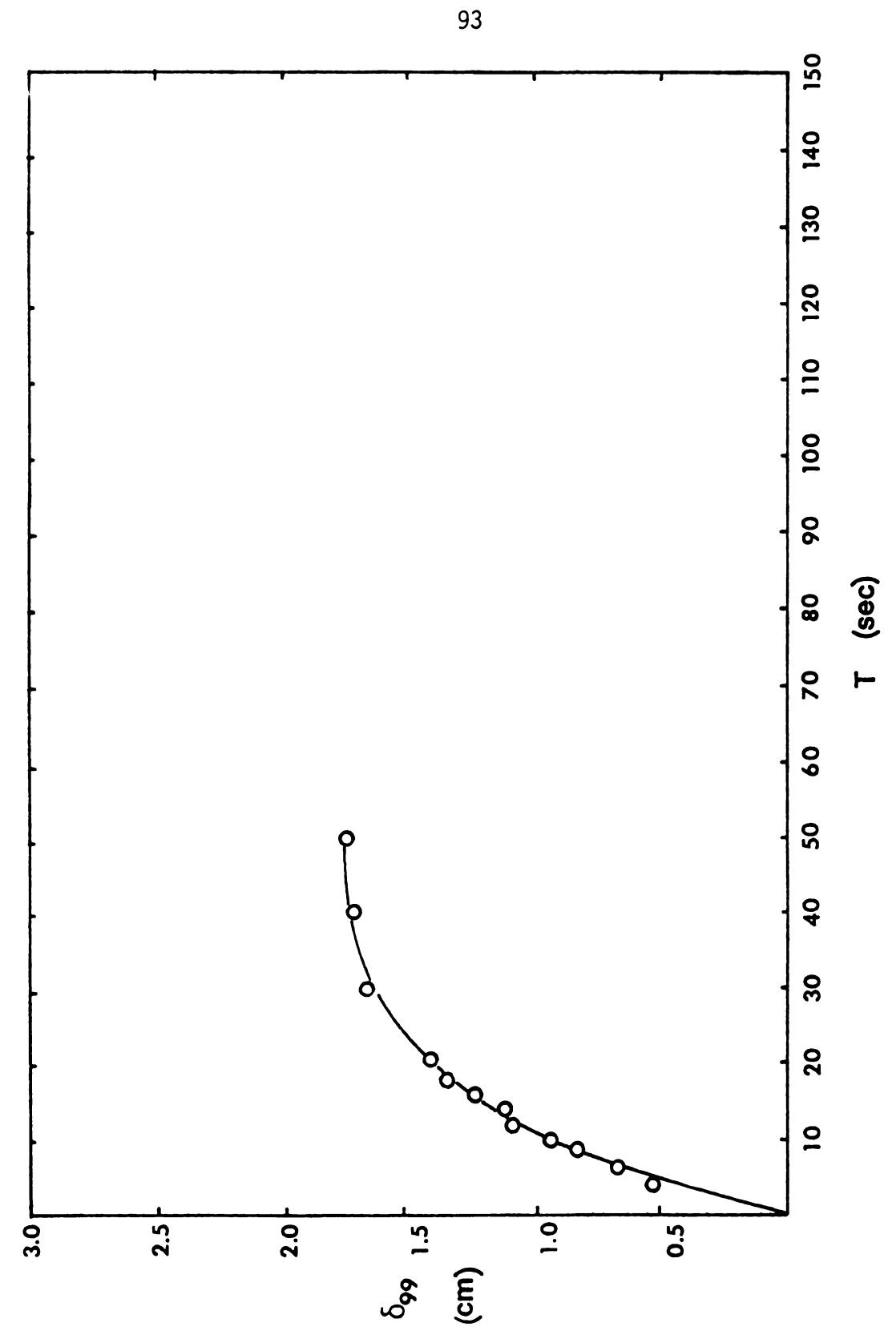


Figure 2.31 Boundary Layer Thickness at $U_{\rm W}$ =9.84 cm/sec

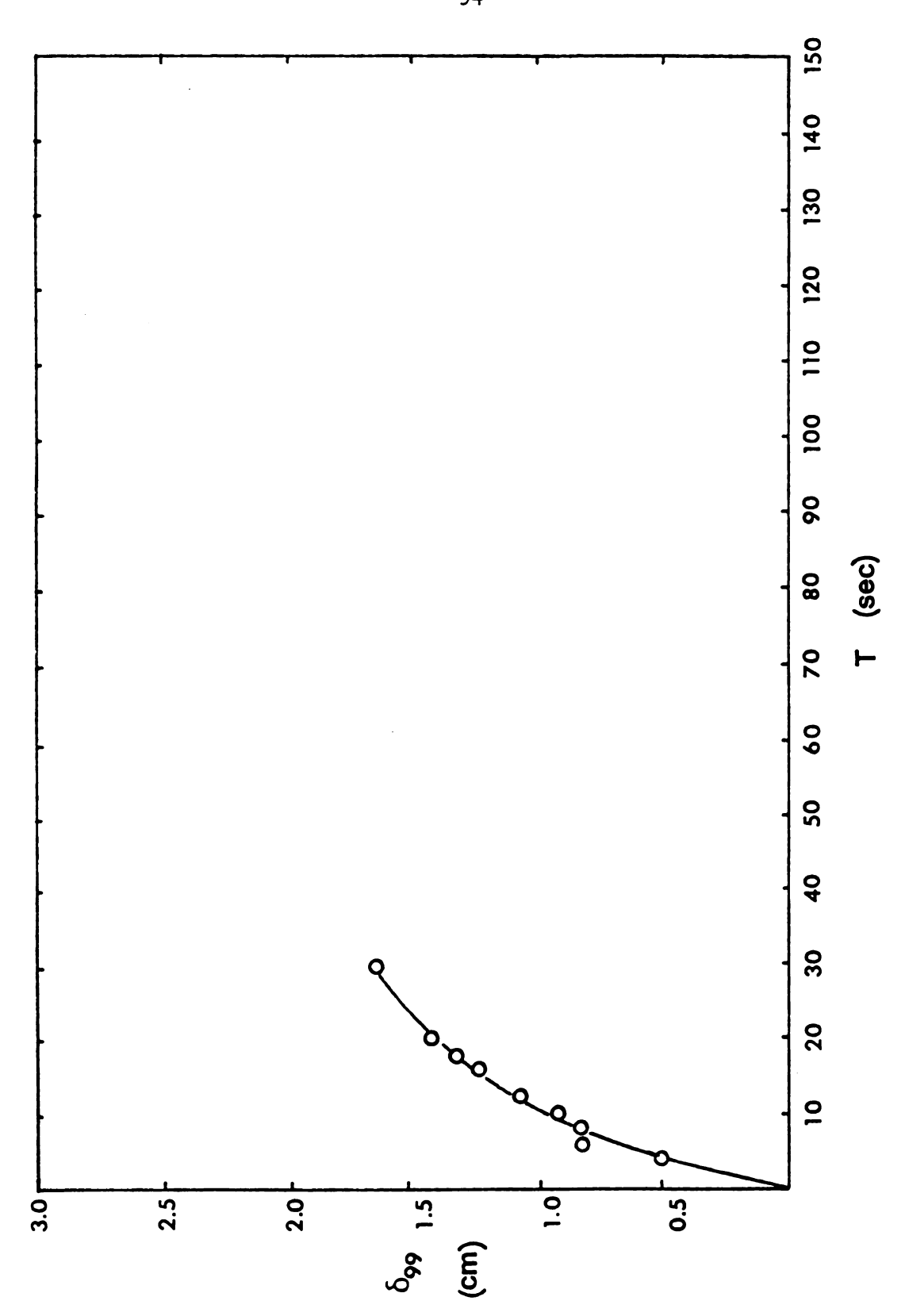


Figure 2.32 Boundary Layer Thickness at U_W =11.42 cm/sec

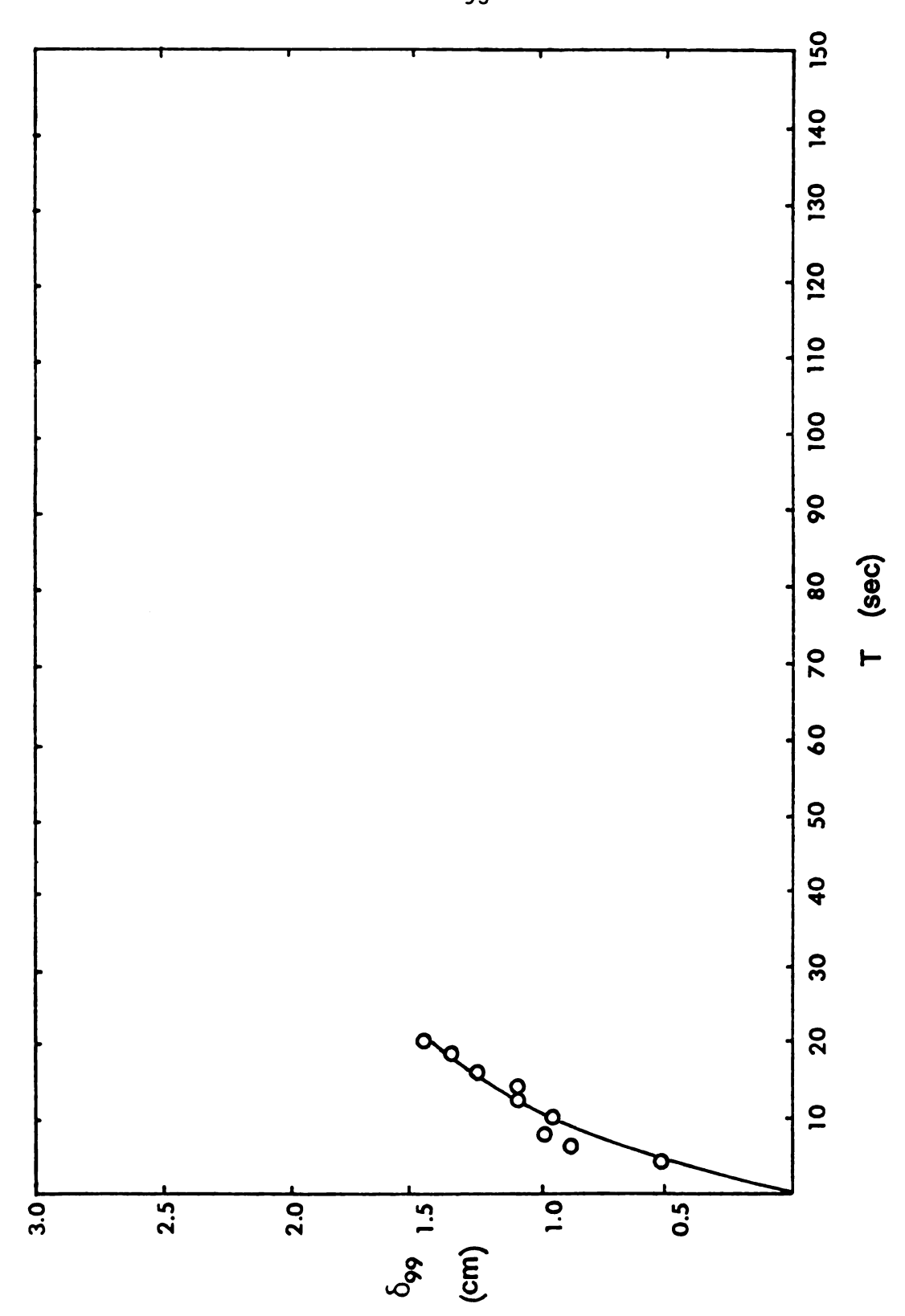


Figure 2.33 Boundary Layer Thickness at U_W =13.30 cm/sec

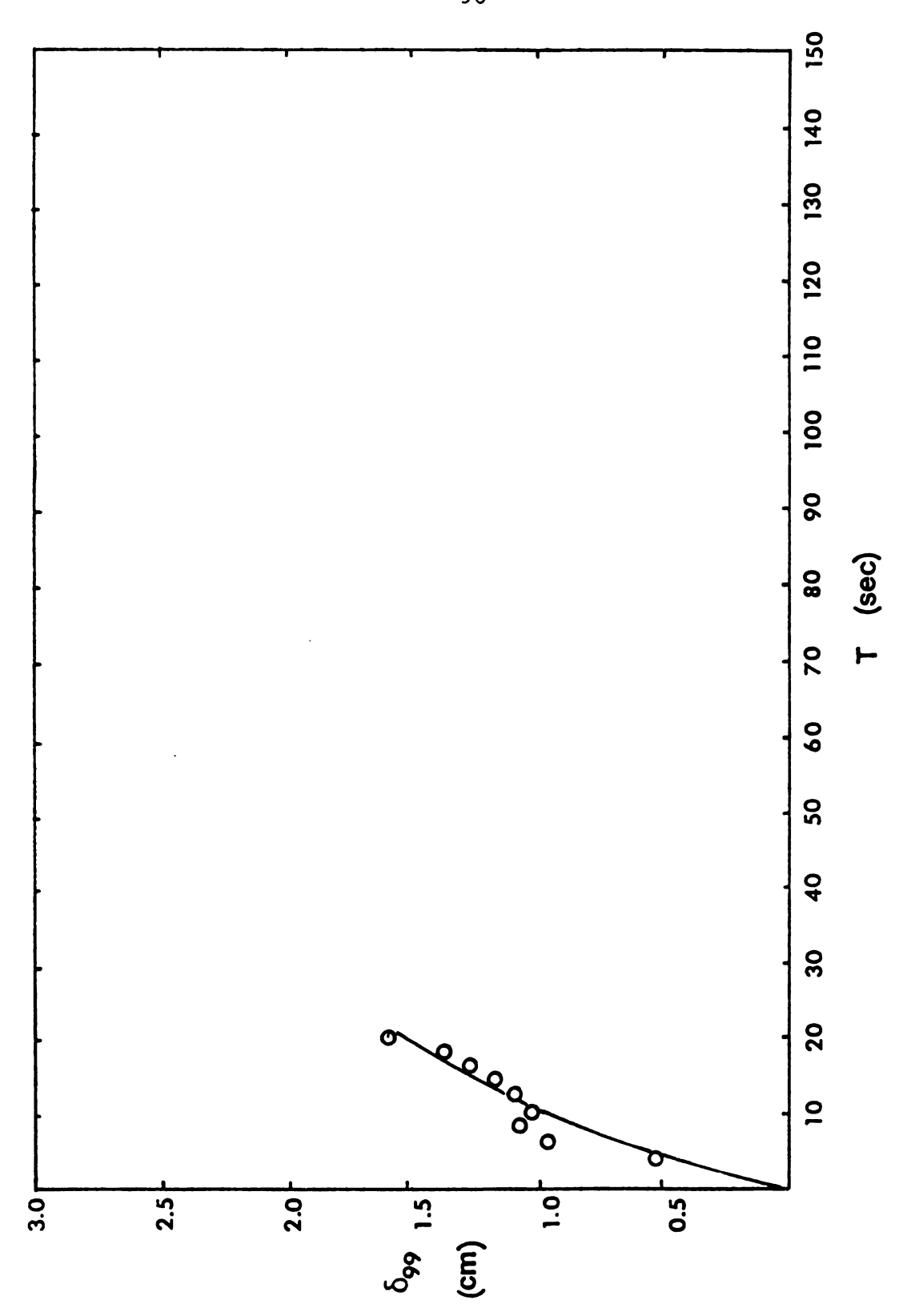


Figure 3.34 Boundary Layer Thickness at $U_{\rm W}$ =19.2 cm/sec

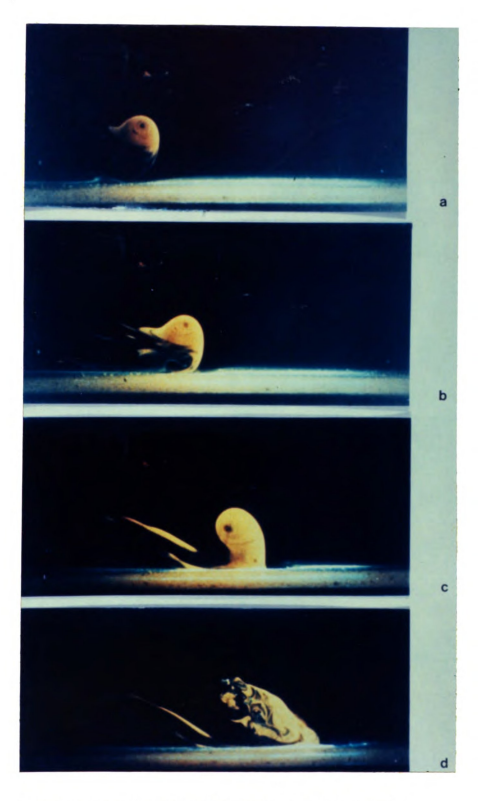


Figure 3.1 An Unstable Interaction at 15 Degrees

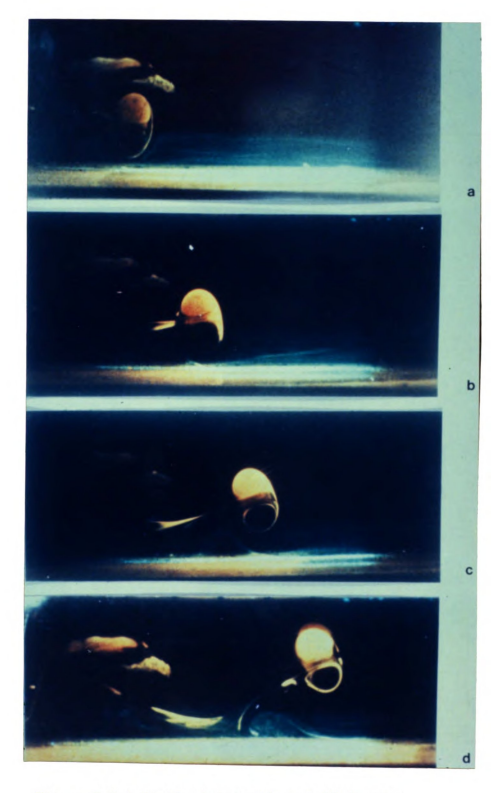


Figure 3.2 A Stable Interaction at 15 Degrees

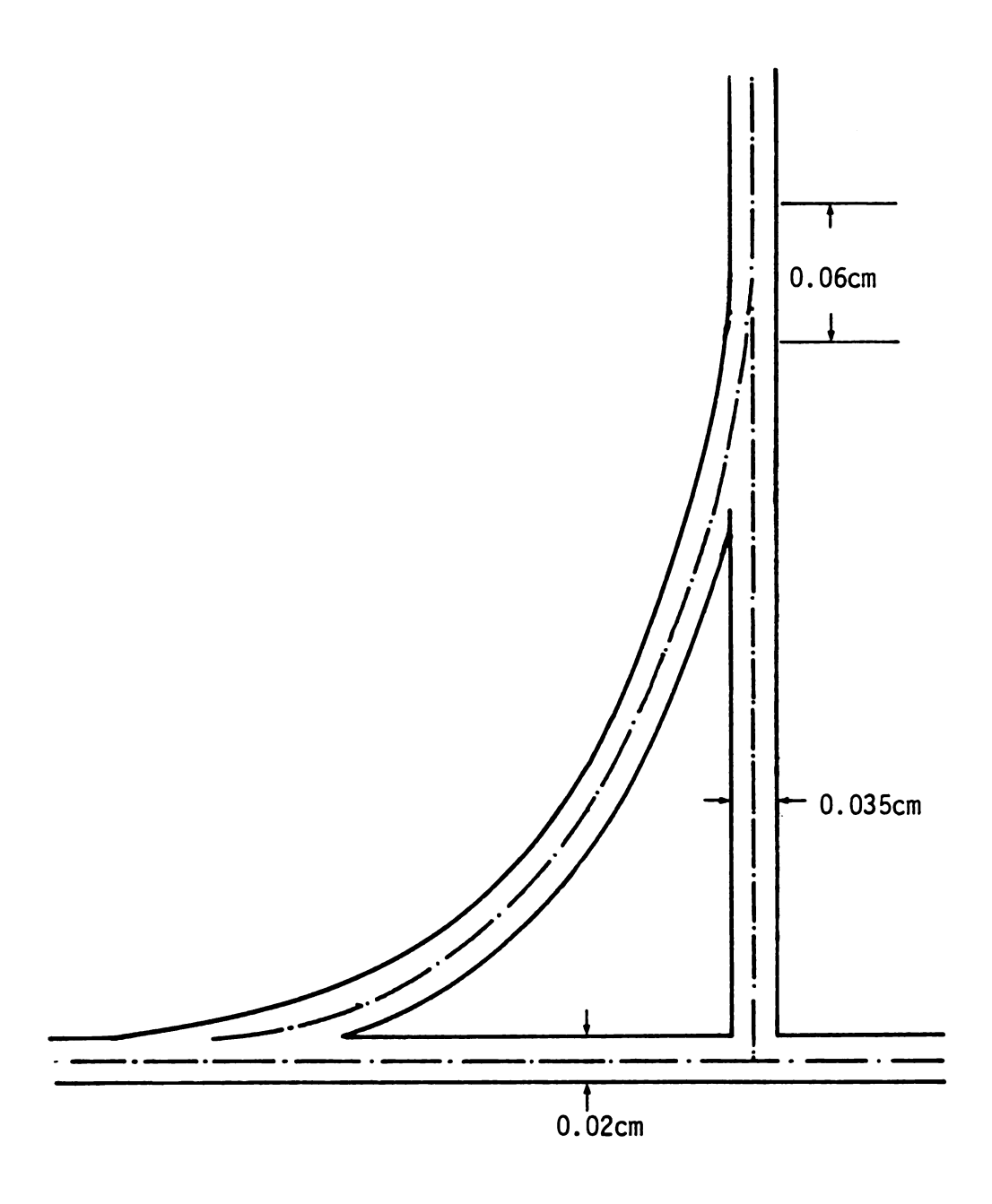


Figure 3.3 Measurement Error Introduced by the Thicknesses of Traces and the Wall Surface $\frac{1}{2}$

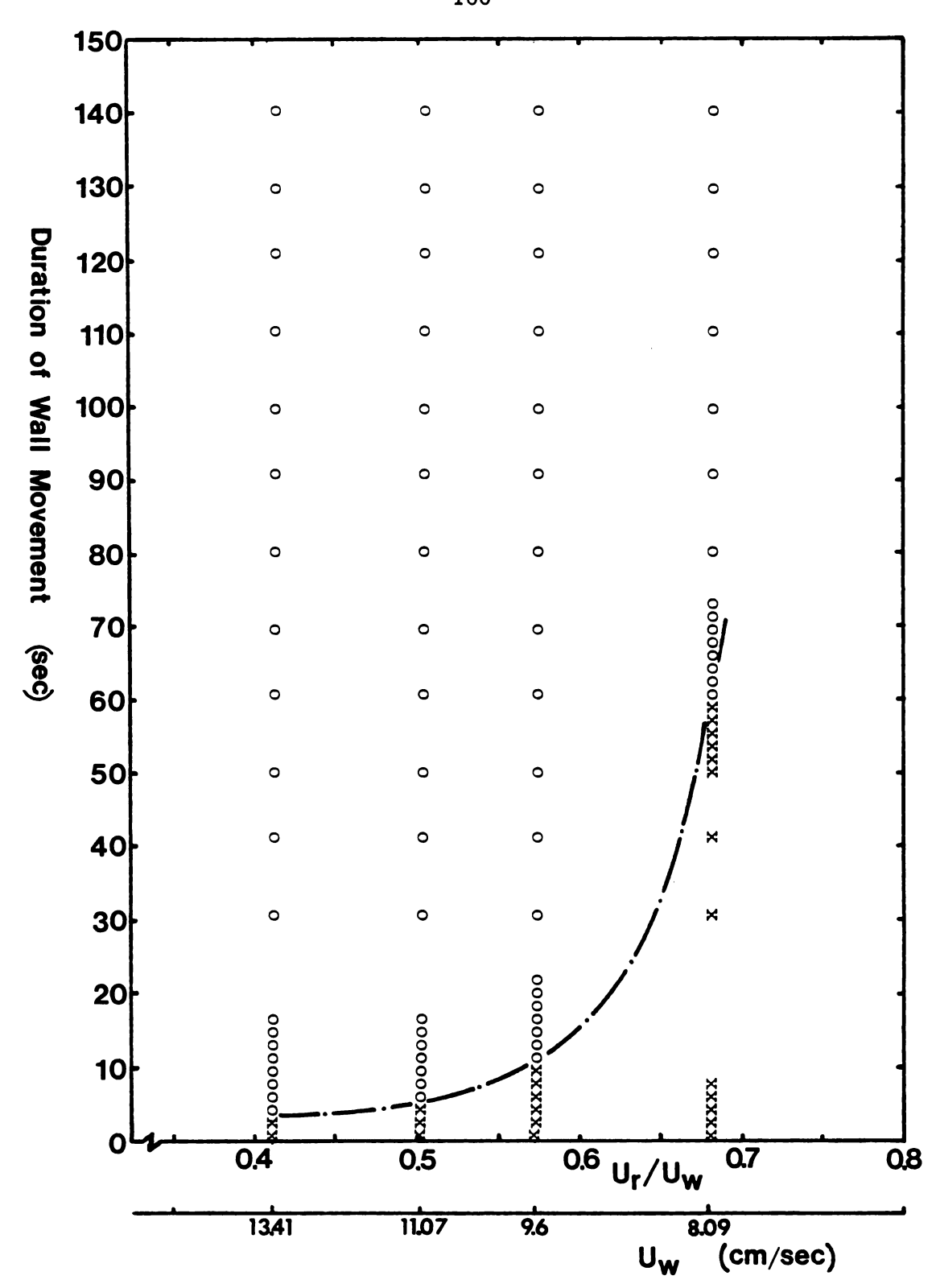


Figure 3.4 Interaction Stability under Various Conditions, x denotes an unstable interaction, o denotes a stable one. The angle of interaction is 15 degrees, velocity of ring is $5.50~\rm cm/sec$

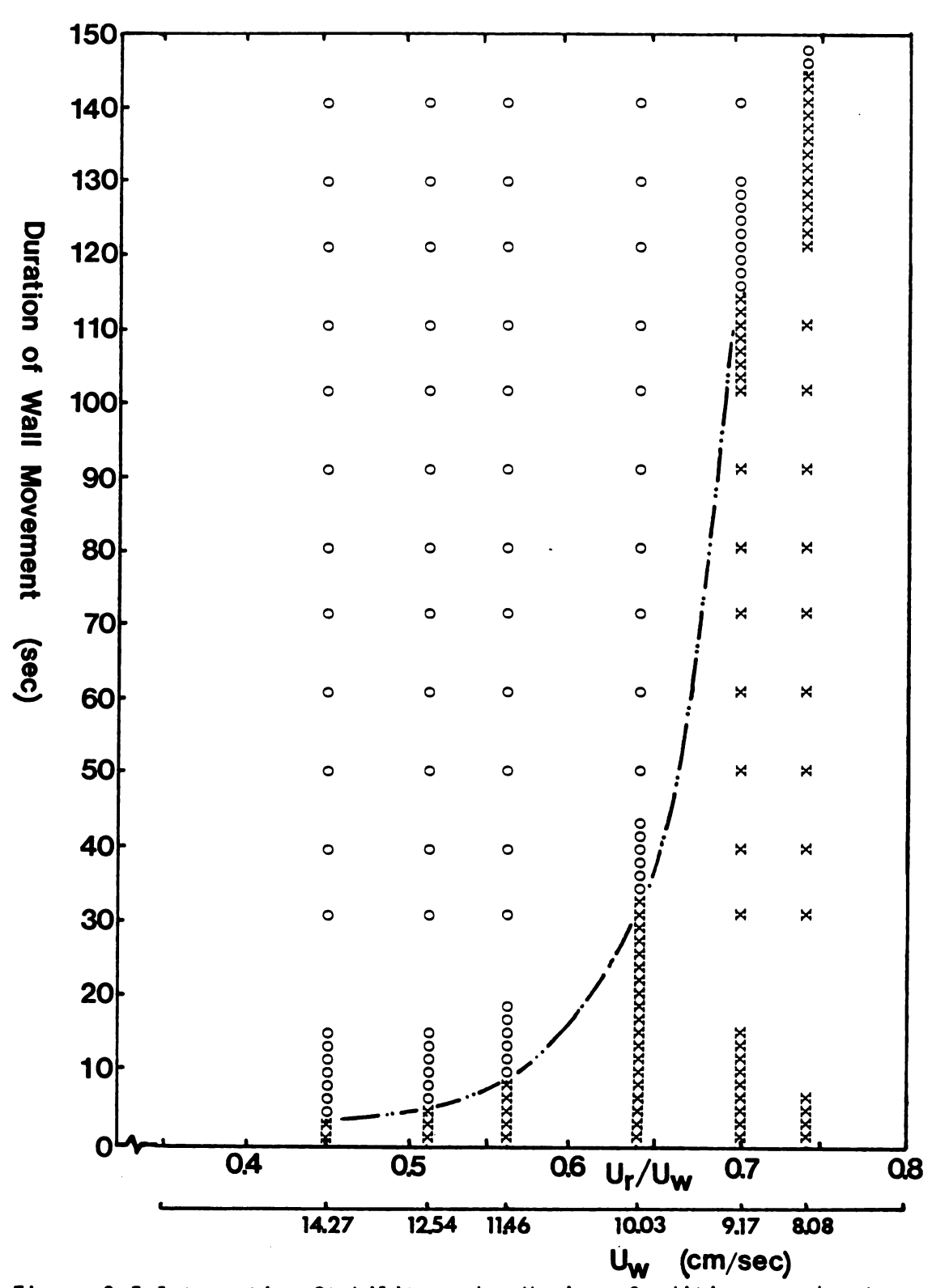


Figure 3.5 Interaction Stability under Various Conditions, x denotes an unstable interaction, o denotes a stable one. The angle of interaction is 15 degrees, velocity of ring is 6.42 cm/sec

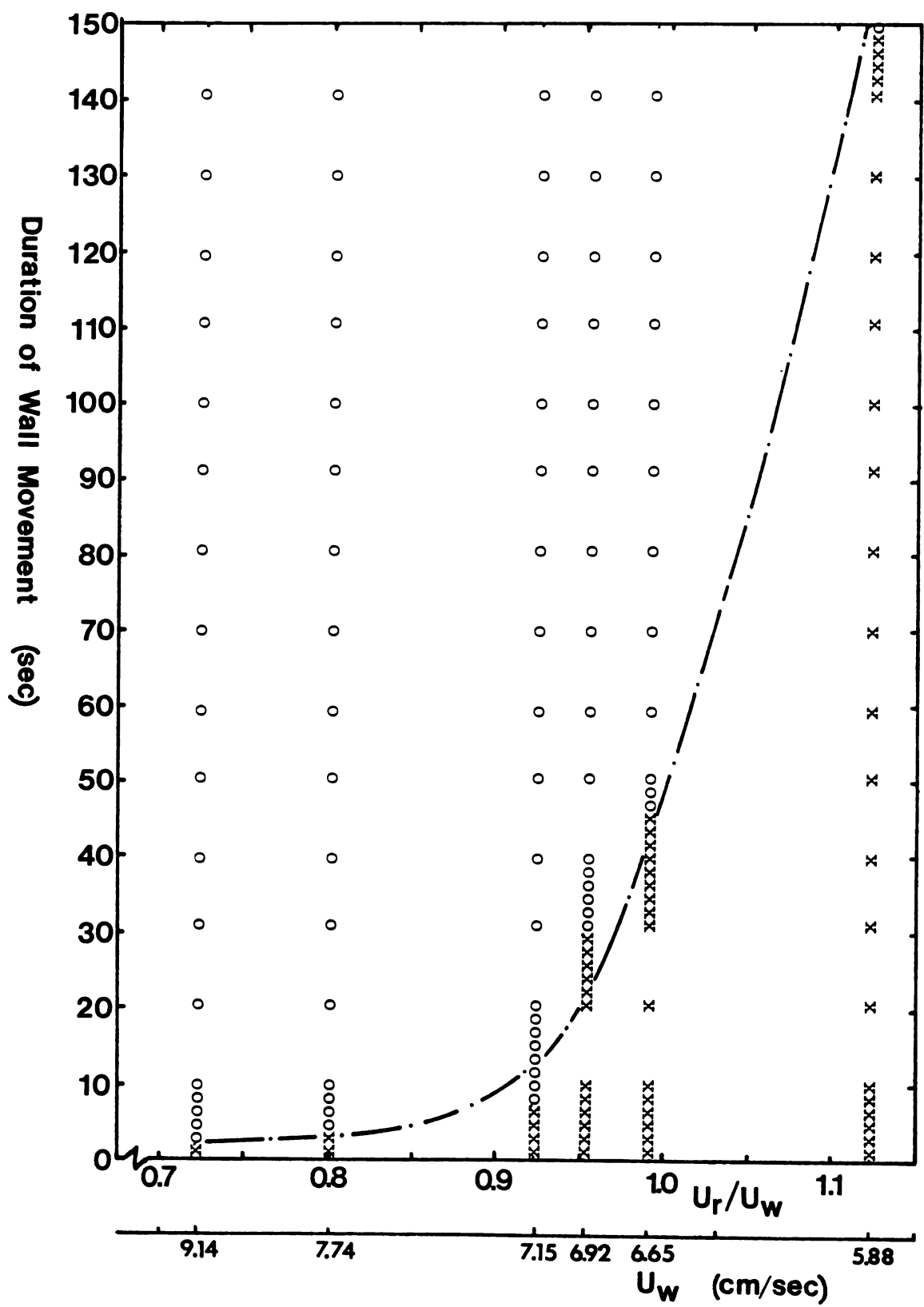


Figure 3.6 Interaction Stability under Various Conditions, x denotes an unstable interaction, o denotes a stable one. The angle of interaction is 9 degrees, velocity of ring is 6.58 cm/sec

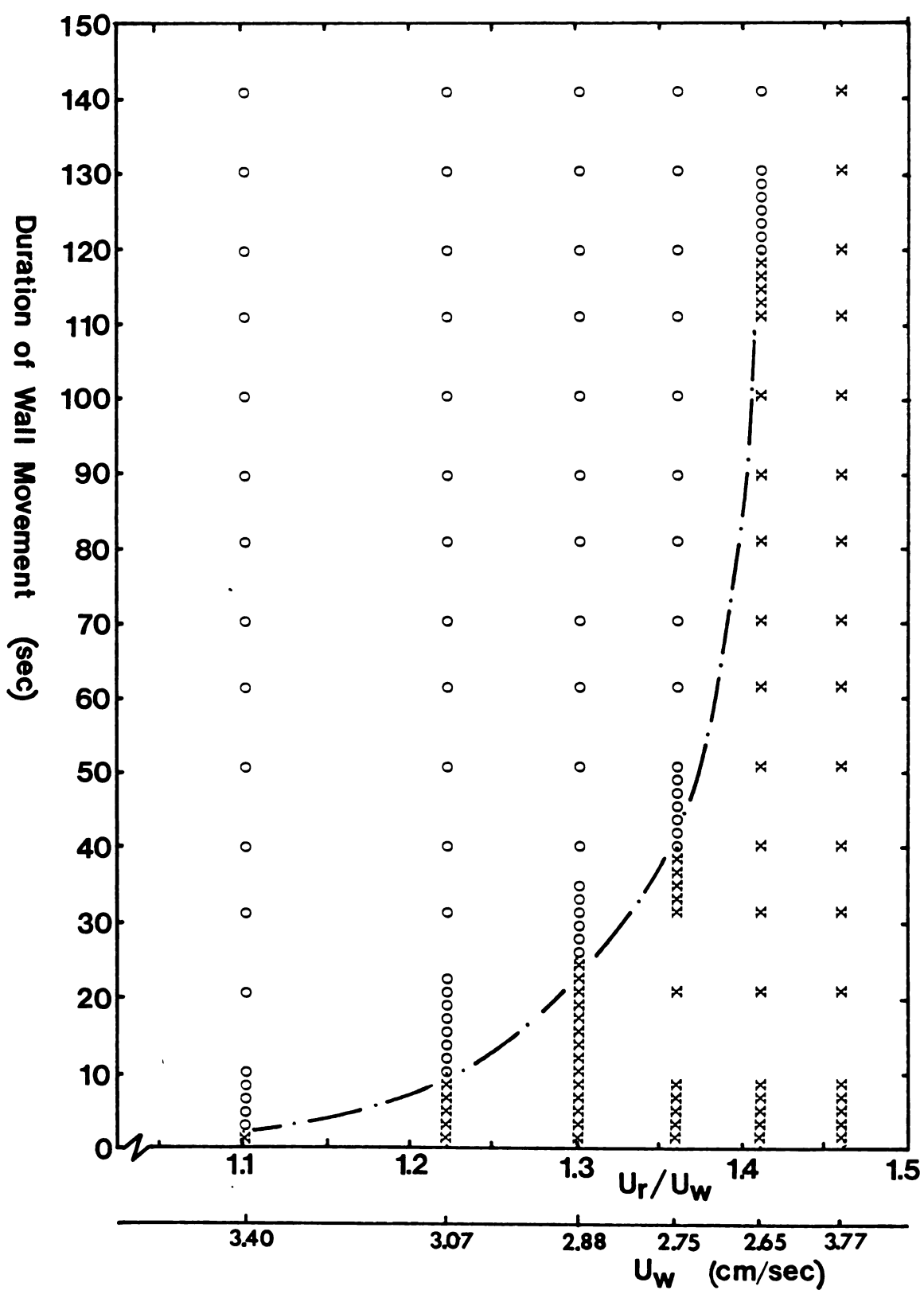


Figure 3.7 Interaction Stability under Various Conditions, x denotes an unstable interaction, o denotes a stable one. The angle of interaction is 3 degrees, velocity of ring is 3.74 cm/sec

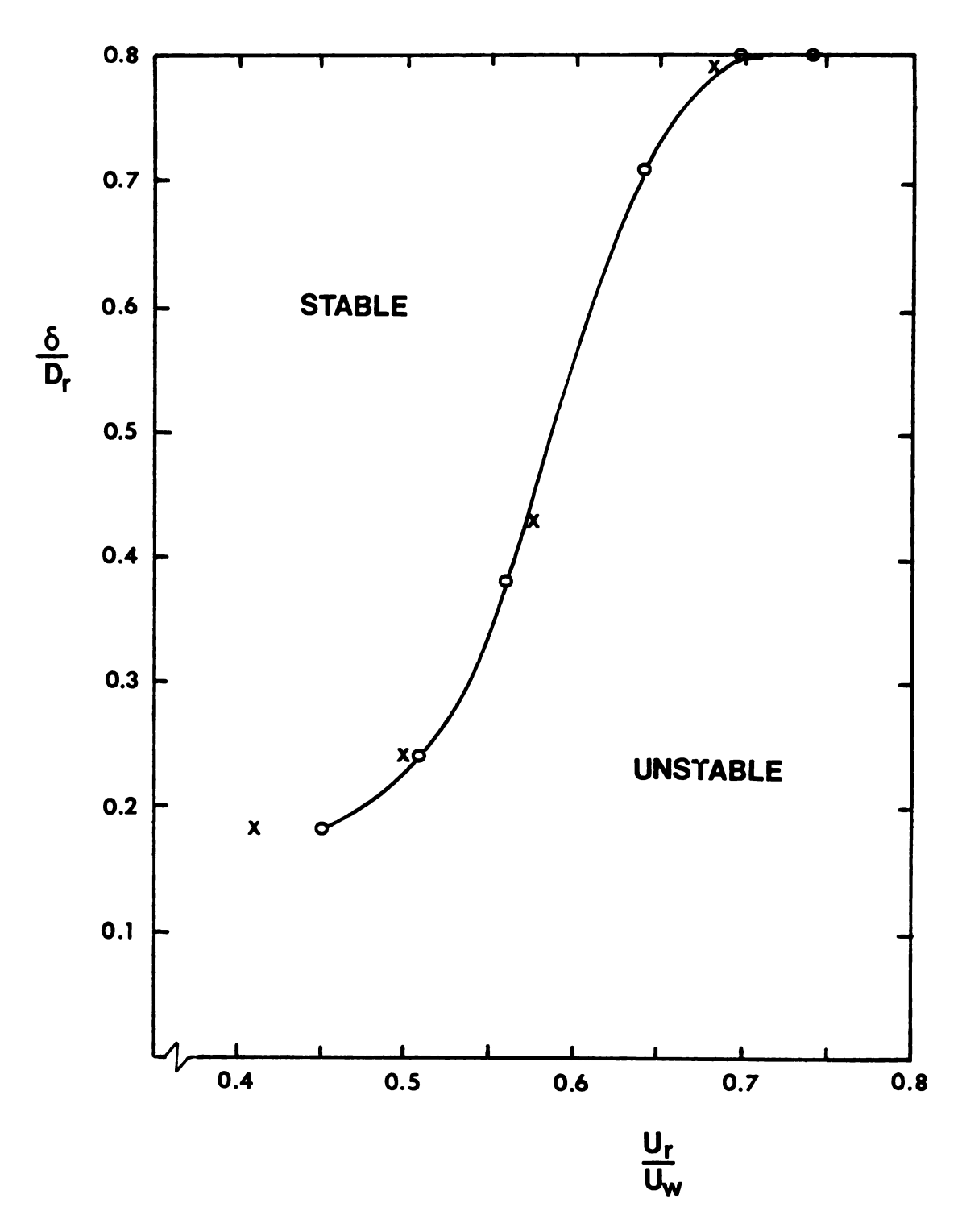


Figure 3.8 Stability Map for Interaction Angle of 15 Degrees

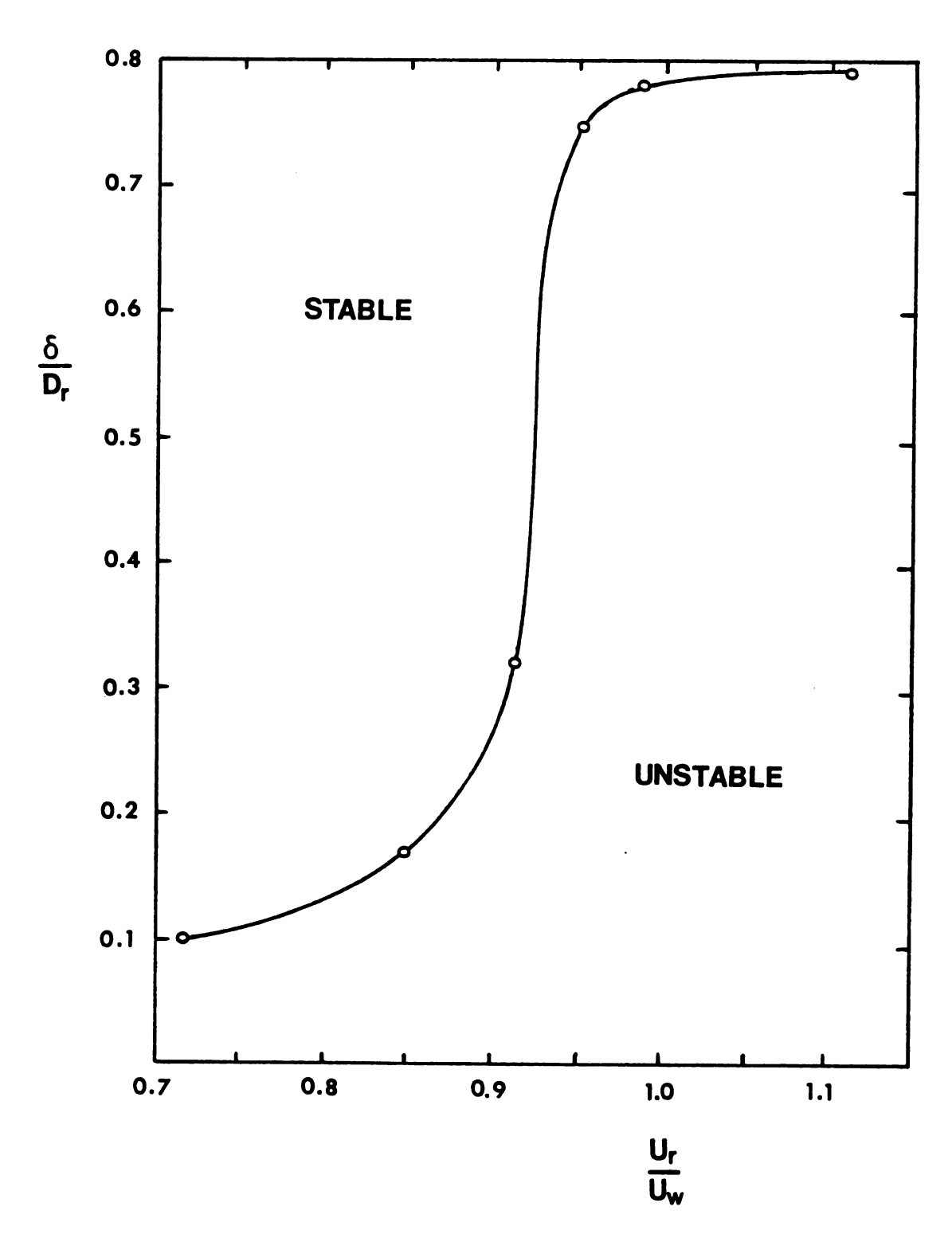


Figure 3.9 Stability Map for Interaction Angle of 9 degrees

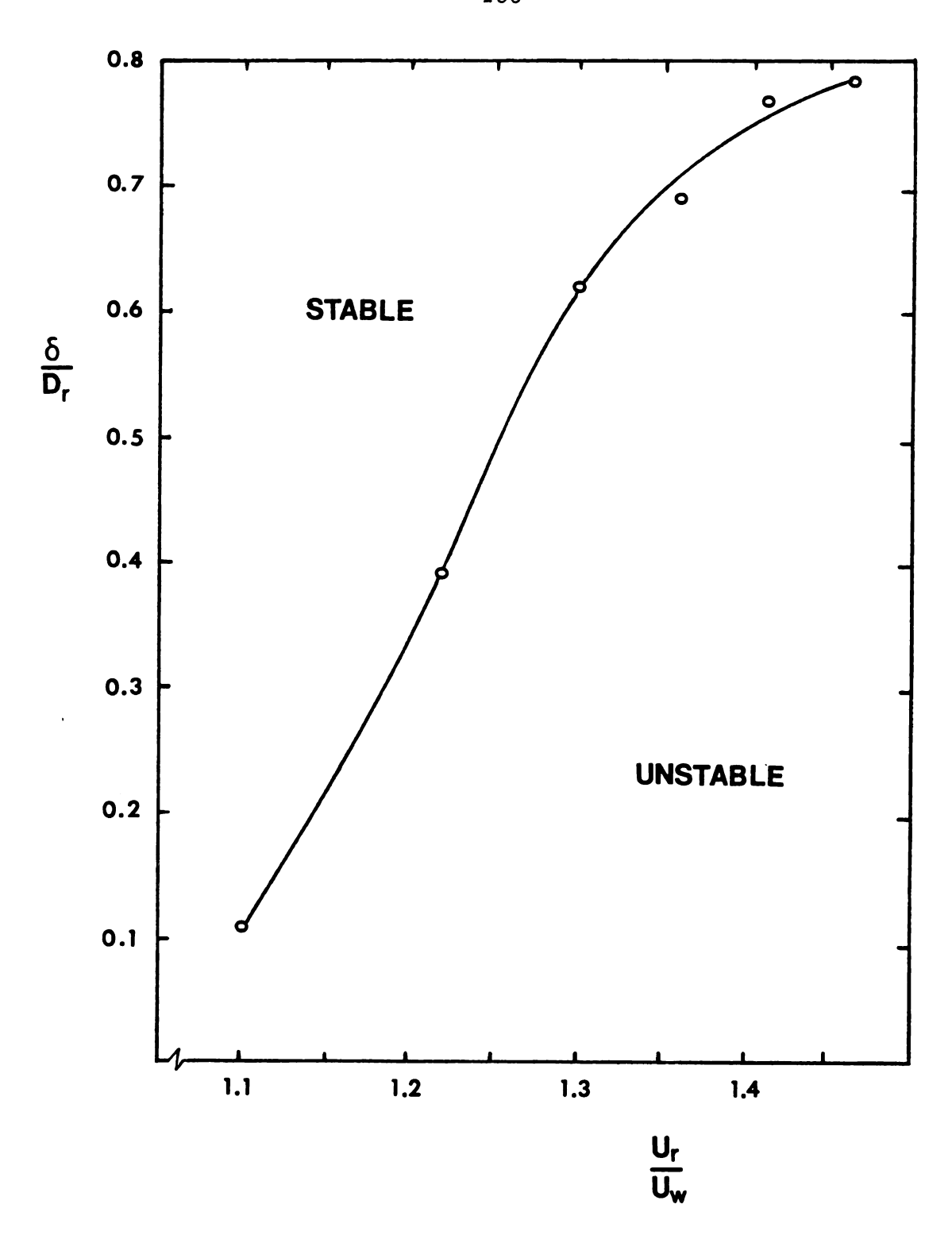


Figure 3.10 Stability Map for Interaction Angle of 3 Degrees

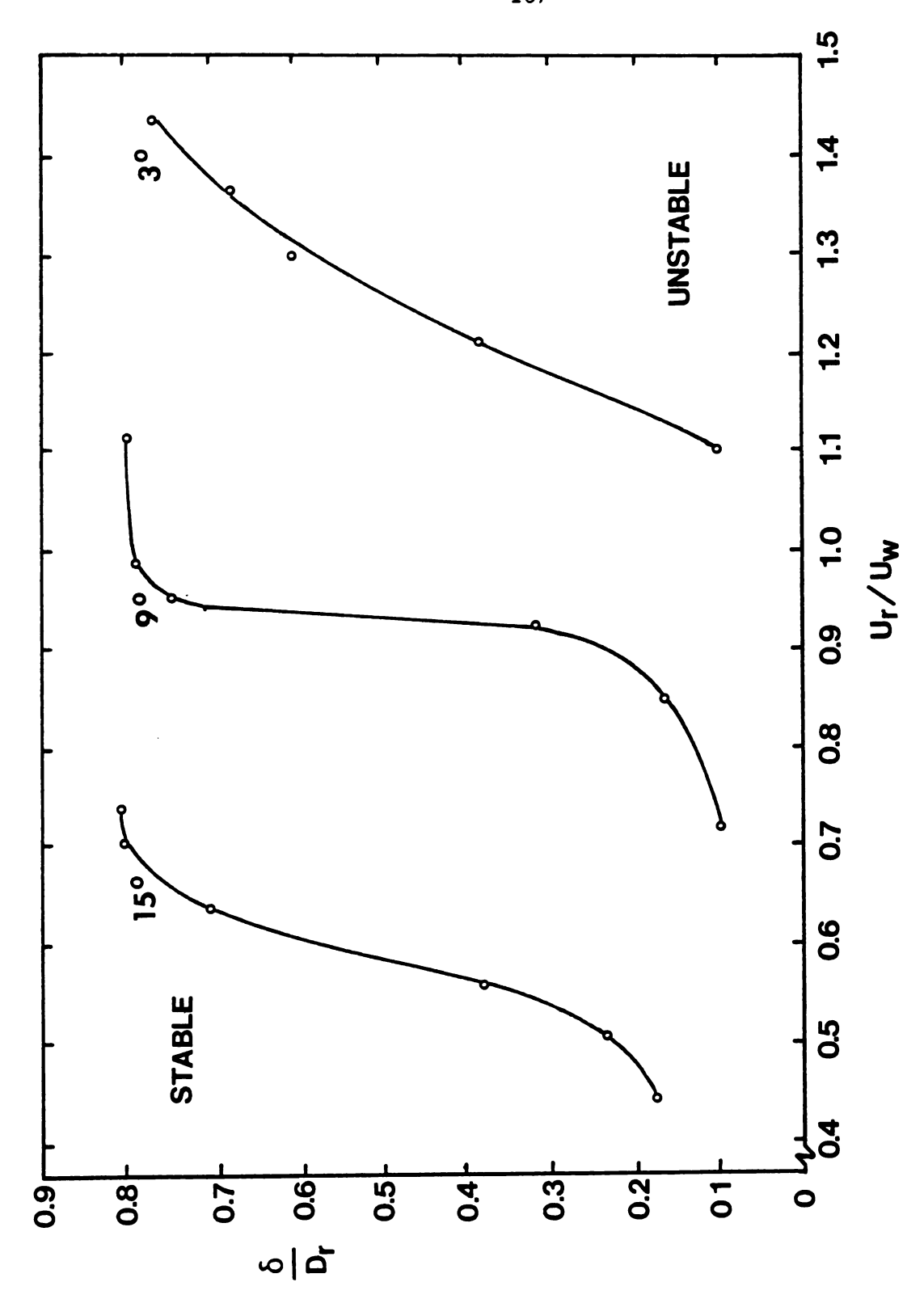
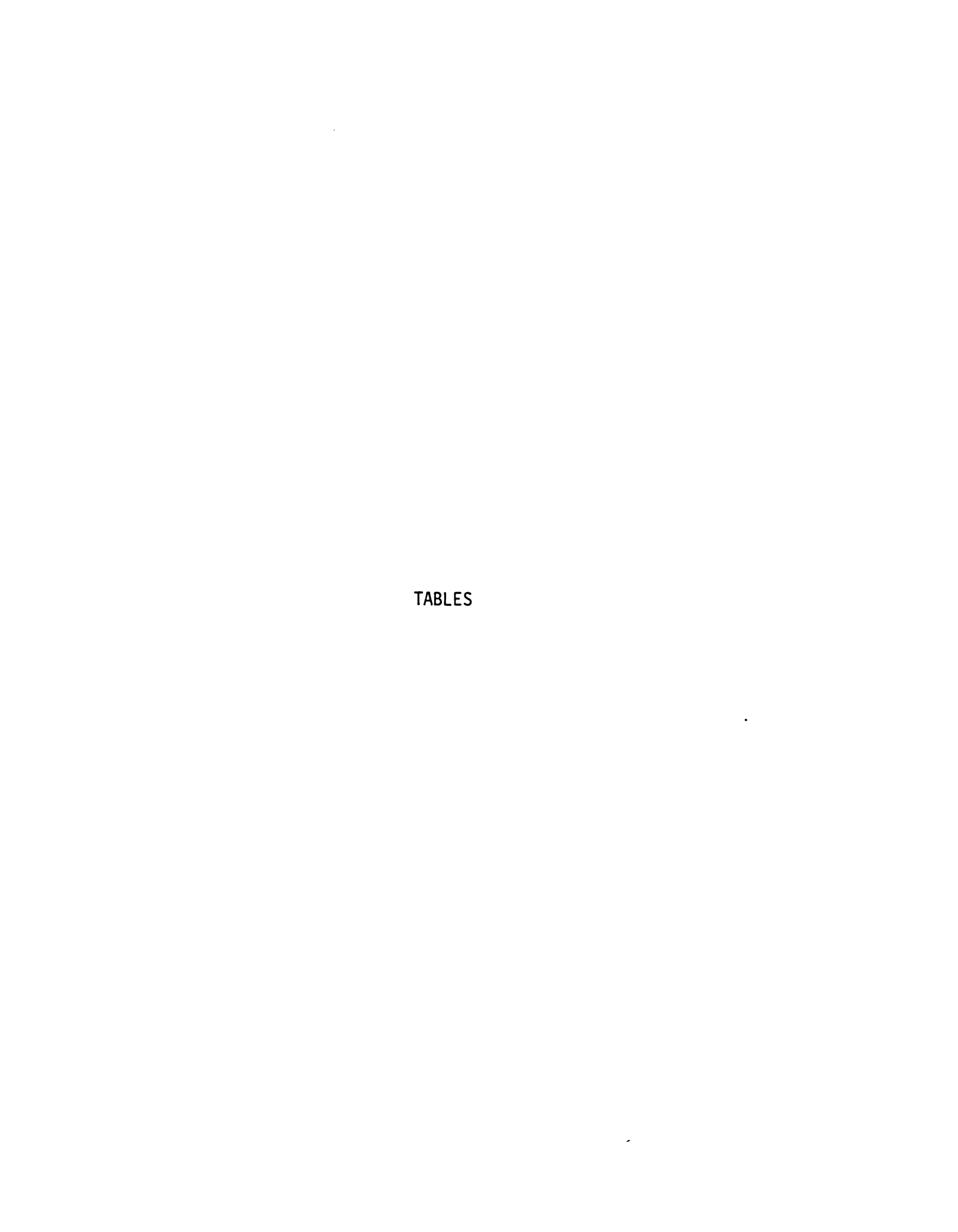


Figure 3.11 Overall Stability Map



Potentio- meter Settings	L ₁	T1	٨٦	L 2	Т2	٧2	L ₃	Т3	٧3	(V)av	(V)av (V ²)av	Standard Diviations
7.0	75.4	10.46	7.21	75.0	11.59	6.47	76.5	11.05	6.92	6.86	47.24	0.42
7.5	72.3	10.18	7.10	76.2	10.54	7.23	75.3	10.47	7.19	7.17	51.46	0.23
8.0	78.3	10.23	7.68	77.2	9.92	7.78	74.3	9.71	7.65	7.70	59.34	0.22
8.5	73.1	8.71	8.39	75.2	8.47	8.88	69.5	7.99	8.70	8.66	74.98	0.12
9.0	76.4	8.22	9.24	74.6	8.22	9.08	78.6	8.65	9.09	9.14	83.49	0.23
9.5	77.9	7.72	10.09	77.1	7.69	10.03	76.3	7.60	10.05	10.06	101.13	0.27
10.0	75.8	6.76	11.21	77.6	6.93	11.20	71.7	6.40	11.21	11.21	125.59	0.27
10.5	76.1	6.77	11.24	76.1	6.67	11.41	79.0	6.98	11.32	11.32	128.22	0.28
11.0	72.1	5.93	12.16	76.7	6.11	12.55	72.3	5.80	12.47	12.40	153.62	0.37
11.5	74.0	5.64	13.12	72.3	5.74	12.60	75.6	5.88	12.85	12.86	165.34	0.20
12.0	73.5	5.20	14.13	74.8	5.49	13.62	74.8	5.33	14.04	13.93	194.10	0.22
12.5	72.4	4.80	15.09	75.7	5.03	15.06	74.1	4.95	14.96	15.04	226.10	0.31
13.0	76.2	4.69	16.25	74.8	4.66	16.04	74.5	4.56	16.34	16.21	262.78	0.13

Table 1 A typical Set of Wall Speed Calibration Data

Figure No.	Interaction Angle	Interaction Valve Opening Angle Time (sec)	Ur (cm/sec)	U_{r}/U_{w}	U_{r} U_{r}/U_{w} Delay Time (sec)
2.18	15	0.32	4.67	0.8	10
2.19	15	0.32	4.67	0.5	10
2.20	6	0.38	2.35	1.7	0
2.21	6	0.38	2.35	0.85	80
2.11	က	0.38	2.35	1.7	0
2.23	က	0.38	2.35	1.1	0

Table 2 Initial Conditions for Figure 2.18 through 2.23

NII								
T	1.35	2.68	5.01	6.57	9.84	11.42	13.30	19.20
4	0.44	0.50	0.45	0.45	0.53	0.51	0.52	0.53
6	0.58	0.60	0.59	0.59	0.71	0.80	0.86	0.94
8	0.72	0.72	0.71	0.75	0.82	0.81	0.98	1.10
10	0.88	0.83	0.82	0.90	0.93	0.96	0.95	1.04
12	0.94	0.95	0.96	1.01	1.11	1.09	1.12	1.14
14	0.99	1.03	1.04	1.06	1.16	1.09	1.13	1.23
16	1.08	1.08	1.13	1.18	1.28	1.26	1.27	1.33
18	1.14	0.96	1.14	1.24	1.38	1.36	1.39	1.40
20	1.21	1.20	1.22	1.32	1.43	1.44	1.46	1.54
30	1.36	1.41	1.54	1.62	1.64	1.62		
40	1.40	1.45	1.64	1.67	1.69			
50	1.47	1.64	1.70	1.69	1.73			
60	1.55	1.60	1.67	1.72				
70	1.70	1.63	1.71	1.71				
80	1.64	1.67	1.72	1.69				
90	1.62	1.65	1.67	1.73				
100	1.64	1.64	1.68	1.72				
110	1.64	1.63	1.72	1.72				
120	1.64	1.64	1.69	1.69				
130	1.62	1.65	1.68	1.73				
140	1.64	1.64	1.71	1.72				
150	1.64	1.65	1.68	1.73				

Table 3 Boundary Layer Thickness at Various Time Durations (sec) and Wall Speed (cm/sec)